QUAD Lift Workability Analysis

Evaluating the Dynamic Interaction Between Two Dual-crane Vessels using a Frequency Domain Modelling Technique

Niels van Duijn

Master of Science Thesis

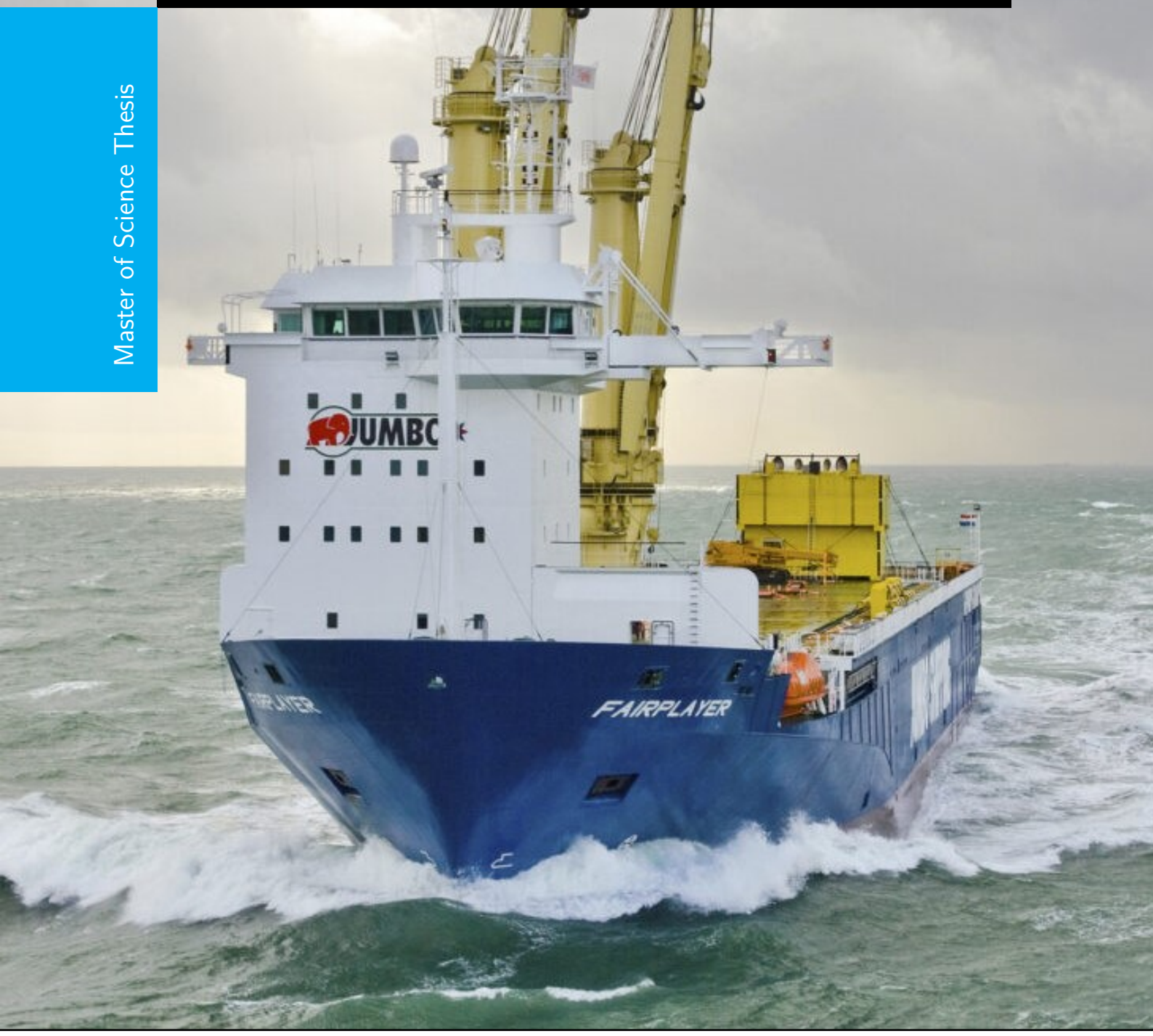

TU Delft Delft University of Technology

Offshore & Dredging Engineering

QUAD Lift Workability Analysis

Evaluating the Dynamic Interaction Between Two Dual-crane Vessels using a Frequency Domain Modelling Technique

Master of Science Thesis

For the degree of Master of Science in Offshore and Dredging Engineering at Delft University of Technology

Niels van Duijn

October 20, 2020

Faculty of Mechanical, Maritime and Materials Engineering (3mE) · Delft University of Technology

The work in this thesis was supported by Jumbo Maritime.

Copyright © Offshore and Dredging Engineering (ODE)
All rights reserved.

Delft University of Technology
Department of
Offshore and Dredging Engineering (ODE)

The undersigned hereby certify that they have read and recommend to the Faculty of Mechanical, Maritime and Materials Engineering (3mE) for acceptance a thesis entitled

QUAD Lift Workability Analysis

by

Niels van Duijn

in partial fulfillment of the requirements for the degree of

Master of Science Offshore and Dredging Engineering

Dated: October 20, 2020

Supervisor(s):

Prof. A. Metrikine, TU Delft

Assist. Prof. O. Colomés, TU Delft

ir. K. van der Heiden, Jumbo Maritime

Reader(s):

Abstract

A QUAD lift is a new lifting method in which dual crane vessels combine their vessel capability to increase their offshore lift performance. The use of the Jumbo J-Class vessels in a QUAD lift creates the opportunity to increase the offshore lift capacity and to install structures with larger dimensions. When floating vessels are close to each other in an offshore environment, their motion will be different than in the freely-floating situation because of hydrodynamic coupling and wave diffraction forces. The main objective of this thesis is to create a model of the QUAD Lift method which predicts the vessel and load motions and evaluate the workability such a lift.

Both potential solvers AQWA and OrcaWave are used to assess the hydrodynamic parameters of the interacting vessels. The gap between the vessels is 40 m and the vessel configuration is such that the cranes are parallel to each other. In between the vessels, transversal wave resonance induces peaks in the frequency dependent radiation forces of the vessels. An additional damping lid in between the vessels effectively reduces the resonance behaviour, which is overestimated by potential solvers. The damping lid has an negligible effect on the final workability of the QUAD lift.
A 18-DoF linear Matlab model is created which includes the mechanical connection between the vessels and the load. The cranes and the cables are modelled as linear springs. The natural frequencies and eigenvectors show large coupling between the vessel roll and the load sway motion. Tugger lines between the vessel and load are added to shift the natural frequencies of the system and to decrease the large horizontal responses of the load.

A parametric study is done on the effect of the load mass, cable lengths and wave directions on the system motion in the most probable wave condition in the Central North Sea. An increase of the mass of the load leads to larger vessel and load motions. The shorter the cable length, the larger the vessel and load motions. The motions are most severe in beam and quarter waves. Depending on the stiffness of the tugger lines the workability can be improved up to 85, 55 and 24 % in respectively head, quarter and beam waves. The limiting factor for the workability is the off-lead angle of the cranes. Broadening of the off-lead angle limit of the crane shows great potential to further increase the workability.

Table of Contents

Acknowledgements **xiii**

1 Introduction **1**
1-1 About Jumbo Maritime . . . 2
1-1-1 Jumbo J-Class vessels . . . 2
1-2 Simple example of a possible QUAD Lift installation . . . 3
1-3 Problem Statement . . . 4
1-3-1 Thesis Objectives . . . 4
1-4 Scope . . . 5
1-5 Approach . . . 5
1-6 Report overview . . . 6

2 Waves **7**
2-1 Introduction . . . 7
2-2 Airy Wave Theory . . . 8
2-2-1 Energy Density Spectra . . . 9
2-3 Response spectra . . . 10
2-3-1 Statistics . . . 12

3 Motion of the vessels **13**
3-1 Introduction . . . 13
3-2 QUAD lift vessel lay-out . . . 13
3-3 Diffraction calculation . . . 13
3-3-1 Vessel Geometry . . . 14
3-3-2 Mesh . . . 15
3-3-3 Irregular Frequencies . . . 16
3-4 Vessel motions . . . 16
3-4-1 Superposition of motion . . . 18

3-4-2 Matrices and Coupling Terms . . . 19
3-5 Response Amplitude Operator (RAO) . . . 19
3-5-1 Resonance waves . . . 20
3-5-2 Overestimation resonance waves . . . 21
3-5-3 Viscous Roll Damping . . . 22
3-5-4 Damping Lid . . . 25
3-5-5 Analysis of lid damping factor . . . 25
3-5-6 Behaviour of Fairplayer vs Literature . . . 28
3-6 Natural Frequencies . . . 28
3-6-1 DP system . . . 31
3-7 Analysis of J-type responses for different gap widths . . . 31
3-7-1 Validation of Roll Response Marin . . . 32
3-8 AQWA vs OrcaWave . . . 32

4 QUAD Lift Model **35**
4-1 Introduction . . . 35
4-2 Metacentric height . . . 35
4-2-1 Minimal GM during lift . . . 36
4-3 Position of the CoG . . . 36
4-3-1 Change of CoG . . . 36
4-3-2 Hydrostatic coefficients . . . 37
4-3-3 Hydrodynamic coefficients and change of CoG . . . 38
4-4 QUAD Lift Model . . . 39
4-4-1 Crane stiffness . . . 41
4-4-2 Derivation Equations of Motion . . . 42
4-5 Coupled Responses . . . 44
4-5-1 Vessel Responses . . . 44
4-5-2 Load Responses . . . 44
4-5-3 Vessel Roll Response . . . 47
4-5-4 Dynamic crane forces . . . 47
4-6 Coupled Natural Frequencies . . . 49
4-7 Tugger lines . . . 52
4-7-1 Tug method . . . 52
4-7-2 Tugger line lay-out . . . 53
4-7-3 Tugger line model . . . 54
4-7-4 Tugger line stiffness analysis . . . 55
4-7-5 Natural Frequencies and Eigenvectors . . . 60

5 Results: Parametric study and Workability **65**
5-1 Introduction . . . 65
5-2 Response Spectra . . . 65
5-3 Parametric Study . . . 67
5-3-1 Variation of Load mass . . . 68
5-3-2 Variation of tugger stiffness values . . . 70
5-3-3 Variation of cable length . . . 71
5-4 Workability . . . 72
5-4-1 Free Floating Vessels . . . 72
5-4-2 QUAD Lift without tugger lines . . . 73
5-4-3 QUAD lift with tugger lines . . . 74

6 Conclusions and Recommendations **79**
6-1 Conclusions and Discussion . . . 79
6-1-1 Vessel motions and interaction . . . 79
6-1-2 QUAD Lift . . . 80
6-1-3 Parametric study and Workability . . . 80
6-2 Recommendations . . . 81

A Responses **83**
A-1 Free floating vessels . . . 83
A-2 QUAD Lift . . . 84
A-2-1 Vessel Response . . . 85
A-2-2 Load Response . . . 86

B QUAD Lift Matrices **87**

C Scatter Diagram **91**

D Literature Review **93**
D-1 Introduction . . . 93
D-2 Literature review hydrodynamic body interaction . . . 93
D-2-1 Strip theory . . . 93
D-2-2 Panel method . . . 94
D-2-3 Finite element method . . . 94
D-3 Potential Theory . . . 94
D-3-1 Conservation Principles . . . 94
D-3-2 Velocity Potential . . . 95
D-3-3 Potential Flow Elements . . . 96
D-4 Potential theory of a body in waves . . . 98
D-4-1 Forces and moments . . . 100
D-4-2 Solving the potentials . . . 103

Bibliography **105**

Glossary **109**

List of Acronyms 109

List of Symbols 109

List of Figures

1-1 Fairplayer Rotterdam. 2

1-2 First 2 phases of installation. The barge and HLCV's are floated to the correct location.(phase 1) The crane cables are attached to the installation piece.(phase 2) 3

1-3 Phase 3 and 4 installation. The structure is lifted in the air (phase 3) and the barge is moved from underneath. (phase 4) 3

1-4 Overview of thesis approach. 5

2-1 Superposition of wave trains with equal height, frequency, direction and length. . 7

2-2 Different wave theories. 8

2-3 Wave record analysis 9

2-4 JONSWAP and Pearson-Moskowitz spectra for different peak periods. The significant wave height is 4 m. 11

2-5 Multi-directional JONSWAP for a peak period of 8 s. The significant wave height is 4 m. The dominant wave direction is 0 degrees. 11

3-1 Quad lift vessel lay-out. The position of the vessels is such that the cranes are parallel to each other. 14

3-2 Fairplayer hull geometry. The left figure shows the original Fairplayer hull, including rudder and thrusters. The figure on the right shows the adjusted hull geometry suited for the AQWA diffraction analysis. 15

3-3 Comparison hydrodynamic data for different meshes Fairplayer. 15

3-4 Meshed vessels side-by-side in ANSYS AQWA with a gap distane of 30m 16

3-5 Effect of internal lid on added mass for heave of side-by-side laying Fairplayer with gap distance of 30m. 17

3-6 Vessel heading conventions 18

3-7 Fairplayer sway radiation damping with characteristic resonance peaks. 22

3-8 Wave patterns of side laying vessels for incident head waves. 22

3-9 Side view of relative wave elevation in between the vessels at frequency of 1.30 rad/s. The gap distance is 40m. 23

3-10 Dimensionless roll damping contributions vs the dimensionless frequency. 24
3-11 RAO's vs freqency in rad/s of FSRU in heave and sway motion for head waves calculated by HYDROSTAR and results of model test executed by Fournier et al.(2006) [10]. The gap distance between vessels is 20 m. 26
3-12 RAO's vs freqency in rad/s of LNG carrier in heave and sway motion for head waves obtained by Chen et al. (2007) [6]. The gap distance between vessels is 20 m. 26
3-13 Hydrodynamic data and RAO's for sway motion of vessel relative to fixed wall for different gap distances by Peña et al.(2016) [28]. 27
3-14 Responses of Fairplayer in head waves with a gap distance of 20 m. 28
3-15 Dimensionless hydrodynamic data for different damping factors for Fairplayer with a gap distance of 40 m. 29
3-16 RAO's for different damping factors of the side-to-side laying Fairplayer in beam waves coming from the non-vessel side. The gap distance is 40 m. 30
3-17 Roll RAO for beam waves compared to experimental data Marin 32
3-18 RAO's of fairplayer for beam waves for different gap widths d in between side to side laying vessels. 33
3-19 Comparison RAO's of both vessels in beam waves between AQWA and OrcaWave. The vessels are in beam waves, V1 indicates the front laying vessel and V2 is not directly exposed to the incident waves. The relative distance between both vessels is 40 m. 34

4-1 Stability floating object 36
4-2 Vertical distance from CoG to load 37
4-3 Single pendulum mechanics 39
4-4 Overview QUAD Lift Model 40
4-5 Top view QUAD Lift with dimensions 41
4-6 Comparison RAO's of free floating vessel and vessel in QUAD Lift for head waves. The mass of the load is 1000 t and the vessel to vessel distance is 40 m. 45
4-7 Horizontal responses of load during QUAD Lift for head and beam waves. 46
4-8 Off-lead and side-lead angles for each of the four cranes of the vessels in head and beam waves, respectively. 46
4-9 Roll Responses for vessels in beam waves for different load conditions. The vessel to vessel distance is 40 m. 47
4-10 Vertical response of crane tips and load attachment points in QUAD Lift. The vessels are in head waves. 48
4-11 Elongation and elongation forces of cranes and cables in QUAD Lift. The vessels are in head waves. 48
4-12 RAO's vessel during QUAD Lift including natural frequencies(vertical lines). The vessels are subjected to quarter waves. 49
4-13 Eigenvectors for the 10 natural frequencies. The subscripts added to DoF on the x-axis indicate the DoF for the different bodies, 1: vessel 1, 2: vessel 2 and L: the load. 51
4-14 Top view of QUAD lift including green tugger lines. 53
4-15 Front view of QUAD lift including green tugger lines. 54
4-16 Load RAO's for different low stiffness values of tugger lines. The vessels are in quarter waves. 57

4-17 Vessel Roll RAO for different small stiffness values of tugger lines. The vessels are in quarter waves. 57
4-18 Vessel RAO's for different small stiffness values of tugger lines. The vessels are in quarter waves. 58
4-19 Load RAO's for different large stiffness values of tugger lines. The vessels are in quarter waves. 59
4-20 Vessel Roll RAO for different large stiffness values of tugger lines. The vessels are in quarter waves. 59
4-21 Vessel RAO's for different large stiffness values of tugger lines. The vessels are in quarter waves. 60
4-22 Vessel RAO's in a QUAD lift with tugger lines with a stiffness of 200 kN/m. The vertical black lines indicate the natural frequencies. The vessel is in quarter waves. 61
4-23 Eigenvectors for the first set of natural frequencies. The subscripts added to DoF on the x-axis indicate the DoF for the different bodies, 1: vessel 1, 2: vessel 2 and L: the load. 63

5-1 Two dimensional response spectra for Fairplayer during QUAD Lift calculated by use of the JONSWAP spectrum with Hs = 2 m and Tp = 9 s and a dominant wave direction of 90 degrees 66
5-2 Probability of sea conditions at the Central North Sea as a function of specific significant wave height Hs and peak period Tp. 67
5-3 Polar plot of SDA of rotational motions of Fairplayer during QUAD Lift configuration for different loads. Tugger lines are not applied. 69
5-4 Polar plot of SDA of lead angles of Fairplayer during QUAD Lift configuration for different loads. Tugger lines are not applied. 69
5-5 Polar plot of SDA of crane parameters during QUAD Lift for different loads. Tugger lines are not applied. 70
5-6 Polar plot of SDA of lead angles during QUAD Lift for different tugger lines stiffnesses. 70
5-7 Polar plot of SDA of lead angles during QUAD Lift for different crane cable lengths. 71
5-8 Polar plot of SDA of vessel rotations during QUAD Lift for different crane cable lengths. 71
5-9 Workability results for free-floating vessels in beam waves. The green and red cells indicate a workable or not workable sea state, respectively. 73
5-10 Workability results for QUAD Lift configuration without tugger lines in head and beam waves. The green and red cells indicate a workable or not workable sea state, respectively. 74
5-11 Workability results of QUAD Lift with different tugger stiffness values in head, quarter and beam waves. 75
5-12 Off-lead angle response during QUAD Lift in beam waves for different tugger stiffness values. 76
5-13 Off-lead angle response during QUAD Lift in beam waves for different tugger stiffness values. 77
5-14 Off-lead angle response during QUAD Lift in beam waves for different tugger stiffness values. The limiting SDA off-lead angle is set to 2 degrees instead of 1 degree. 77

A-1 Comparison RAO's of free floating Fairplayers in quarter waves. The red line indicates the foremost vessel in the sense of that the wave first reaches this vessel. 84

A-2 RAO's of Fairplayer during QUAD lift in quarter waves. 85
A-3 RAO's of load during QUAD lift in quarter waves. 86

B-1 QUAD Lift stiffness matrix generated by Maple 89
B-2 Tugger line stiffness matrix generated by Maple 90

C-1 Wave Scatter diagram of Central North sea, numbers in the diagram are given in percentages. 91

D-1 Strip theory, the cross section is treated hydrodynamically as a infinite long cilinder. 94
D-2 Uniform potential flow, [18]. 97
D-3 Radial potential flow [18]. 97
D-4 Potential flow elements and superposition [18]. 98

List of Tables

3-1 Approximated natural frequencies of sloshing modes for different gap distances in [rad/s] . . . 23

3-2 Natural Frequencies Fairplayer for different gap distances . . . 31

4-1 Vessel and crane parameters . . . 40

4-2 Load parameters . . . 41

4-3 Mass of cables . . . 42

4-4 Natural Frequencies QUAD Lift . . . 50

4-5 Tugger line parameters . . . 56

4-6 Natural frequencies and critical damping related to the horizontal load motions for different tugger stiffnesses. . . . 56

4-7 Natural Frequencies QUAD Lift with tugger lines with different stiffness values. . . . 61

5-1 Vessel and crane configurations for parametric and workability analysis. The cable length of the cranes and load masses change in the parametric analysis. . . . 68

Acknowledgements

This thesis is the final work of my master to obtain a masters degree in Offshore & Dredging Engineering at the Delft University of Technology. The research is commissioned by Jumbo Maritime. The work has been executed under approval of the graduation committee.
First I want to thank the company Jumbo Maritime for creating the opportunity and thesis subject of the graduation. I want to thank my company supervisor Kasper van der Heiden for his help and guidance during the project. Also in times of personal health problems, you gave me the time to recover and to work at my own pace. I think you should be proud for creating such a working environment.
I received lots of help from both the chairman of the graduation committee Andrei Metrikine and university supervisor Oriol Colomés. Thank you Andrei for all your feedback during the progress meetings. For all the knowledge and questions you shared, which pushed me to work at my best level. Thank you Oriol for your help. Our meetings gave me the assurance to continue the work. A lot of the choices and solutions made in this thesis were discussed during the meetings. You always gave me new perspectives on the to be taken approach. I could not do it without you.

For me personally, this graduation means that life as a student is over. During these years, I did not only learn some engineering skills and knowledge. I also have learned a lot about life itself, about who I am and what I want to be. I have experienced that life does not always move in the direction that I wanted. Nevertheless, I am proud and grateful to graduate. For sure, I could not achieve this without the people around me.
First I would like to thank my family, especially my parents. Thank you for your support, for your help and for your confidence. At some points in life, I have the feeling that you even know me better than I do. Your guidance and lessons helped me to be the person who I am today.
Finally, I would also thank my room-mates for their support. In those seven years, I have enjoyed our friendship. There always has been room for a good talk, both about our personal life or study related topics. We have had amazing times and I am sure that our story will continue.

Delft, University of Technology — Niels van Duijn
October 20, 2020

Chapter 1

Introduction

The offshore heavy lift market is always looking for innovative solutions to face the challenges in their discipline. Immense structures need to be (de-)installed in a harsh offshore environment. Examples of these structures are jackets, topsides and sub-sea equipment. The weight of these structures can vary up to 110,000 tons. To perform a safe installation all kind of installation methods are developed. A example of installation vessels are semi-submersible heavy-lift ships. These vessels use their draft to install the structure at its right position. Examples of these semi-submersibles are the BOKA Vanguard and the Pioneering Spirit. The Vanguard can float from under a floating structure to install it at an offshore location. The Pioneering Spirit has a catamaran shape to be able to install or decommission topsides attached to a jacket structure. A very different kind of installation method is to use crane vessels. Crane vessels have the advantage to be able to install a large range of structures at different heights or water depths. The heavy lift crane vessels vary in dimensions and positioning systems depending on which main speciality they are build for. Semi-submersible crane vessels like the Sleipnir and Thialf are capable to install large topsides up to 20,000 tons. Next to these semi-subs, there are jack-up crane vessels which maintain their position during installation by fixing the legs to the sea-bed. These jack-up crane vessels are nowadays frequently used in the build up of an offshore wind park. Another method to maintain the position of the installation vessels is the use of a Dynamic Positioning (DP) system. This system uses thrusters to control the vessel position and to execute a safe installation. This allows all kind of vessels to perform a heavy lift without being connected to the sea floor.

An increase in the lifting capacity of the vessels opens new possibilities in the offshore market. Therefore, companies are always trying to improve and find new ways to improve their offshore capabilities. On October 22, 2018 Heerema Marine Contractors successfully tested the QUAD lifting method. The test involved two dynamically positioned semi-submersible vessels, the Thialf and the Balder. In a QUAD Lift two vessels use both their cranes to perform a lift. This method of lifting creates several advantages and opportunities compared to a single vessel lift[12]:

- Fully-integrated topside installation for lower overall project costs

- Onshore commissioning for all hookup items for predictable offshore delivery
- Design freedom in all lifted structure dimensions, weights and Center of Gravity (CoG) positions
- Compatibility with any type of foundation
- Fabrication flexibility to optimize procurement strategy
- Transportation possibilities aligned with fabrication scope

1-1 About Jumbo Maritime

Jumbo Maritime is a company specialized in shipping and installation of heavy lift equipment. The company owns and operates a versatile fleet of in-house designed heavy lift vessels with lifting capacities ranging from 650 to 3,000 tons. Since 2003, Jumbo rapidly established a sound track record in the offshore sub-sea and mooring system installation market.

1-1-1 Jumbo J-Class vessels

The J-class vessels dedicated for offshore operations are the Construction Support Vessels (CSVs) Jumbo Fairplayer and Jumbo Javelin. The vessels are both equipped with two mast cranes, manufactured by Huisman, with a safe working load of 900 tons each. The dual cranes provide tandem heavy lift capacity, dual crane upending capability as well as deep-water lowering capability. The vessels are specialized in a high transit speed and a large cargo capacity. Both vessels are equipped with a Dynamic Positioning (DP) class 2 station keeping system to perform reliable offshore transportation and installation.

Figure 1-1: Fairplayer Rotterdam.

Jumbo J-Class QUAD Lift

The execution of a QUAD lift by the vessels of Jumbo Maritime will give the company the possible opportunity to increase their offshore lift capacity. Next to this increase in lift

capacity, the QUAD lift enables the vessels to install pieces of larger dimensions. The crane range will not be a limited factor for the structure dimensions any more.

1-2 Simple example of a possible QUAD Lift installation

The QUAD Lift method could be used in both installation and decommissioning projects. In this section, a simple example of the different phases of a possible offshore QUAD Lift installation are given.
The first phase is the transport of the installation piece to the decided offshore location. This transport could be done by one of the Heavy Lift Crane Vessels (HLCV's) or by the use of a barge. The advantage of the transport by an external transport vessel is that the HLCV's can directly perform the QUAD Lift at the correct location. When the barge floats to the correct location, the cranes can be attached to the to be lifted structure, in this example a sub-sea installation piece.

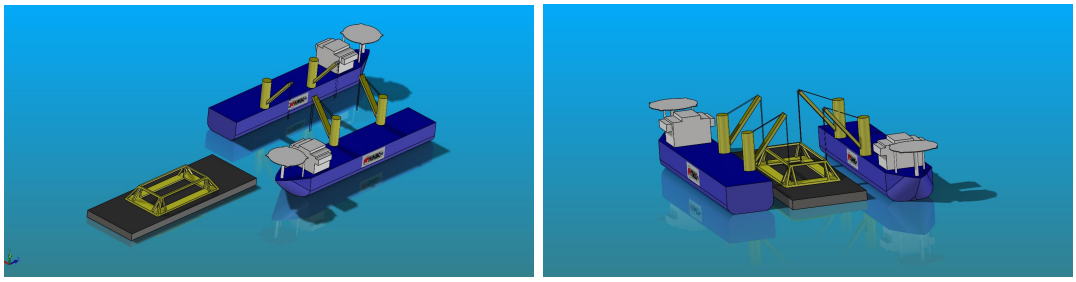

(a) Installation phase 1. **(b)** Installation phase 2.

Figure 1-2: First 2 phases of installation. The barge and HLCV's are floated to the correct location.(phase 1) The crane cables are attached to the installation piece.(phase 2)

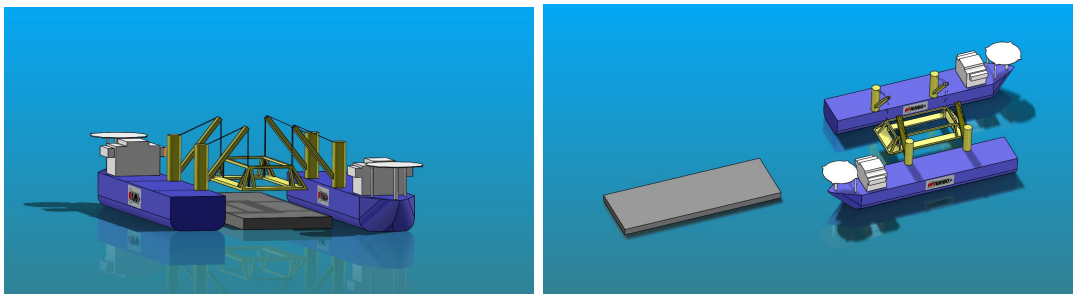

(a) Installation phase 3. **(b)** Installation phase 4.

Figure 1-3: Phase 3 and 4 installation. The structure is lifted in the air (phase 3) and the barge is moved from underneath. (phase 4)

After the attachment of the cables to the transition piece, the sub-sea structure can be detached from the barge and be lifted up by the cranes. Possible tugger lines can be attached to prevent large motions of the structure to perform a safe installation. When the sub-sea structure is in the air, the vessels or barge could float such that the barge is moved from

underneath the lifted structure. Then, the installation piece can be lowered into the sea and be placed at the correct location on the sea-bottom.

1-3 Problem Statement

The analysis of an offshore QUAD lift is associated with the following three research problems:

1. In an offshore environment, waves will influence the motions of the vessels. In case of the presence of a vessel close to another one, the vessel motion will be different in case of a freely floating vessel. Not only the waves could be captured by the front laying vessel, also the motions of both vessel have an influence on each other. In other words, the vessel motions are hydro-dynamically coupled to each other.

2. When two structures are close together in open waves, waves in between these structure could have a resonance behaviour which could lead to the increase of the wave height. This will have an influence on the motion of the vessel as well.

3. The moment when the vessels start to lift a structure, the vessel motions will not only be hydro-dynamically coupled but also coupled via the cranes and the load. This coupling will influence the motion behaviour of the vessels and load.

4. The coupling leads to new and change of natural frequencies in the system. Natural frequencies are also influenced by the addition of tugger lines. The natural frequencies will influence the motion behaviour in the waves of both the vessels and the load.

1-3-1 Thesis Objectives

These problem statements lead to a different set of research objectives. The motion behaviour of a single vessel executing a lift is already a topic of research in the company. The interaction of vessels is however not, therefore this thesis contains the following objectives:

- Perform a study on the effects of interacting vessels based on the Jumbo J-type vessels. Analyse different interaction phenomenons and compare the data with the literature.
- Create a model which analyses the dynamic behaviour of the J-type vessels performing a QUAD Lift.
- Analyse the effects of motion control of the load by the addition of tugger lines. Analyse the effects of different type of tugger lines in terms of material and stiffness's.
- Perform a study on the motion effects of different lift parameters. Examples are cable length, the weight of the load and crane configurations.
- Perform a workability analysis of the QUAD lift at an offshore location. This will give an indication for the company potential of the execution of the QUAD Lift.

1-4 Scope

Since the QUAD Lift is a new possible lifting method to use in the company and to use with the Jumbo J-Class vessels, this thesis is just a simple starting point in the engineering development. This thesis will give an idea of possible problems regarding structure interaction and a combined vessel lift. A workability study is executed to indicate the possible utility of such a lift. This workability analysis is calculated for installation phase 4, shown in Figure 1-3. Effects on the vessel behavior like the moment of take up of the cargo, the interaction of the barge and the lift down through the splash zone are not a subject of analysis in this thesis.
This thesis will just focus on the linear behaviour of the vessels and load. The calculations are executed in the frequency domain. The effects of non-linear behaviour and time-control are neglected in this study.

1-5 Approach

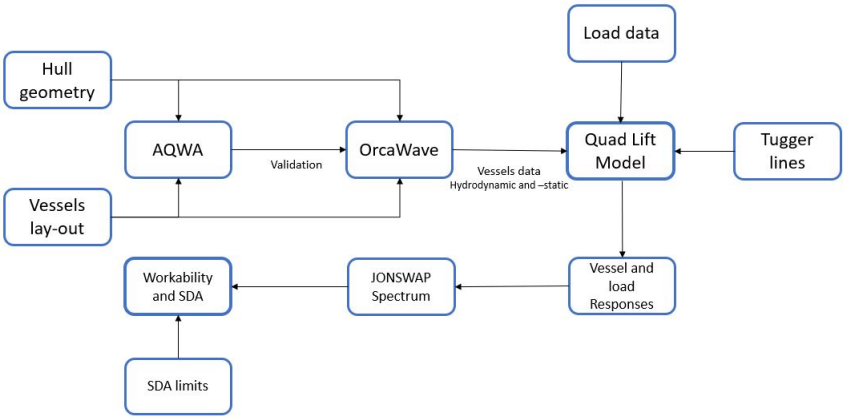

Figure 1-4: Overview of thesis approach.

The first step in the achievement of the thesis objectives is the analysis of effects on the motion behaviour of side-by-side laying vessels. The software packages ANSYS AQWA and OrcaWave are used to obtain the hydrodynamic parameters based on the geometry hull of the Fairplayer. Additionally several vessel interaction phenomena are analysed and the diffraction analysis is adjusted such that it shows identical output compared to the literature.

The next step is the addition of the coupling model of the vessels and the QUAD lift load system. A 18 Degrees of Freedom model (12 DoF of the two vessels and 6 DoF of the load) of the Quad Lift is modelled in MATLAB. The equations of motion with the new mass and stiffness matrix are obtained by use of the software program Maple.
To control the load motions, tugger lines are added to the Quad Lift model. These tugger lines are represented by linear springs.
The final step is a parametric study on the different QUAD lift scenarios including different

crane outreaches, sea conditions and loads. The limiting sea state will be evaluated for the each scenario. Based on the maximum allowable limiting responses during an offshore lift of the vessels and the cranes, the workability is calculated. The limiting responses (Significant Double Amplitude (SDA)) for the QUAD Lift are defined as follows:

- Vessel Roll angle: 1.5 deg
- Vessel Pitch angle: 1.5 deg
- Vessel Roll+ Pitch angles: 2.5 deg
- Crane Off-lead angle 1 deg
- Crane Side-Lead angle 2 deg

1-6 Report overview

This thesis has the following layout:

1. **Chapter 1: Introduction**
   In this chapter, the QUAD lift method is explained as well as the interest of the company for the thesis subject. The problem statements, objectives and the approach are given.
2. **Chapter 2: Waves**
   A short information section about wave theory and statistics are explained which are applied in the diffraction calculations explained in chapter 3 and the final workability calculation in chapter 4.
3. **Chapter 3: Motion of the vessels**
   This chapter elaborates on the method used to gather the hydrodynamic vessel data and to create the equation of motion of the two vessels. Different kind of vessel-vessel interaction phenomenons are discussed.
4. **Chapter 4: QUAD Lift Model**
   This chapter explains the method to connect the vessels to the load and to create the final QUAD lift model. The effects of the addition of tugger lines are analysed.
5. **Chapter 5: Results: Parametric study and Workability**
   This chapter shows the effects on the system motion of the change of different parameters in the QUAD lift model. Also the workability is calculated for different sea directions and QUAD lift configurations.
6. **Chapter 6: Conclusion and Recommendations**
   The results of the thesis are presented and discussed. Recommendations for further work are given.

Chapter 2

Waves

2-1 Introduction

This chapter will introduce all the theory about ocean waves. The waves that are normally of interest during offshore operation are the waves generated by the vessel motions and the waves generated by wind. Wind generated waves can be classified into two categories: sea and swell. Sea is a train of waves driven by a local wind field. The waves have a very irregular behaviour, high waves are followed by low waves and the crests propagate in different directions. A swell is is a series of waves that have propagated out of the local wind area at which they were generated. The waves have a long length and the wave height is more predictable.

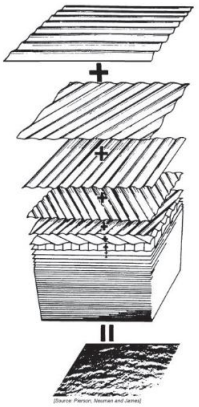

Figure 2-1: Superposition of wave trains with equal height, frequency, direction and length.

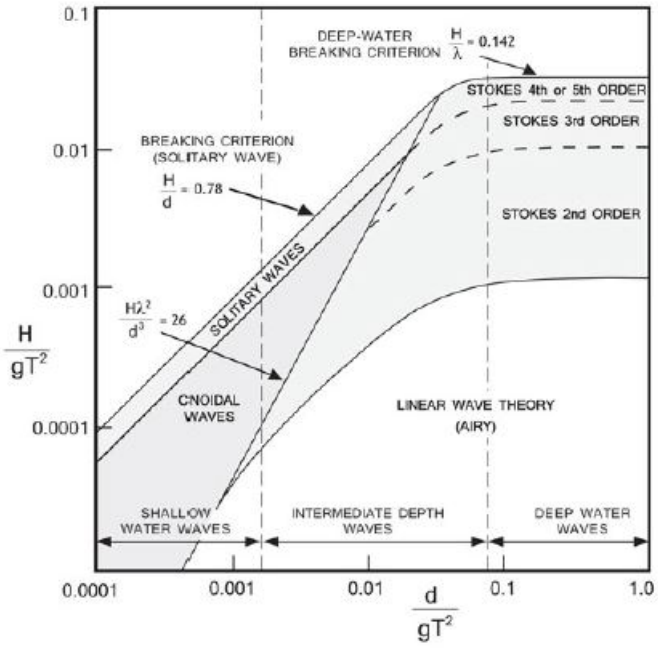

Figure 2-2: Different wave theories.

2-2 Airy Wave Theory

The irregular sea can be seen as a superposition of many regular harmonic waves, each with its own amplitude, frequency, length and direction. This allows to predict very complex irregular behaviour in terms of much simpler theory of regular waves. The superposition of the waves is shown in Figure 2-1.

There are different models to describe the waves. An overview of the different models are shown in Figure 2-2. The legitimation of using a theory depends on the steepness of the wave and the relative water depth. Most offshore operations are executed in calm water with a small periods of waves, compared to the water depth. Therefore, linear wave theory is applicable.

The water profile of a linear regular wave moving in x-direction can be described by:

$$\zeta = \zeta_a \cos(kx - \omega t) \tag{2-1}$$

In which k is the wave number and ω is the frequency of the wave. The frequency is related to the wave number and water depth h via the dispersion relation:

$$\omega^2 = kg \tanh(kh) \tag{2-2}$$

Based on the superposition principle the irregular wave elevation over time is described as:

$$\zeta(t) = \sum_{n=1}^{N} \zeta_{a_n} \cos(k_n x - \omega_n t + \epsilon_n) \tag{2-3}$$

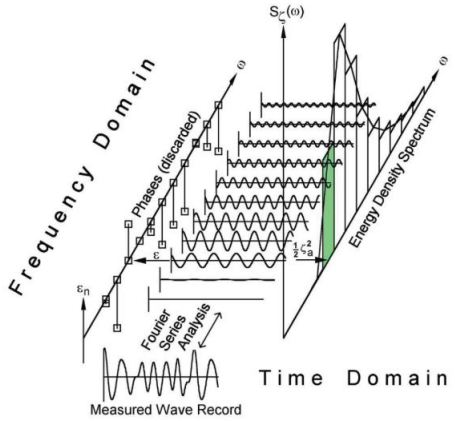

Figure 2-3: Wave record analysis

In which N is the number of different regular wave trains and ϵ is the random phase angle of the each wave train.

2-2-1 Energy Density Spectra

The wave energy of a regular wave per surface area is given by:

$$E = \frac{1}{2}\rho g \zeta_a^2 \tag{2-4}$$

All the regular waves contain their own energy. Each regular wave with its own frequency and amplitude covers a certain region on a energy density spectrum. In a mathematical way the wave spectrum of the regular waves can be expressed as:

$$S_\zeta(\omega_n) \cdot \Delta\omega = \sum_{\omega_n}^{\omega_n+\Delta\omega} \frac{1}{2}\zeta_{a_n}^2(\omega) \tag{2-5}$$

if the frequency step $\Delta\omega$ tends to zero, the definition of the wave energy spectrum becomes:

$$S_\zeta(\omega_n) \cdot d\omega = \frac{1}{2}\zeta_{a_n}^2 \tag{2-6}$$

A graphical interpretation of the wave energy spectrum is shown in Figure 2-3. The phases of the waves are not incorporated in the energy density spectrum and are thrown away. The spectra can be created by measurement at a certain location at the worlds oceans. Two very popular wave density spectra are the Brentschneider and Joint North Sea Wave Project (JONSWAP) spectra. The Brentschneier or Pearson-Moskowitz spectra contains the information of the wave energy of fully developed seas. The JONSWAP spectrum, which is a adjusted variant of the Pearson-Moskowitz spectrum, contains the information about fetch-limited wind generated seas and is based on measurements in the North-Sea. Both spectra are shown in Figure 2-4. The formulation for the JONSWAP spectrum is given as:

$$S_\zeta(\omega) = \frac{320 \cdot H_{1/3}^2}{T_p^4} \cdot \omega^{-5} \cdot \exp\left\{\frac{-1950}{T_p^4} \cdot \omega^{-4}\right\} \cdot \gamma^A \tag{2-7}$$

in which:

- $H_{1/3}$ is the significant wave height. The average of the highest one-third of the wave heights in a wave-record.
- T_p is the peak period. The period with the highest spectral energy.
- γ^A is the peak enhancement factor. In this study γ is equal to 3.3.
- $A = \exp\left\{\left(\frac{-\frac{\omega}{\omega_p} - 1}{\sigma\sqrt{2}}\right)^2\right\}$

Equation (2-7) covers only the information for uni-directional waves, the waves are coming from one direction. A frequency spectrum alone is not sufficient for describing natural ocean waves since the individual components propagate in various directions. To include wave directionality in a spectrum, directional wave components are superimposed to show the wave energy distribution with respect to both frequency and direction [33]. The equation of a two-dimensional spectrum can be expressed by a spreading function:

$$S_\zeta(\theta, \mu) = D(\theta) S_\zeta(\omega) \tag{2-8}$$

in which $D(\theta)$ is the directional spread function. A cosine-fourth rule is often used to introduce directional spreading μ to the wave energy spectrum. [31] The total energy density in the two-directional spectrum must be the same as the corresponding one dimensional spectrum, so the integral of the spread functions over all the directions has to equal one. This requirement can be accomplished by use of the gamma function:

$$D(\theta) = \left(\frac{2^{2s-1}}{\pi}\right)\left(\frac{\Gamma^2(s+1)}{\Gamma(2s+1)}\right) cos^{2s}\left(\theta - \bar{\theta}\right) \tag{2-9}$$

The gamma function is defined as:

$$\Gamma(s+1) = s! \tag{2-10}$$

s is chosen to be four. The dominant wave direction is indicated as $\bar{\theta}$. A multi-directional JONSWAP for a dominant wave direction $\bar{\theta}$ of 0 degrees is shown in Figure 2-5.

2-3 Response spectra

The response spectrum of a vessel motion can be found by the transfer function of the motion and the wave spectrum:

$$S_r(\omega, \theta) = |H_r|^2 \cdot S_\zeta(\omega, \theta) \tag{2-11}$$

The significant double amplitude (SDA) of the response, the mean value of the highest one-third part of the highest response amplitudes are given by:

$$H_{r,1/3} = 4\sqrt{m_{0r}} \tag{2-12}$$

in which the moments of the response spectrum m_{nr} can be calculated by:

$$m_{nr} = \int_0^{2\pi}\int_0^{\infty} \omega^n S_r(\omega, \theta) d\omega d\theta \tag{2-13}$$

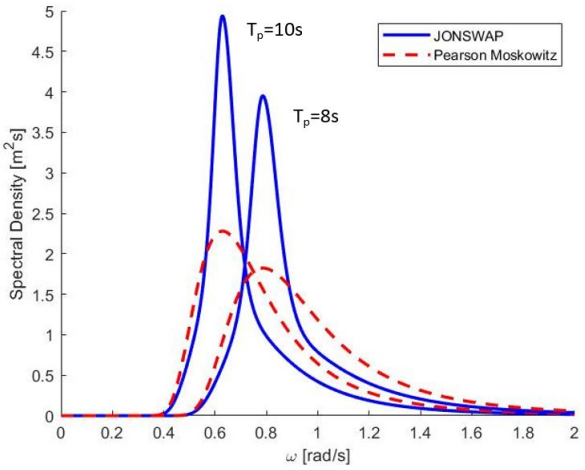

Figure 2-4: JONSWAP and Pearson-Moskowitz spectra for different peak periods. The significant wave height is 4 m.

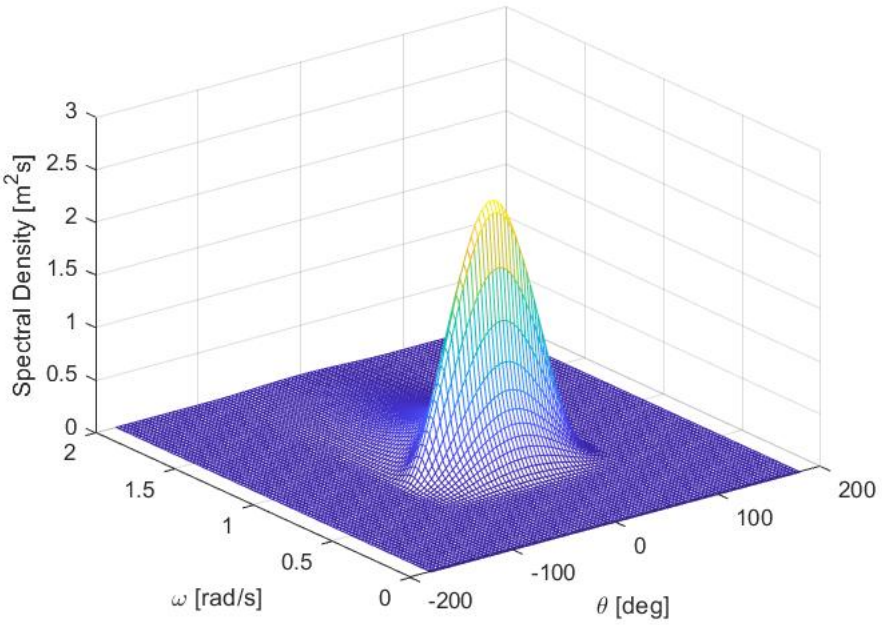

Figure 2-5: Multi-directional JONSWAP for a peak period of 8 s. The significant wave height is 4 m. The dominant wave direction is 0 degrees.

2-3-1 Statistics

The probability density function with the maximum and minimum values of the response follows a Rayleigh distribution:

$$f\left(H_r\right) = \frac{H_r}{m_{0r}} \cdot \exp\left\{\frac{-H_r^2}{2m_{0r}}\right\} \tag{2-14}$$

The probability that the response exceeds a certain threshold value a is given by:

$$P\left(H_r > a\right) = \exp\left\{\frac{-a^2}{2m_{0r}}\right\} \tag{2-15}$$

The average number of times per hour that this will happen is given by:

$$N_{hr} = \frac{3600}{T_{2r}} \cdot P\left(H_r > a\right) \tag{2-16}$$

in which T_{2r} is the mean zero crossing period. The mean zero crossing period is given by:

$$T_{2r} = 2\pi\sqrt{\frac{m_{0r}}{m_{2r}}} \tag{2-17}$$

Given that the wave amplitudes are Rayleigh distributed the Most Probable Maximum (MPM) can be calculated by:

$$\zeta_{mpm} = \sqrt{2m_{0r}\ln\left(N\right)} \tag{2-18}$$

in which N is the number of oscillations in a given timespan. The duration is usually taken as three hours, the approximate timespan in which a sea state is assumed to be constant. N can be calculated by dividing the timespan by the mean zero crossing period of the motion. The most probable maximum can be calculated to give an indication of the performance of the concept.

Chapter 3

Motion of the vessels

3-1 Introduction

This chapter explains the method used to model the response of two vessel at an offshore location. The hydrodynamic data is obtained by a diffraction calculation of two software programs AQWA and OrcaWave. Multiple numerical and potential theory aspects, such as irregular frequencies and standing waves are explained.

3-2 QUAD lift vessel lay-out

The position of the vessels is for importance to perform a sufficient QUAD Lift. The cranes of both vessels need to be at the lifting side. Since two identical vessels are used, the vessels have a 180 degrees different surge direction. A second requirement is that the lifted object need to be in the range of the four vessel cranes. The QUAD lift analysis will be done, such that the cranes do not have a rotation. Given the fact that the crane position of the vessels are not in an amidships symmetry position, it means that the vessels are shifted in the surge direction relative to each other. The vessel lay-out can be seen in Figure 3-1.

3-3 Diffraction calculation

To obtain the vessel hydrodynamic coefficients and interaction forces the numerical program ANSYS AQWA and OrcaWave are used. ANSYS AQWA is a three dimensional panel method software to perform radiation and diffraction analysis of floating bodies. AQWA uses a graphical user interface in which bodies geometries can be imported and meshed so that a diffraction analysis can be executed.
OrcaWave is a diffraction analysis program in the environment of Orcina. This software package is used in-house at Jumbo Maritime and is used afters problems with the interpretation

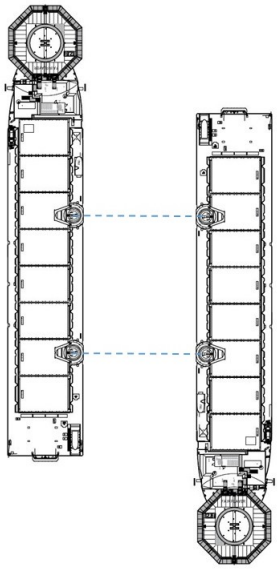

Figure 3-1: Quad lift vessel lay-out. The position of the vessels is such that the cranes are parallel to each other.

of the hydrodynamic data of AQWA. It was not possible to recreate the responses of the vessels based on the hydrodynamic coupled data. For an uncoupled single vessel diffraction calculation, this was not a problem. An advantage of the use of both programs is that the hydrodynamic results can be compared and validated. Since hydrodynamic interaction and potential diffraction programs is still a subject of research, both programs can be used to create a valid analysis of the calculation.

The radiation and diffraction analysis meets the following limitations of potential theory and assumptions:

- The bodies have zero forward speed.
- The fluid is inviscid and incompressible. The fluid flow is irrotational.
- The incident regular wave train is of small amplitude compared to its length: $2\zeta < \frac{1}{7}\lambda$
- The motions are to the first order and hence must be of small amplitude. All body motions are harmonic.

3-3-1 Vessel Geometry

The hull geometry of the Fairplayer Rotterdam is delivered by Jumbo Maritime. However, the hull model was only suited to create 3D views, not to use in a panel method software. In between the different faces of the vessel hull there were small gaps. The vessel hull is therefore adjusted by both software programs Rhineceros and Spaiceclaim. Next to the stitching of the hull, the rudder and thrusters of the vessel were deleted cause they were not suited to include in the analysis in AQWA. Both vessel hulls are shown in Figure 3-4.

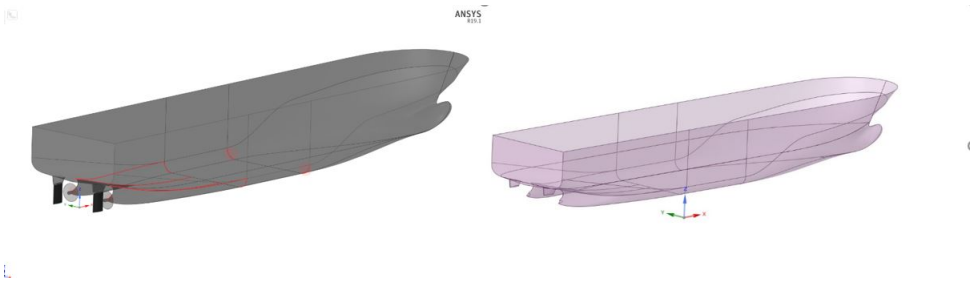

Figure 3-2: Fairplayer hull geometry. The left figure shows the original Fairplayer hull, including rudder and thrusters. The figure on the right shows the adjusted hull geometry suited for the AQWA diffraction analysis.

3-3-2 Mesh

To perform the diffraction analysis the 3D model can be meshed in AQWA. Onto each meshed panel the potential theory and boundary conditions are applied. A large mesh size increases calculation time. The mesh size has an influence on the accuracy of the hydrodynamic data generated by AQWA. In Figure 3-3 the added mass and damping coefficients for different meshes of the Fairplayer are shown. The effect of the given meshes on the hydrodynamic data are small. Next to the influence on the potential theory data the mesh is also linked to

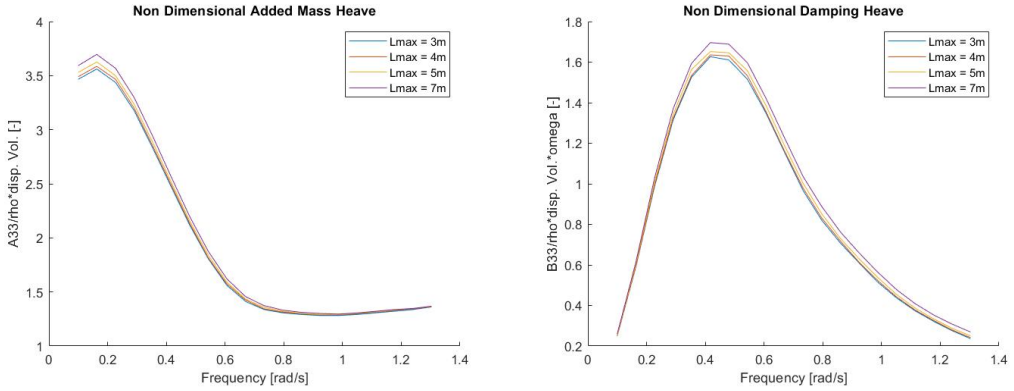

(a) Non-dimensional added mass for heave of Fairplayer for different meshes vs frequency.

(b) Non-dimensional damping for heave of Fairplayer for different meshes vs frequency.

Figure 3-3: Comparison hydrodynamic data for different meshes Fairplayer.

the range of frequencies in AQWA. A requirement in AQWA for the maximum panel length is:

$$L_{max} \leq \frac{1}{7}\lambda \tag{3-1}$$

In the dispersion relation, the wavelength λ is linked to the wave frequency. Therefore, a large mesh size decreases the maximum applicable frequency in the diffraction analysis. The maximum number of frequencies for which in AQWA a diffraction analysis can be performed is restricted to 100. The frequency bounds are 0.1 rad/s (lower limit) and 2 rad/s.(upper limit)

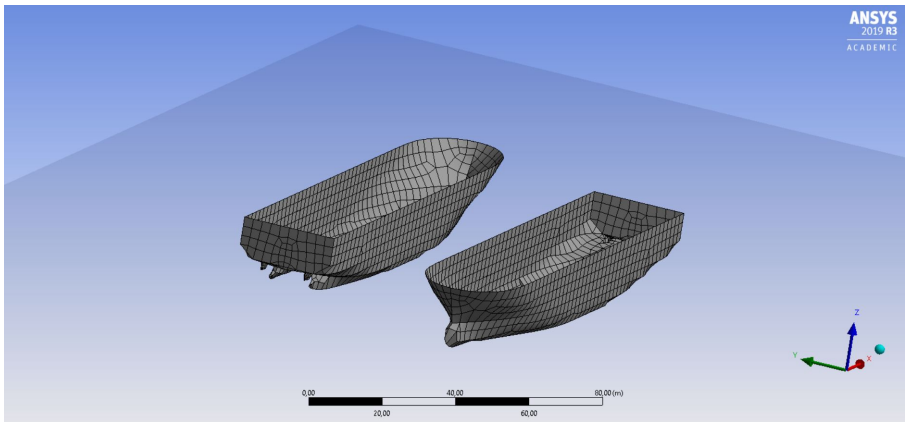

Figure 3-4: Meshed vessels side-by-side in ANSYS AQWA with a gap distane of 30m

3-3-3 Irregular Frequencies

By the use of a boundary integral formulation as it is done in the diffraction analysis can cause numerical errors in the solution of the hydrodynamic coefficients due to the occurrence of irregular frequencies. These irregular frequencies relate to the eigenvalue problem of the imaginary interior fluid motion inside the body with the same free surface condition as the external fluid surrounding the body [17]. Especially in the case of multi-hull structures or hydrodynamic interaction between structures irregular frequencies can occur [3]. To prevent the errors AQWA the internal lid method is employed for the source distribution approach. In this method, it is assumed that a fluid field exists interior to the mean wetted body surface, satisfying the same free-surface boundary condition experienced by the floating body. The vertical component of this interior fluid velocity is forced to be zero.
The effect of the damping lid on the hydrodynamic data of the Fairplayer can be seen in Figure 3-5. The irregular frequencies become visible at the higher values of the frequency. Small peaks in the data occur and are for certain frequencies removed by the internal lid. However, the calculation with an internal lid also increases the values of some peaks.
In OrcaWave, also an interior surface can be added to remove the numerical errors. However, the small peaks in the hydrodynamic data could not be removed by the application of the interior lid. Therefore, AQWA seems to have a more effective method to remove the irregular frequencies.

3-4 Vessel motions

In a three dimensional system the body motion has six degrees of freedom. These six degrees of freedom contain three translations and three rotations:

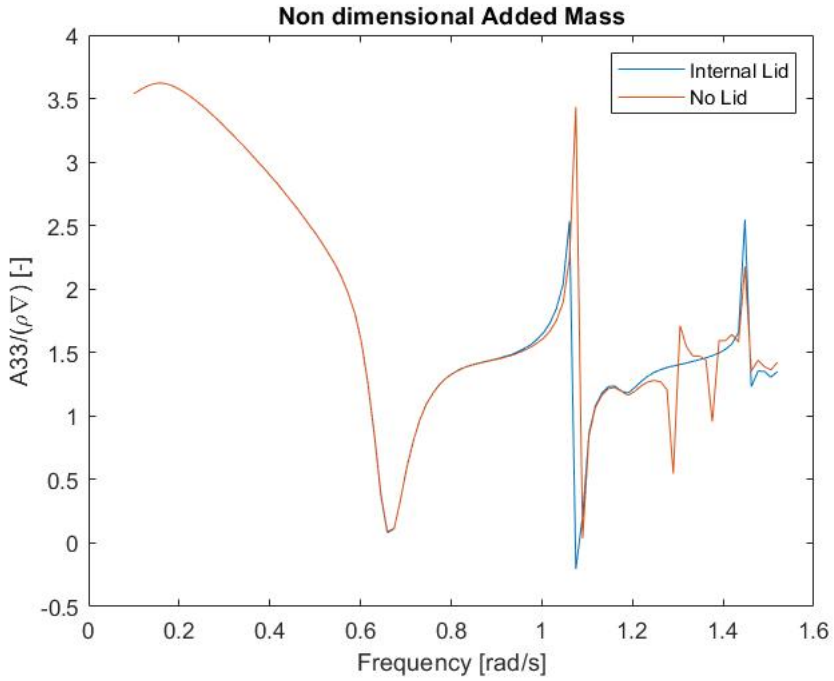

Figure 3-5: Effect of internal lid on added mass for heave of side-by-side laying Fairplayer with gap distance of 30m.

- x - surge - translation along X axis
- y - sway - translation along Y axis
- z - heave - translation along Z axis
- ϕ - roll - rotation around X axis
- θ - pitch - rotation along Y axis
- ψ - yaw - rotation along Z axis

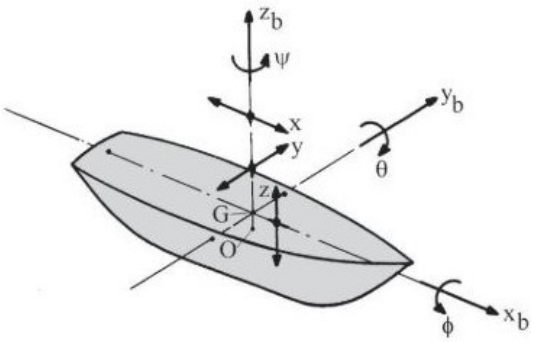

Degrees of freedom of a vessel.

The definition of different headings of the vessels are shown in Figure 3-6. Waves travelling in surge directions are typically known as head waves. Waves travelling in sway direction of the vessel are known as beam waves. The waves in between these directions are indicated as quarter waves.(45 and 135 deg) Since the body lay-out is symmetric, the diffraction calculation needs only be done for the five wave directions shown in Figure 3-6 to create a full 360 degree result. E.g. the response of the second body in beam waves (90 degrees) is the same as to motion of the first body when the waves are from the opposite side. (-90 degrees) This symmetry reduces the calculation time to obtain the hydrodynamic data.

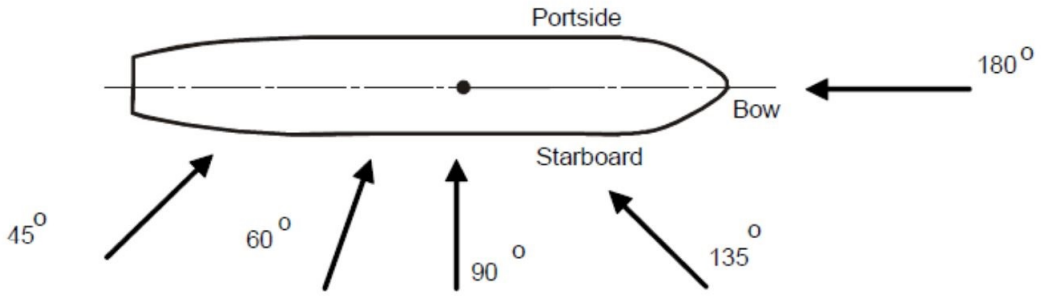

Figure 3-6: Vessel heading conventions

3-4-1 Superposition of motion

If we assume a linear motion model it is allowed to make use of the superposition principle. In the superposition principle the loads of the waves on a fixed body and the loads on the body by the oscillation of the body are calculated separately and added up to define the whole motion system. The equation of motion of two interacting bodies is given by:

$$\mathbf{M}\ddot{\vec{x}} + \mathbf{B}\dot{\vec{x}} + \mathbf{C}\vec{x} = \vec{F} \tag{3-2}$$

in which $\mathbf{M}$ is the system mass matrix, containing the vessel mass and inertia terms as well as the hydrodynamic added mass of the vessels. $\mathbf{B}$ is the radiation damping matrix and $\mathbf{C}$ is the hydrostatic stiffness matrix. The vector $\vec{F}$ is the force vector which contains the Froude-Krylov force due to the pressure on the hull of the incoming waves and the diffraction force due to the disturbing of the wave by the body. For a model of two bodies the number of degrees of freedom is equal to 12. In matrix form the equation of motion is written as:

$$\begin{bmatrix} M_{1,1} & M_{1,2} & \cdots & M_{1,12} \\ M_{2,1} & M_{2,2} & \cdots & M_{2,12} \\ \vdots & \vdots & \ddots & \vdots \\ M_{12,1} & M_{12,2} & \cdots & M_{12,12} \end{bmatrix} \begin{bmatrix} \ddot{X}_1 \\ \ddot{X}_2 \\ \vdots \\ \ddot{X}_{12} \end{bmatrix} + \begin{bmatrix} B_{1,1} & B_{1,2} & \cdots & B_{1,12} \\ B_{2,1} & B_{2,2} & \cdots & B_{2,12} \\ \vdots & \vdots & \ddots & \vdots \\ B_{12,1} & B_{12,2} & \cdots & B_{12,12} \end{bmatrix} \begin{bmatrix} \dot{X}_1 \\ \dot{X}_2 \\ \vdots \\ \dot{X}_{12} \end{bmatrix}$$

$$+ \begin{bmatrix} C_{1,1} & C_{1,2} & \cdots & C_{1,12} \\ C_{2,1} & C_{2,2} & \cdots & C_{2,12} \\ \vdots & \vdots & \ddots & \vdots \\ C_{12,1} & C_{12,2} & \cdots & C_{12,12} \end{bmatrix} \begin{bmatrix} X_1 \\ X_2 \\ \vdots \\ X_{12} \end{bmatrix} = \begin{bmatrix} F_1 \\ F_2 \\ \vdots \\ F_{12} \end{bmatrix} \tag{3-3}$$

The added mass and damping terms vary over the frequency of the waves. The force coefficients are complex because of the fact that the force depends on the phase with respect to the incoming wave. The complex force terms vary over the frequency and the direction of the

incoming regular wave. Therefore, also the responses of the body vary over the frequency and the angle of the incoming wave. The different coefficients given in eq. (3-3) for a two body system ($i, j = 1..12$) and their dependencies are given below:

- $M_{i,j} = m_{i,j} + a_{i,j}(\omega)$ The mass and inertia terms $m_{i,j}$ and the frequency dependent added mass $a_{i,j}(\omega)$.
- $B_{i,j} = b_{i,j}(\omega)$ The frequency dependent damping of the radiation of the waves.
- $C_{i,j} = c_{i,j}$ The hydrostatic stiffness of the vessel.
- $F_i = f_i(\omega, \theta)$ The excitation forces on the vessel as a function of the frequency and the incoming wave angle θ.
- $X_i = x_i(\omega, \theta)$ The responses of the vessels as a function of the frequency and the incoming wave angle θ.

Given that the hydrodynamic coefficients depend on the frequency and the hydrodynamic forces on frequency and incoming wave angle, it means that the equation of motion has a unique solution for every single frequency and angle.

3-4-2 Matrices and Coupling Terms

The matrices can be divided into four quadrants. Each quadrant contains a six by six matrix, the number of degrees of freedom of a single body. The four quadrants of the matix are shown in eq. (3-4). The first quadrant contains the coefficients of the first vessel. The second quadrant contains the coupling terms of the second vessel acting on the first vessel. The third quadrant contains the coupling terms of the first vessel acting on the second vessel. When the vessels are floating close to each other there is only coupling between the vessels in the added mass and damping terms. The mass and stiffness matrix have no coupling so their second and third quadrant contain only zeros. The fourth quadrant contains the coefficients of the second vessel.

$$\left(\begin{array}{c|c} 1 & 2 \\ \hline 3 & 4 \end{array}\right) \rightarrow \left(\begin{array}{c|c} \begin{bmatrix} a_{1,1} & a_{1,2} & \cdots & a_{1,6} \\ a_{2,1} & a_{2,2} & \cdots & a_{2,6} \\ \vdots & \vdots & \ddots & \vdots \\ a_{6,1} & a_{6,2} & \cdots & a_{6,6} \end{bmatrix} & \begin{bmatrix} a_{1,7} & a_{1,8} & \cdots & a_{1,12} \\ a_{2,7} & a_{2,8} & \cdots & a_{2,12} \\ \vdots & \vdots & \ddots & \vdots \\ a_{6,7} & a_{6,8} & \cdots & a_{6,12} \end{bmatrix} \\ \hline \begin{bmatrix} a_{7,1} & a_{7,2} & \cdots & a_{7,6} \\ a_{8,1} & a_{8,2} & \cdots & a_{8,6} \\ \vdots & \vdots & \ddots & \vdots \\ a_{12,1} & a_{12,2} & \cdots & a_{12,6} \end{bmatrix} & \begin{bmatrix} a_{7,7} & a_{7,8} & \cdots & a_{7,12} \\ a_{8,7} & a_{8,8} & \cdots & a_{8,12} \\ \vdots & \vdots & \ddots & \vdots \\ a_{12,7} & a_{12,8} & \cdots & a_{12,12} \end{bmatrix} \end{array}\right) \tag{3-4}$$

3-5 Response Amplitude Operator (RAO)

The RAO is the linear transfer function between the vessel motion and the wave amplitude. The equation of motion for a vessel is:

$$(\mathbf{M} + \mathbf{A})\,\ddot{\vec{x}} + \mathbf{B}\dot{\vec{x}} + \mathbf{C}\vec{x} = \vec{F} \tag{3-5}$$

The motion vector $\vec{x}$ can be further defined, given that all the body motions are harmonic:

$$\begin{aligned} \vec{x} &= \vec{X}e^{-i\omega t} \\ \dot{\vec{x}} &= -i\omega\vec{X}e^{-i\omega t} \\ \ddot{\vec{x}} &= -\omega^2\vec{X}e^{-i\omega t} \end{aligned} \tag{3-6}$$

The forces are also harmonic over time including a phase difference between the wave and the body motion ϵ_ζ.

$$\vec{F} = \vec{f_a}e^{-i(\omega t+\epsilon_\zeta)} = \vec{F}_a e^{-i\omega t} \tag{3-7}$$

The time dependent motion and force terms, eqs. (3-6) to (3-7), can be implemented into the equation of motion eq. (3-2). The time dependent terms can be wiped out of the equation. This will give an equation for the RAO of the 12 DoF($i = 1...12$):

$$RAO_i(\omega,\theta) = \frac{\vec{X}(\omega,\theta)}{\zeta} = \frac{\vec{F}_a(\omega,\theta)}{-\omega^2\left(\mathbf{M}+\mathbf{A}(\omega)\right) - i\omega\mathbf{B}(\omega)+\mathbf{C}} \tag{3-8}$$

in which:

- $\mathbf{M}$ is the [12x12] mass and inertia matrix.
- $\mathbf{A}(\omega)$ is the [12x12xN_ω] frequency dependent added mass matrix.
- $\mathbf{B}(\omega)$ is the [12x12xN_ω] frequency dependent damping matrix.
- $\mathbf{C}$ is the [12x12] hydrostatic stiffness matrix.
- $\vec{F_a}$ is the [12xN_ωxN_θ] frequency and wave angle dependent complex force vector.
- $\vec{X}$ is the [12xN_ωxN_θ] frequency and wave angle dependent complex response vector.

Note: N_ω and N_θ relate to the number of frequencies and the different incoming wave angles respectively.

3-5-1 Resonance waves

In the gap in between the vessels laying side by side, hydrodynamic resonance behaviour of the waves may occur. According to Molin (2001) the resonance behaviour can categorized in different type of sloshing modes [23]. The first mode is known as the piston mode, in which the water inside the gap heaves up and down more or less like a rigid body. The higher modes are categorized into the transversal sloshing mode and the longitudinal sloshing mode. For small gap widths the eigenfrequencies of the transverse sloshing are high. Transverse sloshing becomes only relevant if the gap widths are relative large [8]. The eigenfrequencies of the hydrodynamic resonances in the gap are approximated by:

$$\omega_n^2 = g\lambda_n\frac{1+J_{n0}\tanh\lambda_n h}{J_{n0}+\tanh\lambda_n h} \tag{3-9}$$

For the piston and longitudinal mode J_{n0} is given by:

$$J_{n0}(r) = \frac{2}{n\pi^2 r}\left(\int_0^1 \frac{r^2}{u^2\sqrt{u^2+r^2}}\left[1+2u+(u-1)\cos(n\pi u)-\frac{3}{n\pi}sin(n\pi u)\right]du \right. \\ \left. -\frac{1}{sin\theta_0}+1+2r\ln\frac{1+cos\theta_0}{1-cos\theta_0}\right) \tag{3-10}$$

in which:

- d is the width of the gap in [m]
- l is the length of the gap in [m]
- h is the draft of vessel in [m]
- g is the acceleration of gravity [ms^{-2}]
- $r = d/l$ [-]
- $\lambda_n = n\pi/l \quad$ [m^{-1}]
- $\theta_0 = tan^{-1}(1/r)$ [rad]

The natural frequencies for different transversal sloshing modes can be calculated by a simplified equation given by Lewandowski (2008) [22]:

$$\omega_n = \sqrt{\frac{\pi g n}{d}} \tag{3-11}$$

The frequencies of the sloshing modes correspond to the associated standing waves in the gap. The effects of the transversal sloshing modes can be seen in the radiation data of the vessels. At different standing wave modes, peaks occur in the radiation data. Figure 3-7 shows the vessel sway damping with respect to the gap distance divided by the wave length. The characteristic behaviour of the data is equal to gap size to wavelength ratios close to 0.5,1,..,2.5.

The wave resonance frequencies for different modes are shown in Table 3-1. Only the resonance frequencies inside the frequency spectrum bound are shown. The transversal resonance frequencies match the data peaks shown in Figure 3-7. The large set of longitudinal sloshing frequencies are not directly visible in the hydrodynamic data. Since very crude assumptions have been made in the approximation of the sloshing frequencies, the overview of the natural frequencies gives an idea on the variety of possible modes in the gap and on the complexity of the wave pattern [27]. Different wave patterns are shown in Figure 3-8. The figures indicate the longitudinal sloshing modes and the possibility of transverse sloshing for larger gap widths.

3-5-2 Overestimation resonance waves

A common problem in multi-structure diffraction analyses is the overestimation of the wave amplitude in between structures in waves. This overestimation is caused by the resonance behaviour of the waves in the gap described in the previous section. Pauw (2007) gave two

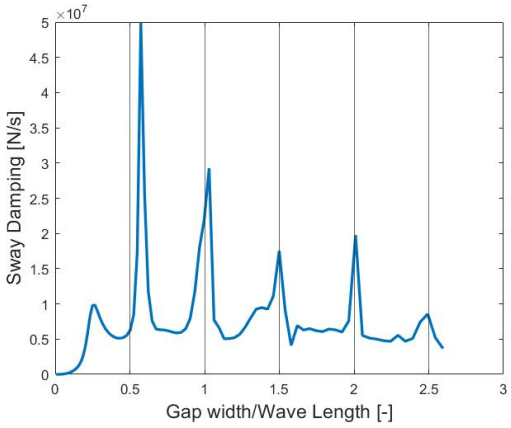

(a) Sway damping with respect to gap width/wave length ratio.

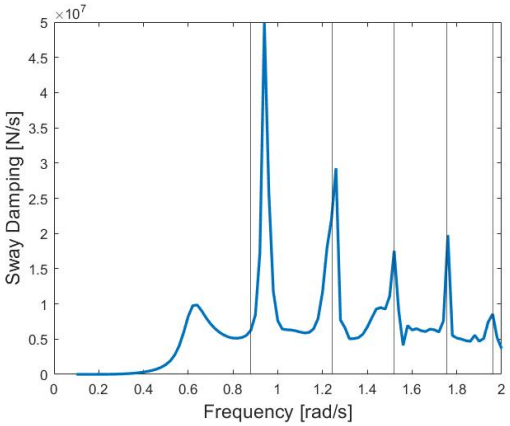

(b) Sway damping with respect to frequency.

Figure 3-7: Fairplayer sway radiation damping with characteristic resonance peaks.

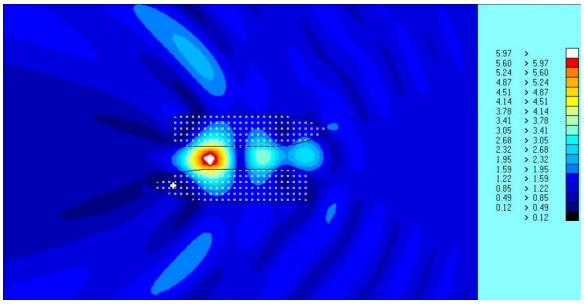

(a) Relative wave heigth for a gap width of 20 m for a frequency of 0.953 [rad/s].

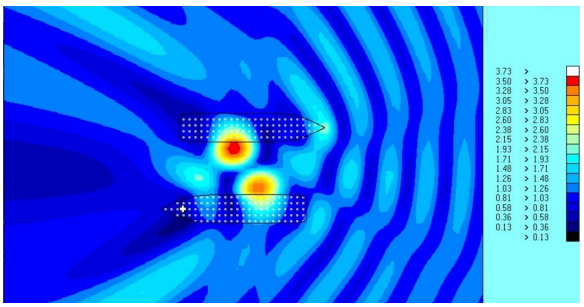

(b) Relative wave heigth for a gap width of 50 m for a frequency of 0.953 [rad/s].

Figure 3-8: Wave patterns of side laying vessels for incident head waves.

reasons for the overestimation of the resonance waves: Non-linear effects in the physics of the waves, like breaking tend to reduce the extreme wave elevations [27]. In diffraction theory these effects are not incorporated. Secondly, viscous effects, also neglected in diffraction theory, may be more dominantly present at the bilges of the keel due to the resonant flow between the two floating bodies. A occurence of a standing wave in between the vessels are shown in Figure 3-9. The relative wave amplitude for a incoming wave of 1 m increases in between the vessel up to almost ten times this amplitude. Since this is a unrealistic representation of reality and it will have a large effect on the outcome of the hydrodynamic data. Therefore adjustments in the diffraction analyse need to be made.

3-5-3 Viscous Roll Damping

An important assumption of potential theory is the neglection of viscous effects. Especially the roll motion is influenced by (non-linear) viscous forces [15]. Additional viscous damping is added to incorporate this non-linear behaviour. The viscous damping is estimated based on the empirical method of Ikeda [19]. This method is recommended by the ITTC Specialist

Modes	Longitudinal Frequency [rad/s]	Transversal Frequency [rad/s]
Piston	0.555	
Mode 1	0.733	0.878
Mode 2	0.883	1.241
Mode 3	1.014	1.520
Mode 4	1.132	1.756
Mode 5	1.240	1.962
Mode 6	1.340	
Mode 7	1.433	
Mode 8	1.520	
Mode 9	1.602	
Mode 10	1.680	
Mode 11	1.755	
Mode 12	1.827	
Mode 13	1.896	
Mode 14	1.962	

Table 3-1: Approximated natural frequencies of sloshing modes for different gap distances in [rad/s]

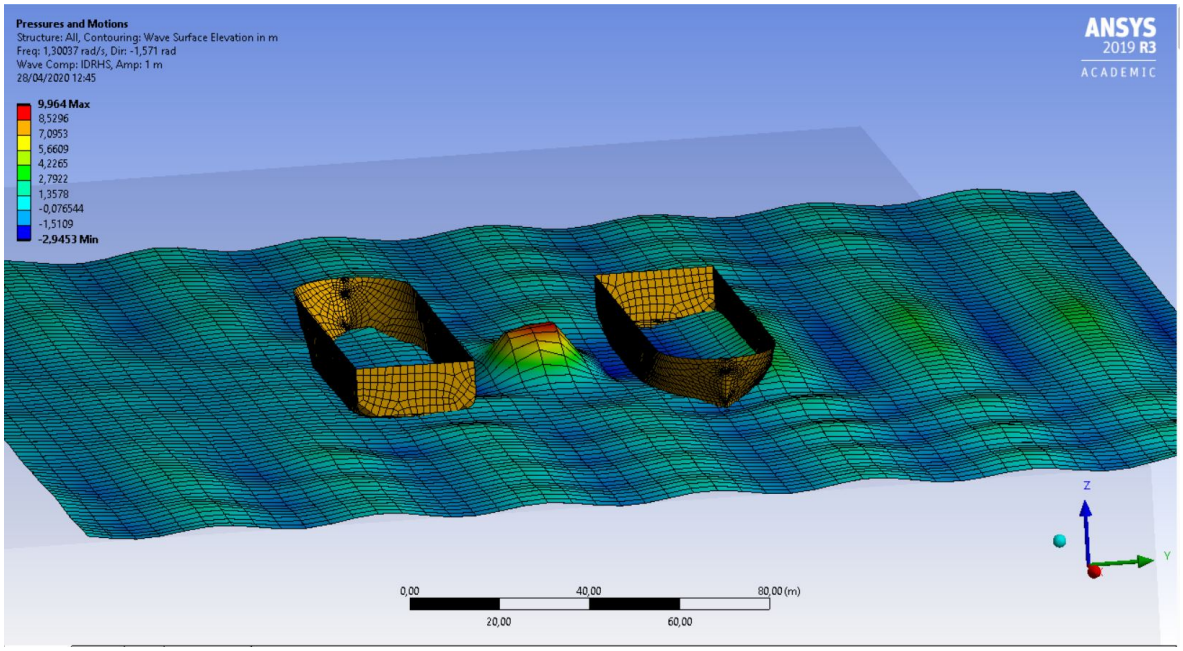

Figure 3-9: Side view of relative wave elevation in between the vessels at frequency of 1.30 rad/s. The gap distance is 40m.

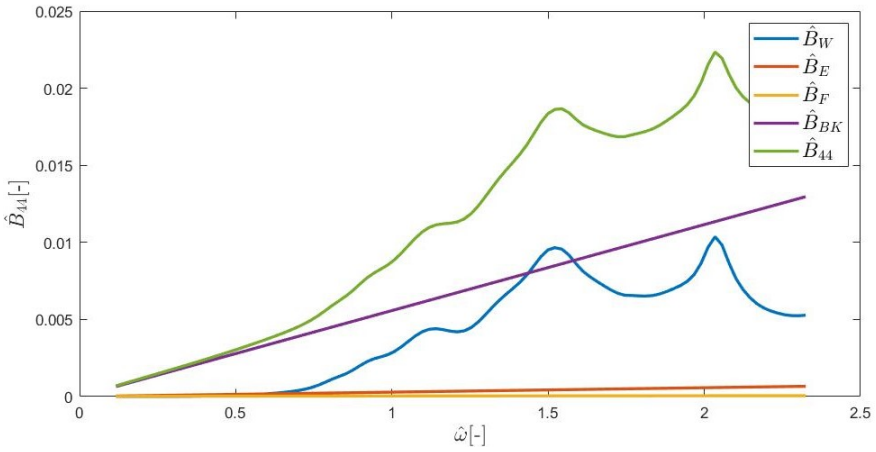

Figure 3-10: Dimensionless roll damping contributions vs the dimensionless frequency.

Committee on Stability in Waves. The roll damping moment of the vessel can be summed up by a number of different contributions: The wave, lift, frictional, eddy and the appendages contributions (bilge keel, skeg, rudder etc.). The total damping coefficient of the vessel can therefore be written as:

$$B_{44} = B_W + B_L + B_F + B_E + B_A \tag{3-12}$$

The wave and lift components are linear, proportional to the roll angular velocity. The lift component is non-zero in case of a forward speed, which is not the situation in this work, so $B_L = 0$. The damping contribution of the appendages is represented by the damping of the bilge keels $B_A = B_{BK}$. The friction, eddy and appendages components are non-linear and assumed to be proportional to the square of roll angular velocity. To calculate the different damping contribution terms use is made of the prediction fit formulas given by Kawahara 2011 [19]. Van Heijst (2015) has already checked the validity of this method onto the J-class vessel on the basis of different vessel parameters [32]. The second order damping term depends on the roll response which is an unknown. It could be determined by means of an iteration process but it is a time consuming process to create such an iterator for the complete matrix system. To gain further simplification of the system, the maximum acceptable Significant Double Amplitude (SDA) of roll of the Fairplayer is used:

$$\phi_a = SDA_{roll} \tag{3-13}$$

The contribution of the dimensionless different damping terms to the total roll damping as a function of the dimensionless frequency is shown in Figure 3-10. The dimensionless damping coefficient is given by:

$$\hat{B}_{44} = \frac{B_{44}}{\rho \nabla B} \sqrt{\frac{B}{2g}} \tag{3-14}$$

The potential wave damping B_W is generated by AQWA. From the figure it is shown that the bilge keels of the vessel play an important role in the addition of the viscous damping. Especially in the low frequency zone where the potential wave damping is zero viscous damping is dominant.

3-5-4 Damping Lid

A method to prevent the unrealistic wave elevation in between the vessels is the addition of an external lid on the surface. The lid adds a certain damping on the wave elevation. This lid method was originally formulated by Chen(2005) [7]. This lid has an adjusted boundary condition to suppress non-realistic high wave elevations between the two floating objects. The boundary conditions for the potential theory are explained in appendix D-4. Equation (D-23) gives the expression for the boundary condition for the water surface:

$$-\omega^2\phi + g\frac{\partial\phi}{\partial z} = 0 \quad \text{for} \quad z = 0 \tag{3-15}$$

The adjusted damped water surface boundary condition is expressed as:

$$\frac{\omega^2}{g}\left(\alpha_d f_1 - 1\right)\phi - 2i\frac{\omega^2}{g}\alpha_d f_1\phi + \frac{\partial\phi}{\partial z} \quad \text{for} \quad z = 0 \tag{3-16}$$

in which α_d is the damping factor and ϕ is the velocity potential. The function f_1 relates to the gap size in between the vessels d_{gap}:

$$f_1 = \begin{cases} \sin^2\left(\frac{\pi}{2}\frac{\omega}{\omega_0}\right) & \text{if} \quad \omega < \omega_0 = \max\left(0.1, \sqrt{\frac{\pi g}{d_{gap}}}\right) \\ \left(\frac{\omega}{\omega_0}\right)^2 & \text{if} \quad \omega \geq \omega_0 \end{cases} \tag{3-17}$$

The damping factor α_d determines the rate of damping of the waves. A value of 0 gives no additional effect to the damping. The correct value of the damping factor can be obtained by the execution of model experiments and can be different for different gap sizes of the vessel. A common method is the measurement of the wave height in between the vessels based on a model experiment. This wave height is then compared to the wave height given by the diffraction analysis. Since the damping factor reduces the wave height, the matching wave height with respect to the model experiment is indicated as the correct damping factor. As model experiments for the Fairplayer laying side-by-side are not available, literature is used to analyse the effects of the damping lid on vessel interaction. Damped diffraction runs are executed in AQWA to analyse the effects on the Fairplayer.

3-5-5 Analysis of lid damping factor

Pauw et al. (2007) analysed the emergence of the standing waves as well as the influence on the hydrodynamic data for side-by-side moored vessels [27]. Unfortunately, only small gap distances were considered, so the outcomes can not compared to the distances that are common in a QUAD lift lay-out. Pauw et al. noticed that the damping lid has a greater effect on the outcomes of the second order wave forces than on the first order quantities. Therefore, the damping factor should ideally be tuned based on the second order forces. However, since second order terms are not included in this study, the damping factor will nevertheless be determined based on the first order terms. Regarding larger gap distances, Peña et al.(2016) investigated the effect of the damping lid between a vessel and a fixed structure [28]. Results are presented for the sway motion for a wave heading of 90 degrees(beam waves). The results

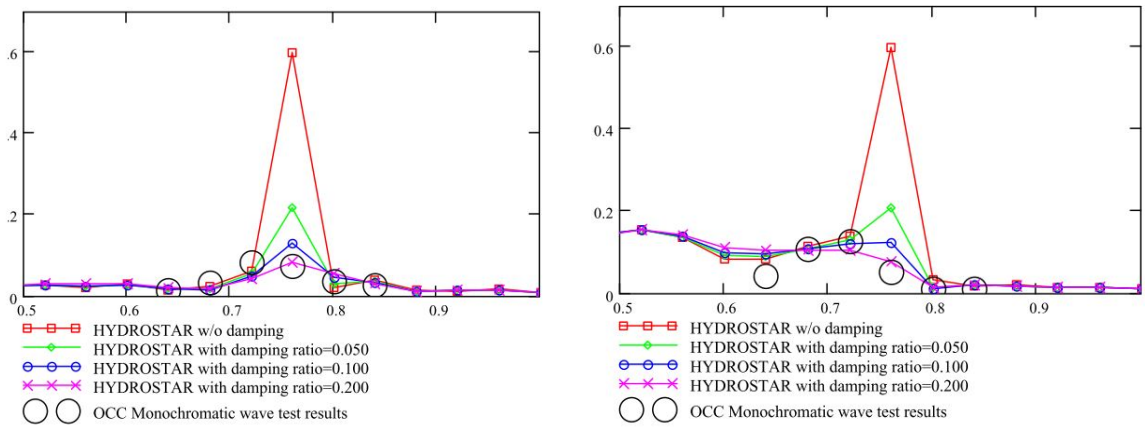

(a) Sway reponse **(b)** Heave response

Figure 3-11: RAO's vs freqency in rad/s of FSRU in heave and sway motion for head waves calculated by HYDROSTAR and results of model test executed by Fournier et al.(2006) [10]. The gap distance between vessels is 20 m.

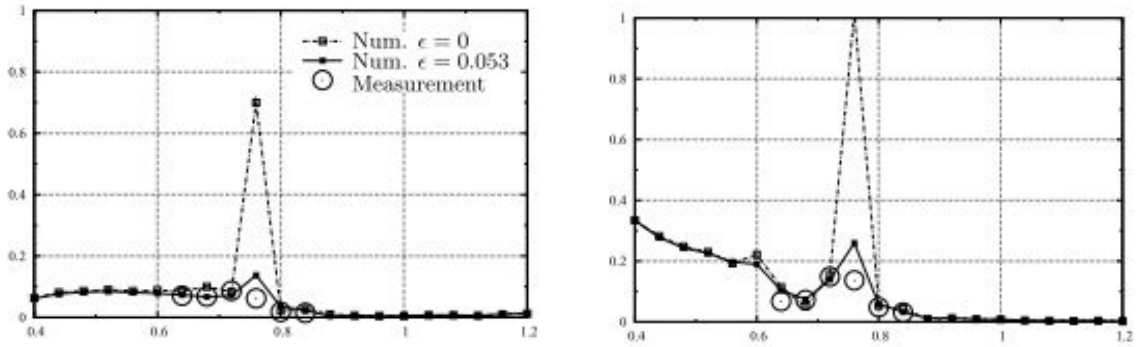

(a) Sway RAO **(b)** Heave RAO

Figure 3-12: RAO's vs freqency in rad/s of LNG carrier in heave and sway motion for head waves obtained by Chen et al. (2007) [6]. The gap distance between vessels is 20 m.

showed the large influence of the damping lid on the hydrodynamic data of the vessel. It was demonstrated that a damping factor of 1 over-damped the system. The addition of lids is necessary when the gap reaches significant dimensions, in their case particular for distances of 18 m or more. Figure 3-13 shows the hydrodynamic data for the vessel in close distance from a fixed wall.

Monochromatic model test to determine the damping coefficient for a LNG carrier and a FSRU moored together side-by-side were executed by Fournier et al.(2006) [10]. They compared model results with the diffraction analysis in the software WAMIT and HYDROSTAR for vessel gaps of 20 and 30 m. Their comparison results for the sway and heave RAO are shown in Figure 3-11. Based on their results it was shown that a damping coefficient of the lid in between the vessels between 0.1 and 0.2 gave a fair agreement with their test results.

Chen et al. (2007) analysed the effect of the damping factor between a LNG carrier and a FSRU [6]. The results were compared to model test. The gap distance between both vessels

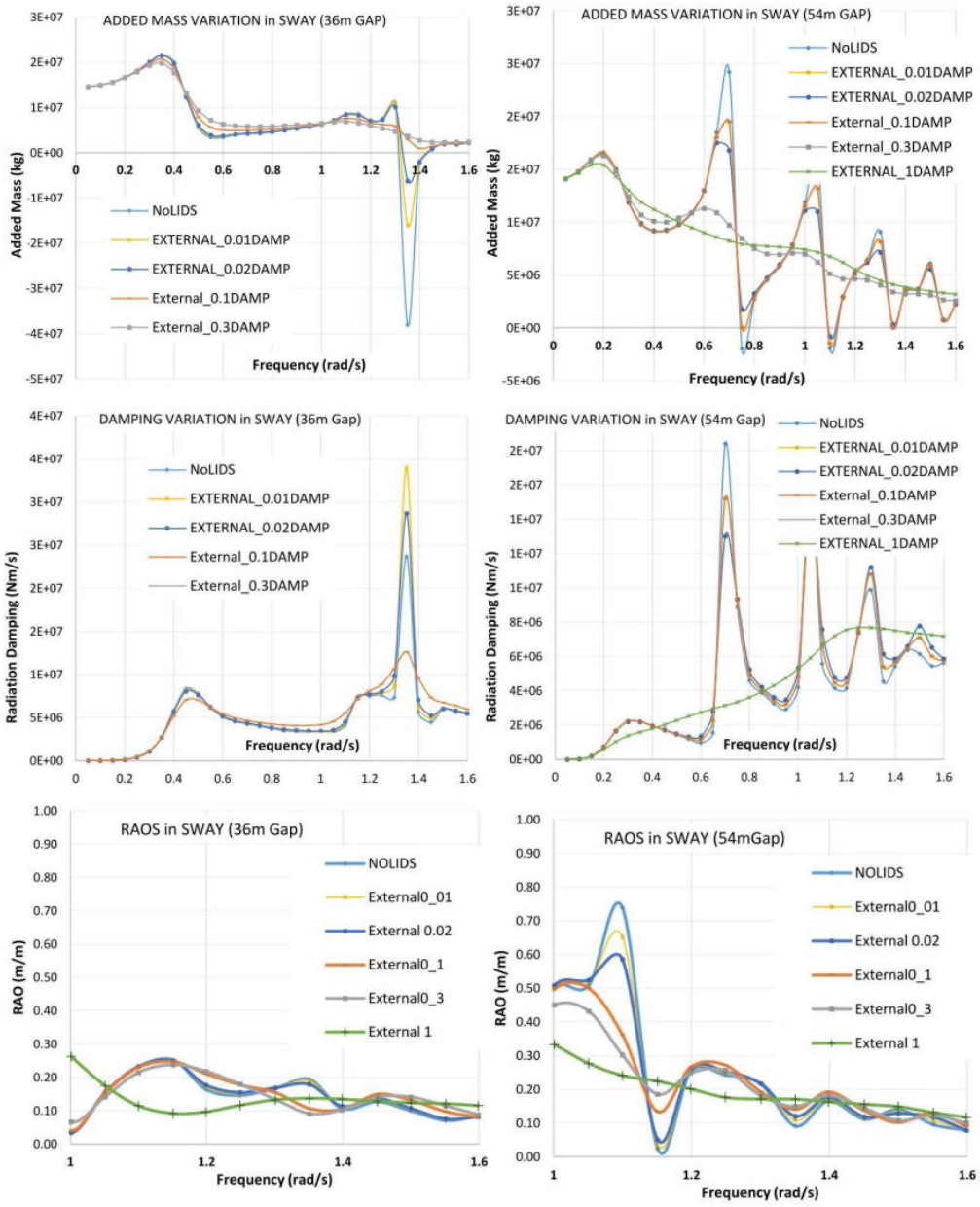

Figure 3-13: Hydrodynamic data and RAO's for sway motion of vessel relative to fixed wall for different gap distances by Peña et al.(2016) [28].

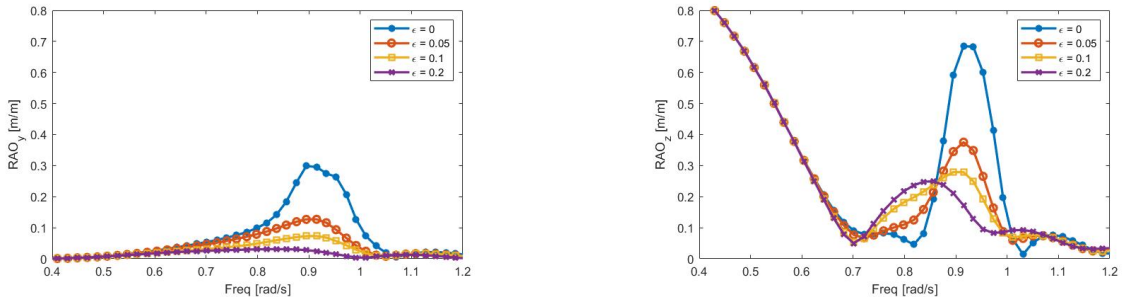

(a) RAO sway **(b)** RAO heave

Figure 3-14: Responses of Fairplayer in head waves with a gap distance of 20 m.

was 20m. The RAO's are shown in Figure 3-12. Based on the comparative study it was found that a damping factor of 0.053 showed a good agreement with the experimental data.

3-5-6 Behaviour of Fairplayer vs Literature

If we look at the responses of the Fairplayer for different damping coefficients, similar phenomena are found. Figure 3-14 shows the same peaks in the sway and heave response as were found by Fournier and Chen showed in Figure 3-11 and Figure 3-12. It should be said that the location and the responses at the peaks differ with respect to the Fairplayer. Different hull layouts and different vessel interaction lay-out could be the reason for this. The hydrodynamic data shows similar behaviour as was found in the study of Peña et al. The dimensionless hydrodynamic coefficients for the side-to-side configurated Fairplayers for a gap distance of 40 m are shown in Figure 3-15. If the damping factor is equal to zero, repetitive resonance peaks in the sway added mass and damping appear. Also, strong negative added masses can be seen in Figure 3-16a. The increase of the damping coefficient is an effective method to remove the peaks from the hydrodynamic data.
The complete responses for the Fairplayer laying side-by-side are shown in Figure 3-16. The increase of the damping factor has a large effect on the sway and heave RAO. The effect on the roll RAO is small. Since it is hard to predict a correct damping factor for the lid, the full model analysis of the QUAD lift is based on the data without addition of the damping lid. The final workability calculation of the QUAD lift is executed for an intensive damped diffraction run with a damping factor of 0.1. The results were hardly different compared to the workability results based on the diffraction calculation without damping lid.

3-6 Natural Frequencies

The free floating Fairplayer has a hydrostatic stiffness in heave, roll and pitch motions. Therefore, it has only natural frequencies in those directions, since the natural frequencies can be calculated by:

$$\left(\mathbf{C} - \omega_n^2 \left(\mathbf{M} + \mathbf{A}\left(\omega_n\right)\right)\right) \vec{v} = 0 \tag{3-18}$$

in which ω_n represent the natural frequencies and $\vec{v}$ is the eigenvector. A problem is however, that the eigenvalues depend on the added mass of the system which depends on the frequency.

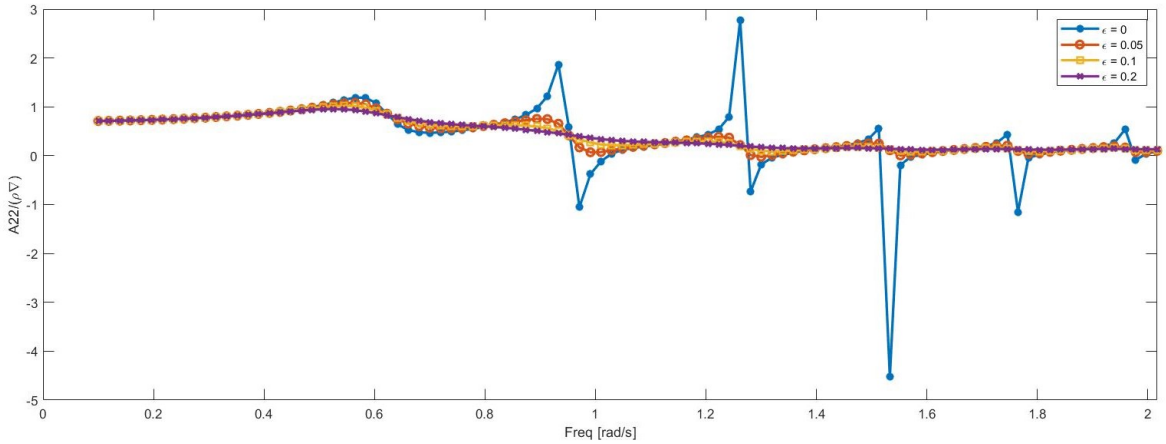

(a) Dimensionless sway added mass vs frequency

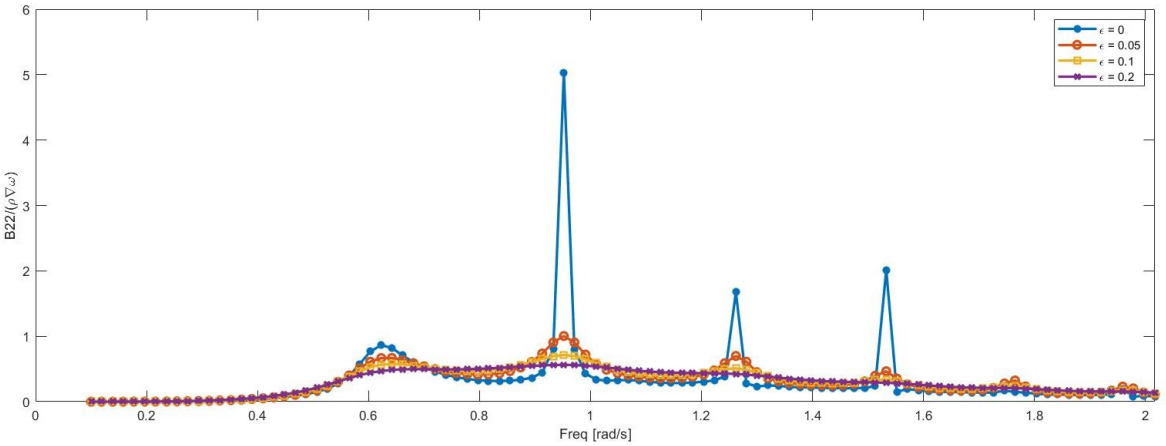

(b) Dimensionless sway damping vs frequency

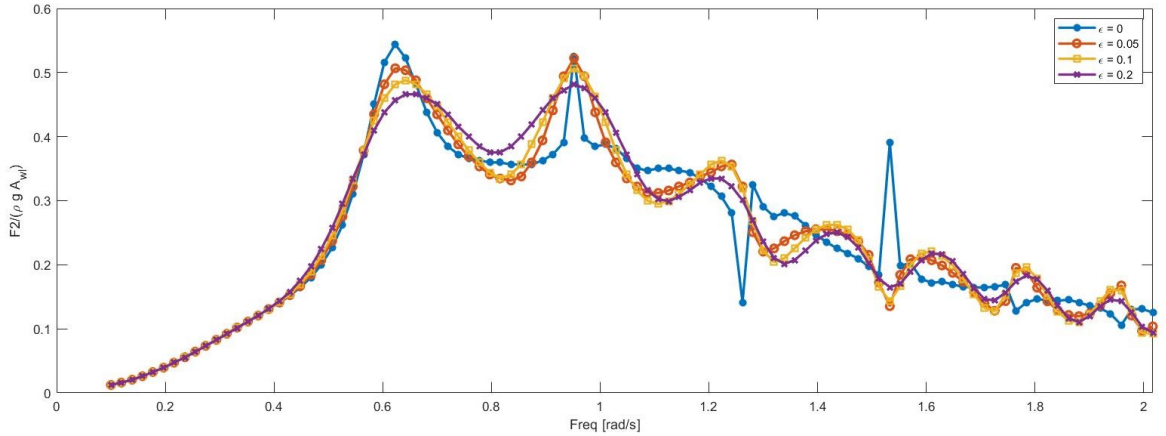

(c) Dimensionless sway excitation forces for beam waves vs frequency

Figure 3-15: Dimensionless hydrodynamic data for different damping factors for Fairplayer with a gap distance of 40 m.

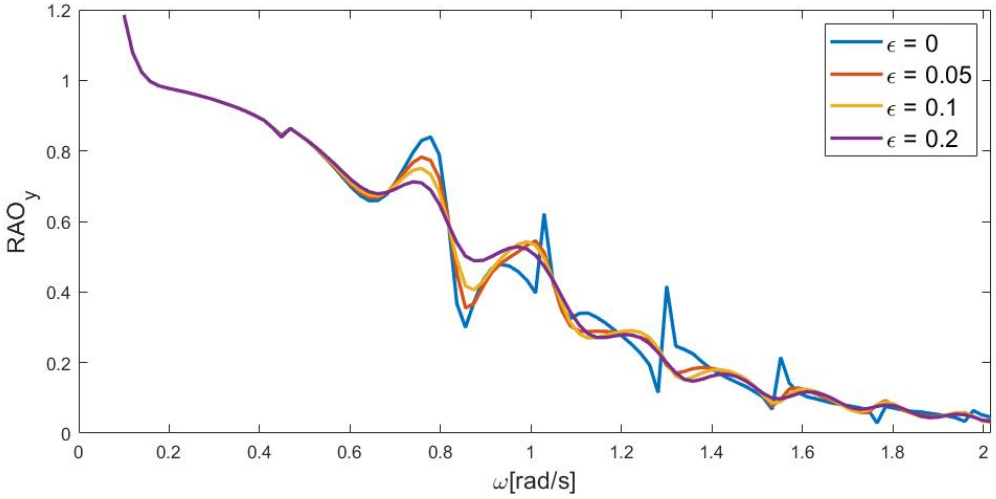

(a) RAO of sway

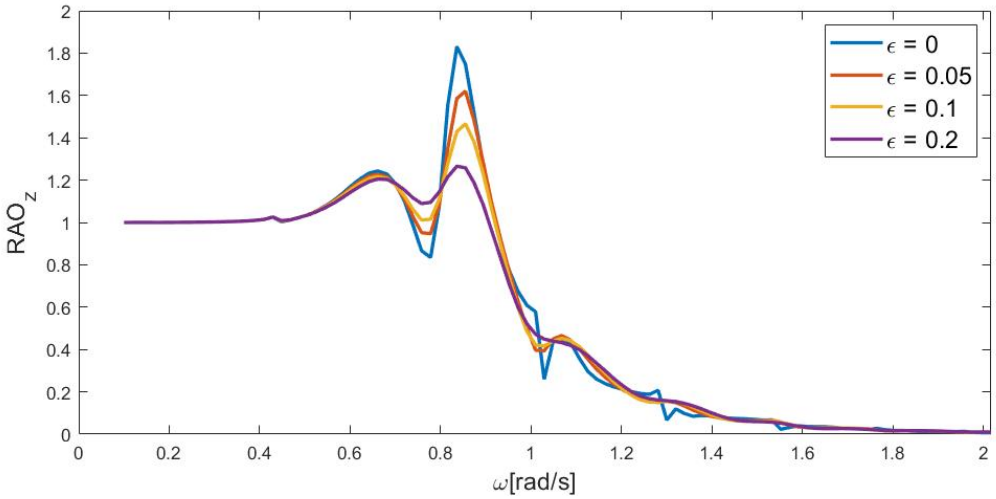

(b) RAO of heave

Figure 3-16: RAO's for different damping factors of the side-to-side laying Fairplayer in beam waves coming from the non-vessel side. The gap distance is 40 m.

	Gap Distances [m]			
Mode	20	30	40	50
Heave [rad/s]	0.86	0.82	0.80	0.80
Roll [rad/s]	0.45	0.45	0.45	0.45
Pitch [rad/s]	0.91	0.88	0.86	0.90

Table 3-2: Natural Frequencies Fairplayer for different gap distances

This means the natural frequency value is only valid if it is determined by a corresponding added mass which depends on the same frequency. The different natural frequencies of the J-type Fairplayer with different vessel gaps are shown in table 3-2.

3-6-1 DP system

The DP system of the vessels is added to the motion model by the addition of different springs. The DP system causes low-frequent reactive response motions which normally are far out of the range of the frequency of the ocean waves. The stiffness of the springs are based on an estimated value of the natural periods of the different motion directions of the DP system which are:

- The natural period for surge motion is 100 s.
- The natural period for sway motion is 100 s.
- The natural period for yaw motion is 100 s.

The natural surge period of the DP-system is related to the stiffness by:

$$T_{n,x} = 2\pi\sqrt{\frac{m_{1,1} + a_{1,1,\omega_{i=1}}}{c_{1,1}}} \tag{3-19}$$

So the surge stiffness of the DP-system is:

$$c_{1,1} = \frac{m_{1,1} + a_{1,1,\omega[i=1]}}{\left(\frac{T_{n,x}}{2\pi}\right)^2} \tag{3-20}$$

For the calculation of the stiffness terms, the added mass value for the lowest frequency ($\omega_{i=1} = 0.1$ rad/s) is taken. The same equations holds in the sway and yaw direction.

3-7 Analysis of J-type responses for different gap widths

The different gap sizes have an influence on the responses of the vessels. The reason of the different responses can be attributed to the differences in the coupling terms of the hydrodynamic matrices. The responses of the vessel for different gap widths are shown in Figure 3-18. It can be seen that the sway and heave responses are influenced due to the presence of the side laying vessel. The roll response barely changes due to the second vessel. Table 3-2 already showed that the natural frequency of the roll response remained constant for different vessel gaps. So the position of the response peaks should also be at the same location which is the case in Figure 3-18c.

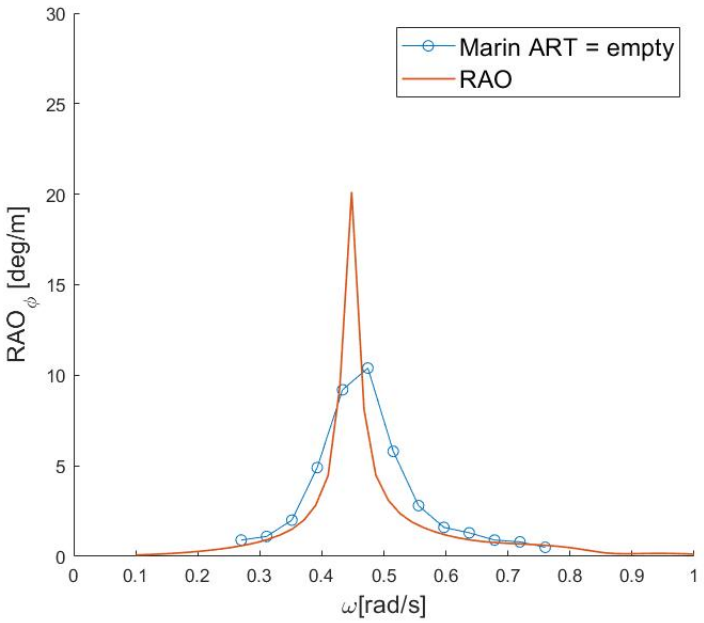

Figure 3-17: Roll RAO for beam waves compared to experimental data Marin

3-7-1 Validation of Roll Response Marin

Since the location of the natural frequency peak for roll response does not change for different gap widths, it can be used to validate the data to sea-keeping tests of the J-class vessel, executed by Maritime Research Institute Netherlands (MARIN). MARIN executed model tests on the implementation of an Anti Roll Tank (ART) for the J-Class vessels. The experimental results of an empty ART can be used in this thesis to compare the roll response curve. The comparison of the roll response and the experimental data is shown in Figure 3-17. The data of Marin shows a peak response at about the same frequency. The response value of the peak response is different. Since this value is strongly dependent on the estimated roll damping, a reason for the difference could be an inaccurate damping estimation by the Ikeda method.

3-8 AQWA vs OrcaWave

From Figure 3-15 it is shown that the hydrodynamic data has a very irregular behaviour. Vessel interaction effects including resonance waves, have a major effect on the data. Especially in case of zero lid damping, repeating peaks in the data are visible. The question could be asked if the data is reliable for an analysis of a coupled motion study. To prevent possible errors in the set up of the diffraction calculations, the data of two diffraction programs is compared.

The first problem in this comparison is that the data of both diffraction codes is given for a different origin. AQWA gives the data with respect to the position of the CoG. OrcaWave gives the data with respect to the body origin. This body origin is defined in the mesh

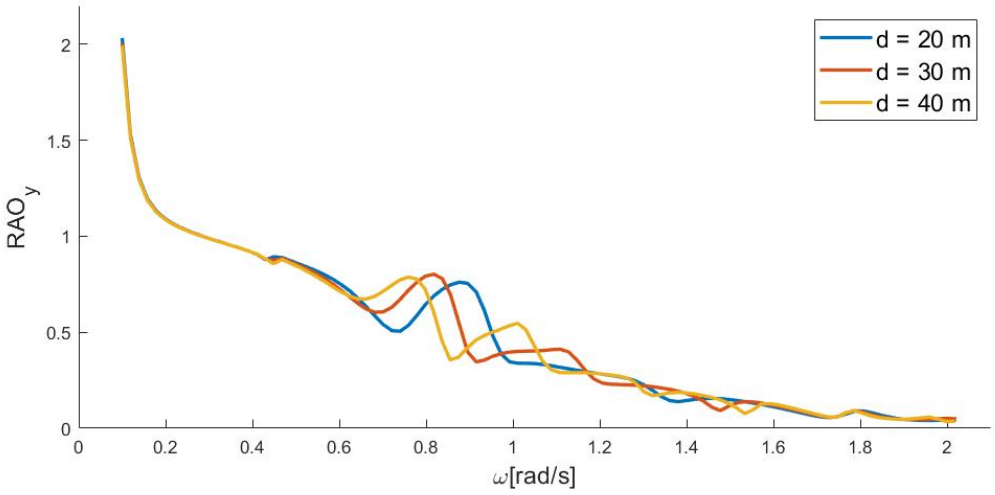

(a) RAO of sway

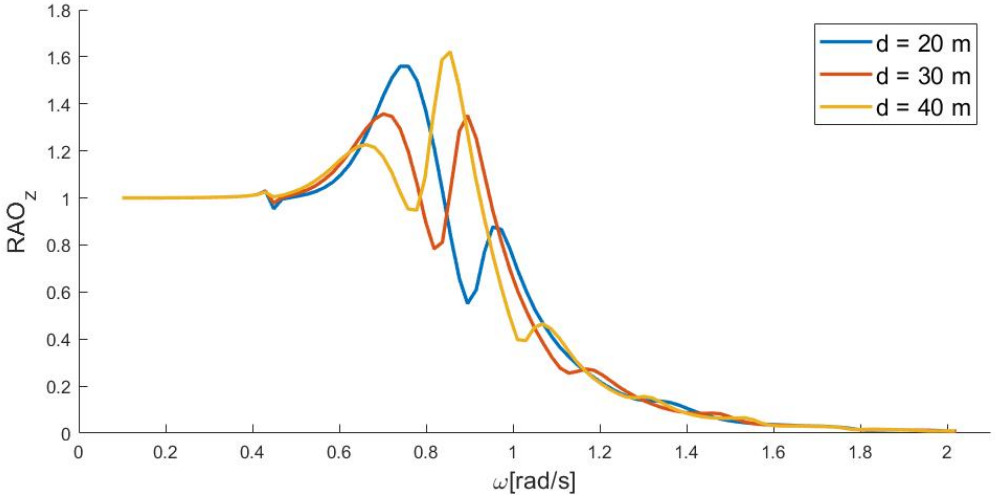

(b) RAO of heave

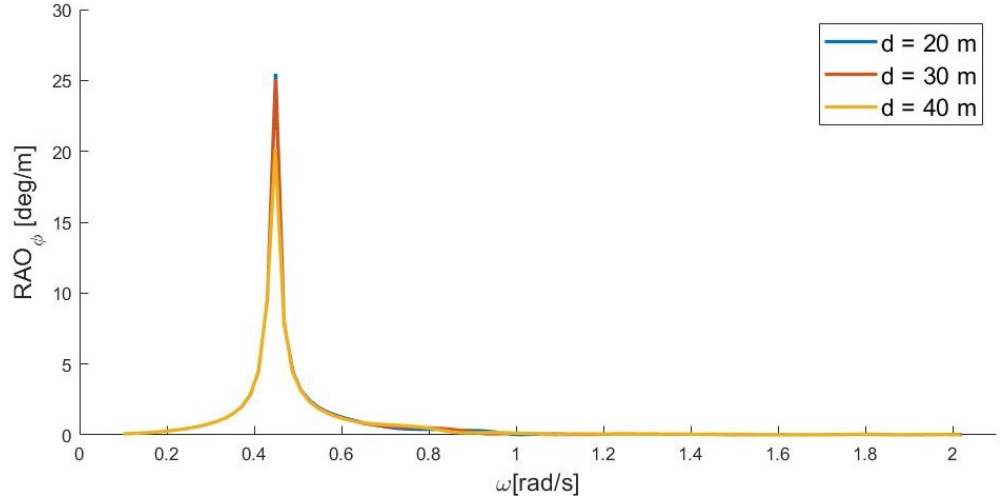

(c) RAO of roll

Figure 3-18: RAO's of fairplayer for beam waves for different gap widths d in between side to side of catamaran hulls

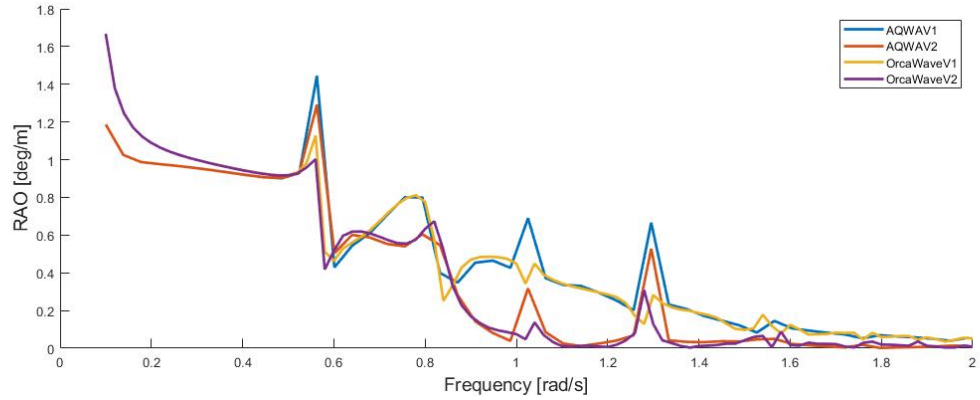

(a) RAO of sway

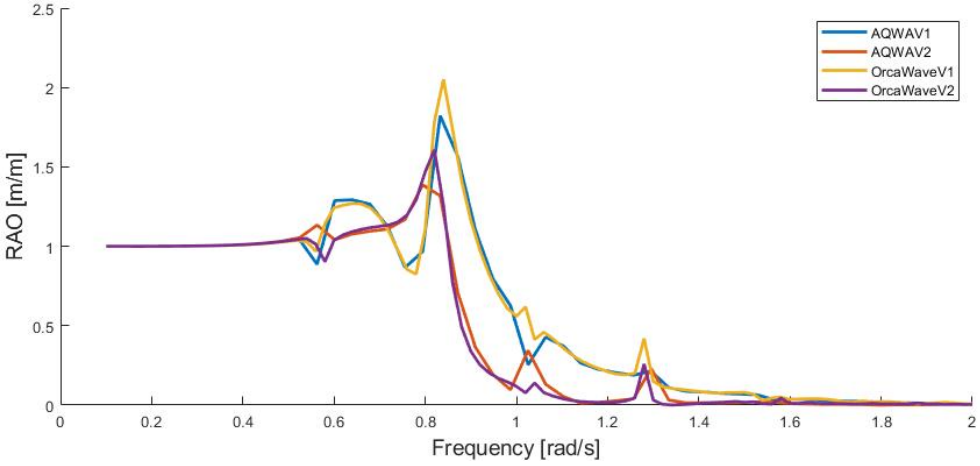

(b) RAO of heave

Figure 3-19: Comparison RAO's of both vessels in beam waves between AQWA and OrcaWave. The vessels are in beam waves, V1 indicates the front laying vessel and V2 is not directly exposed to the incident waves. The relative distance between both vessels is 40 m.

file. To compare the data, a transformation of one of the data sets is required. Figure 3-19 shows the responses of the vessel sway and heave calculated by both diffraction codes, expressed with respect to the CoG of both vessels. Both programs deliver quite the same vessel responses. Only at the resonance frequencies, different peak values can be seen. The resonance frequencies occur in both programs at the same frequencies.

Chapter 4

QUAD Lift Model

4-1 Introduction

This chapter will explain the method used to create the dynamic QUAD lift model. Now the hydrodynamic wave forces and vessel data is known, the model is extended by the coupling of the load. The load introduces 6 new DoF to the equations of motion, which creates a 18 DoF matrix system. Since the equations of motions of the vessels are coupled to the load, the dynamic behaviour of the vessels will change. This dynamic behaviour will be analysed by means of responses, natural frequencies and eigenvectors. To control the load and vessel responses, tugger lines will be introduced.

4-2 Metacentric height

The geometric center height is a value which determines the stability of a floating object in water. In case of a body rotation around the CoG, the Center of Buoyancy (CoB) will shift towards the side at which the displaced water increases by this rotation. Since the CoB is the location at which the buoyancy force is applied, a reaction moment will counteract the rotation. The resulting stability force of a floating object is shown in Figure 4-1. In case of small rotations, the metacentric height is defined as:

$$\overline{GM} = \overline{KB} + \overline{BM} - \overline{KG} \tag{4-1}$$

in which $\overline{KB}$ is the distance from the keel to the center of buoyancy, $\overline{BM}$ is the distance from the center of buoyancy to the initial metacentre and $\overline{KG}$ is the distance from the keel to the center of gravity. The distance $\overline{BM}$ can be calculated by:

$$\overline{BM} = \frac{\nabla}{I_T} \tag{4-2}$$

in which ∇ is the displaced water volume of the object and I_T is the second moment of area of the water plane.

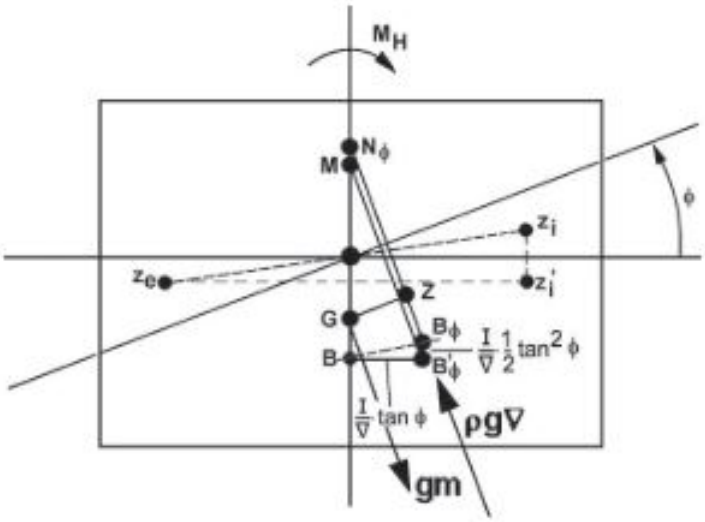

Figure 4-1: Stability floating object

The metacentric height is a indication of the range of stability of the vessel. As long as the distance $\overline{GM}$ is positive, a counteracting moment against the rotation will occur, since the moment lever arm is defined as:

$$\overline{GZ} = \overline{GM} \cdot sin\phi \tag{4-3}$$

4-2-1 Minimal GM during lift

Jumbo uses a rule of thumb to subscribe to minimum required GM for the Fairplayer during an offshore lift: [11]

$$\overline{GM} = 1 + \left(\frac{1.5 \cdot HL}{1800}\right) \tag{4-4}$$

in which HL is the total hook load of the forward and aft crane in tons.

4-3 Position of the CoG

The horizontal position of the CoG is calculated by AQWA and is equal to the centroid of the submerged body. The vertical position of the CoG is given by Jumbo and is 2.1 m above the waterline for a vessel with a draft of 7.5 m. This draft and CoG represents a loaded vessel condition which could be used during offshore activities.

4-3-1 Change of CoG

When a load is applied to the cranes the CoG of the vessel will shift. The displacement of the CoG in the horizontal direction is small and can be counteracted by the use of water tanks. So the horizontal position of the CoG of the vessels does not change in the analysis. There

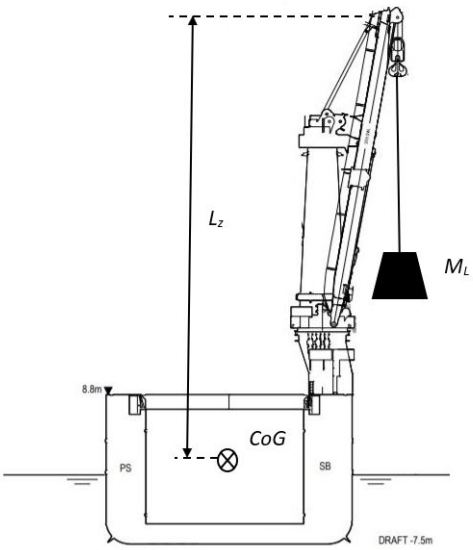

Figure 4-2: Vertical distance from CoG to load

will be however, a vertical change of the CoG. The point of engagement of the load is the crane tip, shown in Figure 4-2. The vertical displacement of the CoG is calculated by:

$$\Delta z = \frac{\sum_i M_{L,i} \cdot L_{z,i}}{M + \sum_i M_{L,i}} \tag{4-5}$$

in which i indicates the effect of each individual crane, $M_{L,i}$ is the mass of the load on the crane, $L_{z,i}$ is the vertical distance of the crane tip to the CoG and M is the mass of the vessel. The applied load on each indivual crane to calculate the change of CoG is based on the static condition: in a QUAD Lift each crane takes one fourth of the total load.

4-3-2 Hydrostatic coefficients

As shown in eq. (4-1) the distance $\overline{GM}$ depends on the vertical position of the CoG. So a vertical change of the position of the CoG has an effect on the metacentric height $\overline{GM}$. The diagonal hydrostatic stiffness terms of the rotation about the horizontal axis depend on the metacentric height values, since they are given by:

$$\begin{aligned} c_{44} &= \rho g \left(\nabla \overline{GM_x} + (y_F - y_G)^2 A_{wl} \right) \\ c_{55} &= \rho g \left(\nabla \overline{GM_y} + (x_F - x_G)^2 A_{wl} \right) \end{aligned} \tag{4-6}$$

in which (x_F, y_F) and (x_G, y_G) represent the position of the center of floatation and the center of gravity in the horizontal plane, respectively. The center of floatation is located at the centroid of the cut water plane area. The other hydrostatic coefficients do not depend on

the vertical change of the CoG. These coefficients are given by:

$$\begin{aligned} c_{34} &= c_{43} = \rho g \left(y_F - y_G\right) A_{wl} \\ c_{35} &= c_{53} = -\rho g \left(x_F - x_G\right) A_{wl} \\ c_{45} &= c_{54} = -\rho g \left(x_F - x_G\right) \left(y_F - y_G\right) A_{wl} \end{aligned} \tag{4-7}$$

The change in the position of the CoG of the vessel leads to the symmetric vessel specific stiffness matrix:

$$\mathbf{C}_v = \begin{bmatrix} 0 & 0 & 0 & 0 & 0 & 0 \\ 0 & 0 & 0 & 0 & 0 & 0 \\ 0 & 0 & c_{33} & c_{34} & c_{35} & 0 \\ 0 & 0 & c_{43} & c_{44} & c_{45} & 0 \\ 0 & 0 & c_{53} & c_{54} & c_{55} & 0 \\ 0 & 0 & 0 & 0 & 0 & 0 \end{bmatrix} \tag{4-8}$$

4-3-3 Hydrodynamic coefficients and change of CoG

The change of the position of the CoG has also an effect on the hydrodynamic data. In OrcaWave the hydrodynamic coefficients are given with respect to the body origin. The body origin is written in the mesh file and is vertically located at the SWL. Horizontally it matches the position of the CoG. The translational responses at a certain position of the vessel can be calculated by the use of a transformation matrix. Besides the indirect transformation of the RAO's, also the hydrodynamic data can be directly tranformed for the new CoG position. The RAO's of the vessels for a shifted CoG can be calculated by application of a transformation matrix $\mathbf{L}$:

$$RAO = \frac{\mathbf{L}^T \vec{F}_a(\omega, \theta)}{\mathbf{L}^T \left(-\omega^2 \left(\mathbf{M} + \mathbf{A}(\omega)\right) - i\omega \mathbf{B}(\omega) + \mathbf{C}\right) \mathbf{L}} \tag{4-9}$$

The vessel transformation matrix to calculate the data for a new position, located at $(\Delta x, \Delta y, \Delta z)$ with respect to the initial origin, is given by:

$$\mathbf{L_v} = \begin{bmatrix} 1 & 0 & 0 & 0 & -\Delta z & \Delta y \\ 0 & 1 & 0 & \Delta z & 0 & -\Delta x \\ 0 & 0 & 1 & -\Delta y & \Delta x & 0 \\ 0 & 0 & 0 & 1 & 0 & 0 \\ 0 & 0 & 0 & 0 & 1 & 0 \\ 0 & 0 & 0 & 0 & 0 & 1 \end{bmatrix} \tag{4-10}$$

In the 12 DoF matrix system for the two vessels the transformation matrix is given by eq. (3-8), the system transformation matrix is given by:

$$\mathbf{L} = \begin{bmatrix} \mathbf{L_v} & 0 \\ 0 & \mathbf{L_v} \end{bmatrix} \tag{4-11}$$

Since all OrcaWave data is given with respect to the body origin, the simplest method to transform the data for a change of CoG is to write all the data with respect to the body origin. In this case, only the stiffness matrix and the mass matrix need to be adjusted. The

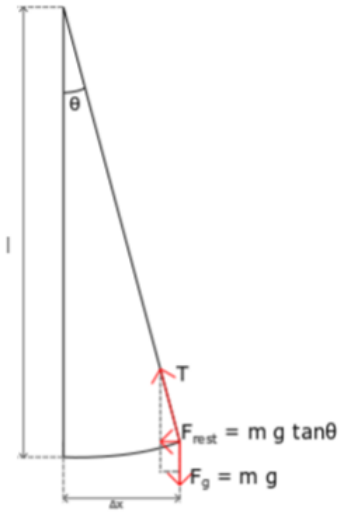

Figure 4-3: Single pendulum mechanics

mass matrix is diagonal when it is expressed in the CoG, therefore the mass matrix with respect to the body origin can be calculated by:

$$\mathbf{M} = \mathbf{L}^T \mathbf{M} \mathbf{L} \tag{4-12}$$

If all the data is known with respect to the body origin, the responses can be calculated. The responses at an arbitrary point p can be simply calculated by application of the transformation matrix to the response vector:

$$RAO_p = \mathbf{L} \cdot RAO \tag{4-13}$$

4-4 QUAD Lift Model

The QUAD lift model is created by the addition of a single load to the four cranes of the two vessels. Now, the system consists of three bodies with each 6 DoF, which makes the QUAD Lift a 18 DoF system. The connection between the load and the vessel is modelled as a linear spring, representing both the vertical cable and crane stiffness. The vertical spring has its attachment point on the vessel at the crane tip and at the corner positions of the load, indicated by the black and red dots in Figure 4-5. The coupling between the load and the vessel is based on the principals of a single pendulum, shown in Figure 4-3. If the load moves horizontally, the tension in the cable has a horizontal component which is related to horizontal displacement and the weight of the load. Based on linear pendulum mechanics a horizontal stiffness value K_r can be obtained:

$$\begin{aligned} F_{rest} &= mg \tan\theta \\ \Delta x &= l \sin\theta \\ F_{rest} = \frac{mg}{l}\Delta x &= K_r \Delta x \\ K_r &= \frac{mg}{l} \end{aligned} \tag{4-14}$$

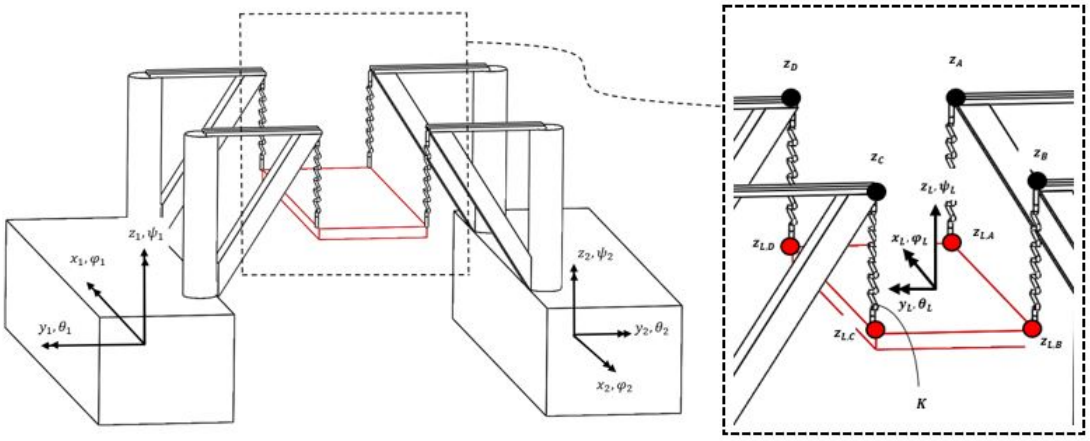

Figure 4-4: Overview QUAD Lift Model

Parameter	Symbol	Value
Vertical position CoG	Z_{CoG}	2.1 [m]
Pos. crane A and C	$(L_{xCr2}, L_{yCr}, L_{zCr})$	(20,23.5,40) [m]
Pos. crane B and D	$(L_{xCr1}, L_{yCr}, L_{zCr})$	(28,23.5,40) [m]
Crane stiffness	k_{crane}	76604 [kN/m]
Cable stiffness	k_{cable}	52622 [kN/m]
Cable length	l	40 [m]
Jib radius	JR	10 [m]
Number of falls	n	16

Table 4-1: Vessel and crane parameters

In case of the QUAD Lift, the load is not lifted by a single but by four cranes. Therefore, the static load on each crane is one fourth of total load. Such that the horizontal stiffness is equal to:

$$K_r = \frac{mg}{4l} \tag{4-15}$$

Quad Lift vessels parameters

The model described in this chapter depends on a large set of parameters. Since this chapter has the purpose to explain the model, a fixed set of vessel parameters is chosen, unless stated otherwise. The distances are given with respect to the body origin axis', horizontally located at the position of the CoG's and vertically at the SWL. The set of parameters is given in Table 4-1.

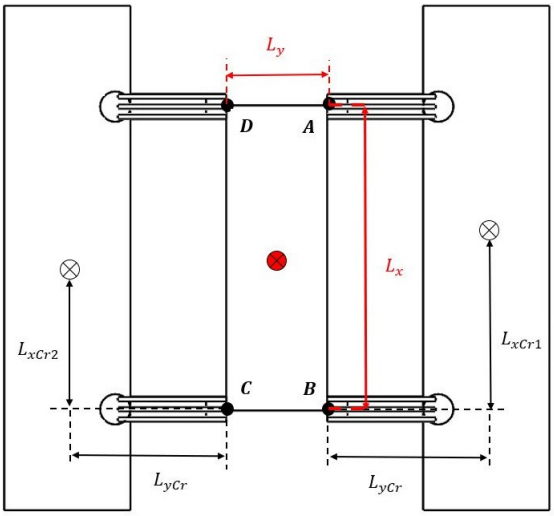

Figure 4-5: Top view QUAD Lift with dimensions

Parameter	Symbol	Value
Length of load	L_x	48 [m]
Width of load	L_y	20 [m]
Height of load	L_x	5 [m]
Weight of load	m_L	1000 [t]
Change of CoG	ΔZ_{CoG}	0.97 [m]
New GM	$(\overline{GM_x}, \overline{GM_y})$	(2.12,198.42) [m]

Table 4-2: Load parameters

Shape of Load

The shape of the load has a influence on the inertia values of the load. Since there is a wide variety in offshore lifted load objects and shapes, a simple rectangular barge is chosen in this study. The height of the barge is 5 m. The barge length and width is such that the attachment points are horizontally equal to the crane tip positions. In case there is no rotation of the cranes, the barge length is equal to the distance between the forward and aft crane which is equal to 48 m. It is assumed that the CoG of the barge is located at the centroid of the object.

4-4-1 Crane stiffness

The total restoring coefficient of one of the vertical springs as shown in Figure 4-5 depends on the crane stiffness and the cable stiffness. The total restoring coefficient is calculated as two springs in series:

$$K = \frac{1}{\frac{1}{k_{crane}} + \frac{1}{k_{cable}}} \tag{4-16}$$

mass cable (open air) per fall	12.14 [kg/m]
submerged mass per fall	10.4 [kg/m]

Table 4-3: Mass of cables

in which the crane stiffness k_{crane} is supplied by the manufacturer of the crane Huisman. The crane stiffness depends on the number of falls and the jib radius. The cable stiffness k_{cable} depends also on the number of falls as well on the cable length in between the load and the crane tip l, the cross sectional area of the cable A and modulus of elasticity E:

$$k_{cable} = \frac{EA}{l} \cdot n_{falls} \tag{4-17}$$

It is assumed that each crane uses 16 falls during the QUAD lift. It is assumed that there is only stiffness in the connection between the vessels an the load. Dissipation of energy via damping in the cables is neglected. The mass of the crane cables per meter is given by Huisman and shown in Table 4-3. If 16 falls are used and the cable length is 40 m, the total mass of the cables in the quad lift is equal to 31.08 t. Compared to the load which has a mass of 1000 t, the cable mass is relative small.(3,1%) To keep the model simple, the effect of the mass of the cables is neglected.

4-4-2 Derivation Equations of Motion

To create the coupled stiffness matrix of the QUAD Lift use is made of the Lagrange method. The coupling is caused by the horizontal and vertical springs, with stiffness K_r and K_z, respectively. The elongation of this springs occurs is the change of distance between the crane tips and the attachment points of the loads. Therefore, the linearised horizontal and vertical displacements of the crane tips $(A, .., D)$ with respect to the vessel origin, are written in terms of generalized coordinates:

$$\begin{aligned}
\Delta x_A &= x_2 + L_{zCr} \cdot \theta_2 + L_{yCr} \cdot \psi_2 \\
\Delta x_B &= x_2 + L_{zCr} \cdot \theta_2 + L_{yCr} \cdot \psi_2 \\
\Delta x_C &= x_1 + L_{zCr} \cdot \theta_1 + L_{yCr} \cdot \psi_1 \\
\Delta x_D &= x_1 + L_{zCr} \cdot \theta_1 + L_{yCr} \cdot \psi_1 \\
\\
\Delta y_A &= y_2 - L_{zCr} \cdot \phi_2 - L_{xCr,2} \cdot \psi_2 \\
\Delta y_B &= y_2 - L_{zCr} \cdot \phi_2 + L_{xCr,1} \cdot \psi_2 \\
\Delta y_C &= y_1 - L_{zCr} \cdot \phi_1 - L_{xCr,1} \cdot \psi_1 \\
\Delta y_D &= y_1 - L_{zCr} \cdot \phi_1 + L_{xCr,2} \cdot \psi_1 \\
\\
\Delta z_A &= z_2 - L_{yCr} \cdot \phi_2 + L_{xCr,2} \cdot \theta_2 \\
\Delta z_B &= z_2 - L_{yCB} \cdot \phi_2 - L_{xCr,1} \cdot \theta_2 \\
\Delta z_C &= z_1 - L_{yCr} \cdot \phi_1 + L_{xCr,1} \cdot \theta_1 \\
\Delta z_D &= z_1 - L_{yCr} \cdot \phi_1 - L_{xCr,2} \cdot \theta_1
\end{aligned} \tag{4-18}$$

Just like the crane tip positions, the relative motion of the attachment points of the cable onto the load with respect to the load origin are written in terms of the generalized coordinates:

$$\begin{aligned}
\Delta x_{L,A} &= x_L + 0.5L_z \cdot \theta_L + 0.5L_y \cdot \psi_L \\
\Delta x_{L,B} &= x_L + 0.5L_z \cdot \theta_L + 0.5L_y \cdot \psi_L \\
\Delta x_{L,C} &= x_L + 0.5L_z \cdot \theta_L - 0.5L_y \cdot \psi_L \\
\Delta x_{L,D} &= x_L + 0.5L_z \cdot \theta_L - 0.5L_y \cdot \psi_L \\
\\
\Delta y_{L,A} &= y_L - 0.5L_z \cdot \phi_L + 0.5L_x \cdot \psi_L \\
\Delta y_{L,B} &= y_L - 0.5L_z \cdot \phi_L - 0.5L_x \cdot \psi_L \\
\Delta y_{L,C} &= y_L - 0.5L_z \cdot \phi_L - 0.5L_x \cdot \psi_L \\
\Delta y_{L,D} &= y_L - 0.5L_z \cdot \phi_L + 0.5L_x \cdot \psi_L \\
\\
\Delta z_{L,A} &= z_L - 0.5L_y \cdot \phi_L - 0.5L_x \cdot \theta_L \\
\Delta z_{L,B} &= z_L - 0.5L_y \cdot \phi_L + 0.5L_x \cdot \theta_L \\
\Delta z_{L,C} &= z_L + 0.5L_y \cdot \phi_L + 0.5L_x \cdot \theta_L \\
\Delta z_{L,D} &= z_L + 0.5L_y \cdot \phi_L - 0.5L_x \cdot \theta_L
\end{aligned} \tag{4-19}$$

The elongation of the springs $(A, .., D)$ in each translational direction can be written as:

$$\begin{aligned}
\Delta X_{A,B} &= \Delta x_{A,B} + \Delta x_{L,A,B} \\
\Delta Y_{A,B} &= \Delta y_{A,B} + \Delta y_{L,A,B} \\
\Delta X_{C,D} &= \Delta x_{C,D} - \Delta x_{L,C,D} \\
\Delta Y_{C,D} &= \Delta y_{C,D} - \Delta y_{L,D,C} \\
\Delta Z_{A,..,D} &= \Delta z_{A,..,D} - \Delta z_{L,A,..,D}
\end{aligned} \tag{4-20}$$

For cranes A and B the horizontal elongation is the sum of both the crane tip and load displacements since the horizontal vessel axis have a different direction with respect to the load.

Euler-Lagrange's equations

To calculate the new equations of motions use is made of the Euler-Lagrange's equations. The Lagrangian is defined as:

$$L = T - V \tag{4-21}$$

in which$T$ and V are the kinetic and potential energy, respectively. The matrices of the vessels are already defined so there is no need to define the equations of motions again. Only the influence of the load need to be added by the defenition of the kinetic and potential energy:

$$\begin{aligned}
T &= 0.5m_L(\ddot{x}_L^2 + \ddot{y}_L^2 + \ddot{z}_L^2) + 0.5I_{xx,L}\ddot{\phi}_L^2 + 0.5I_{yy,L}\ddot{\theta}_L^2 + 0.5I_{zz,L}\ddot{\psi}_L^2 \\
V &= 0.5K_r X_{A,..,D}^2 + 0.5K_r Y_{A,..,D}^2 + 0.5KZ_{A,..,D}^2 + m_L g z_L
\end{aligned} \tag{4-22}$$

Now the equations of motion can be calculated by the application of the Euler-Lagrange equations for the generalized coordinates q_j:

$$\frac{d}{dt}\left(\frac{\partial L}{\partial \dot{q}_j}\right) = \frac{\partial L}{\partial q_j} \tag{4-23}$$

The Euler-Lagrange equations give the equations of motion of the load which can be expressed in the load mass and stiffness matrices, $\mathbf{M_L}$ and $\mathbf{C_L}$, which are are shown in **??**. Since the equations of motion are really large for a 18 DoF system, both matrices are generated by the use of numeric environment Maple.

The coupled equation of motion containing the vessels and load motion is described as follows:

$$\left(-\omega^2 \left(\mathbf{M} + \mathbf{A}(\omega) + \mathbf{M_L}\right) + i\omega\mathbf{B}(\omega) + \mathbf{C} + \mathbf{C_L}\right) \vec{X} = \vec{F}(\omega) \tag{4-24}$$

4-5 Coupled Responses

4-5-1 Vessel Responses

With eq. (4-35) the responses of the vessels and load in a QUAD Lift can be calculated. The QUAD Lift stiffness matrix induces coupling between the load and the vessel motions. The vessel motions for head waves are shown in Figure 4-6. The load is 1000 t and the vessels have a distance of 40 m. The figures show increased response in especially the roll motion during the lift compared to the free floating vessel. Also, in surge, pitch and yaw motion a peak can be seen around a frequency of 0.5 rad/s. Similar coupled response peaks were shown by [13] and [11] for a single crane lift.

4-5-2 Load Responses

Next to the vessel responses, also the load responses during the QUAD Lift are calculated. The horizontal load responses are shown in Figure 4-7. The figures show large resonance behaviour at certain frequencies. The load surge peak at a frequency of 0.5 rad/s is also visible in the vessel surge, pitch and yaw motion. Similar is the load sway peak at a frequency of 0.6 rad/s visible in the roll motion of the vessel.

Off-lead angle and side-lead angle

The horizontal load responses are related to the side-lead (load surge) and off-lead(load sway) angles. These angles need to be limited because large angles could lead to collisions between the load and the vessel. The off-lead ϕ_{OL} and side-lead θ_{SL} angles can be calculated by the relative displacement of the cable attachment point on the load and the crane tip divided by the length of the cable. The relative displacements for each crane are given by eq. (4-33). So, the off-lead and side-lead angles can be calculated by:

$$\begin{aligned} \phi_{OL_{A,..,D}} &= \frac{\Delta X_{A,..,D}}{l} \\ \theta_{SL_{A,..,D}} &= \frac{\Delta Y_{A,..,D}}{l} \end{aligned} \tag{4-25}$$

The off-lead and side-lead angles are shown in Figure 4-8. The off-lead angle is only shown for head waves and the side-lead angle for beam waves since these wave directions give the largest offset as shown in Figure 4-7. Each crane shows similar off-lead and side-lead angles

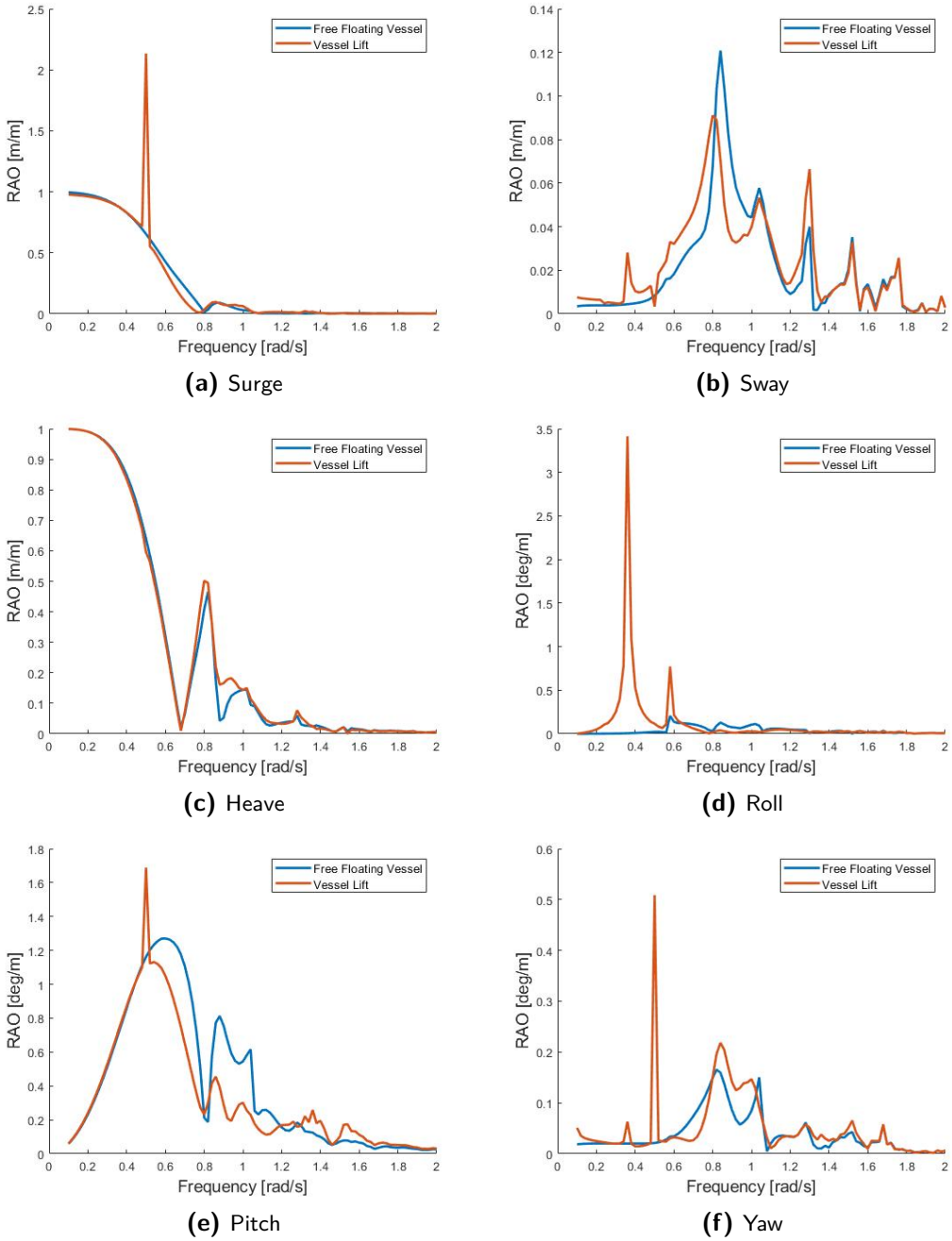

(a) Surge **(b)** Sway

(c) Heave **(d)** Roll

(e) Pitch **(f)** Yaw

Figure 4-6: Comparison RAO's of free floating vessel and vessel in QUAD Lift for head waves. The mass of the load is 1000 t and the vessel to vessel distance is 40 m.

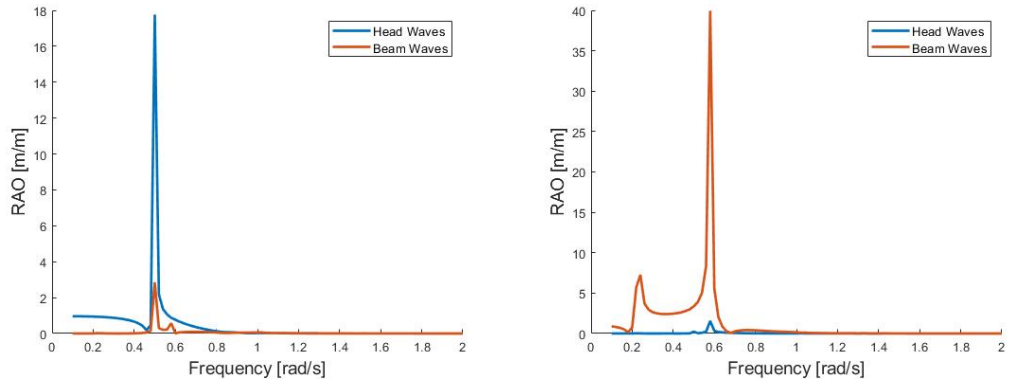

(a) Load surge **(b)** Load sway

Figure 4-7: Horizontal responses of load during QUAD Lift for head and beam waves.

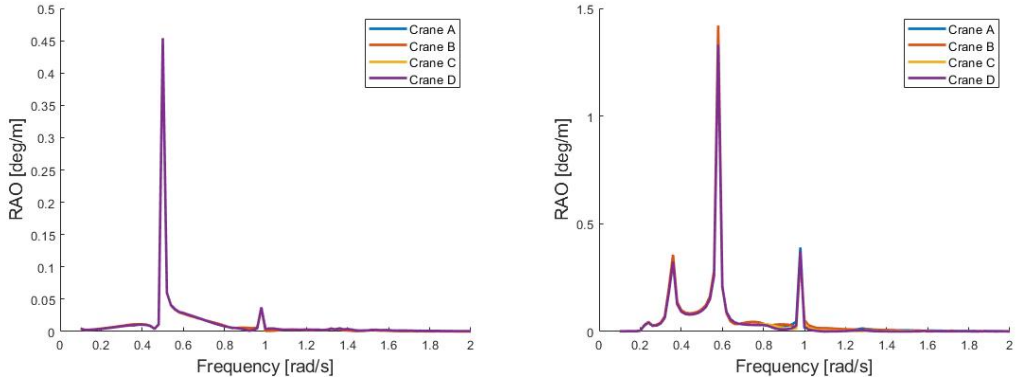

(a) Side-lead angles crane head waves **(b)** Off-lead angles cranes beam waves

Figure 4-8: Off-lead and side-lead angles for each of the four cranes of the vessels in head and beam waves, respectively.

responses. A difference between the load response and the crane lead angles is that the response is zero in the low frequency range. At these frequencies the load has about the same response as the vessels so the relative displacement is almost zero. At certain frequencies, resonance behaviour at the natural frequencies can be seen. A simple formula to calculate the natural frequency for a single pendulum is given by:

$$\omega_n = \sqrt{\frac{K_r}{m_L}} = \frac{g}{l} \tag{4-26}$$

This gives for a cable length of 40 m, a natural frequency of 0.5 rad/s, which matches the natural frequency of the side-lead angle but not exactly the off-lead angle. The QUAD lift system is a coupled system, so other terms have an influence on the natural frequency as well. Since there are large off-lead and side-lead angles for certain frequencies, the application of tugger lines could be an improvement to prevent these angles. The method to apply tugger lines and the results on the motions will be discussed further on in section 4-7.

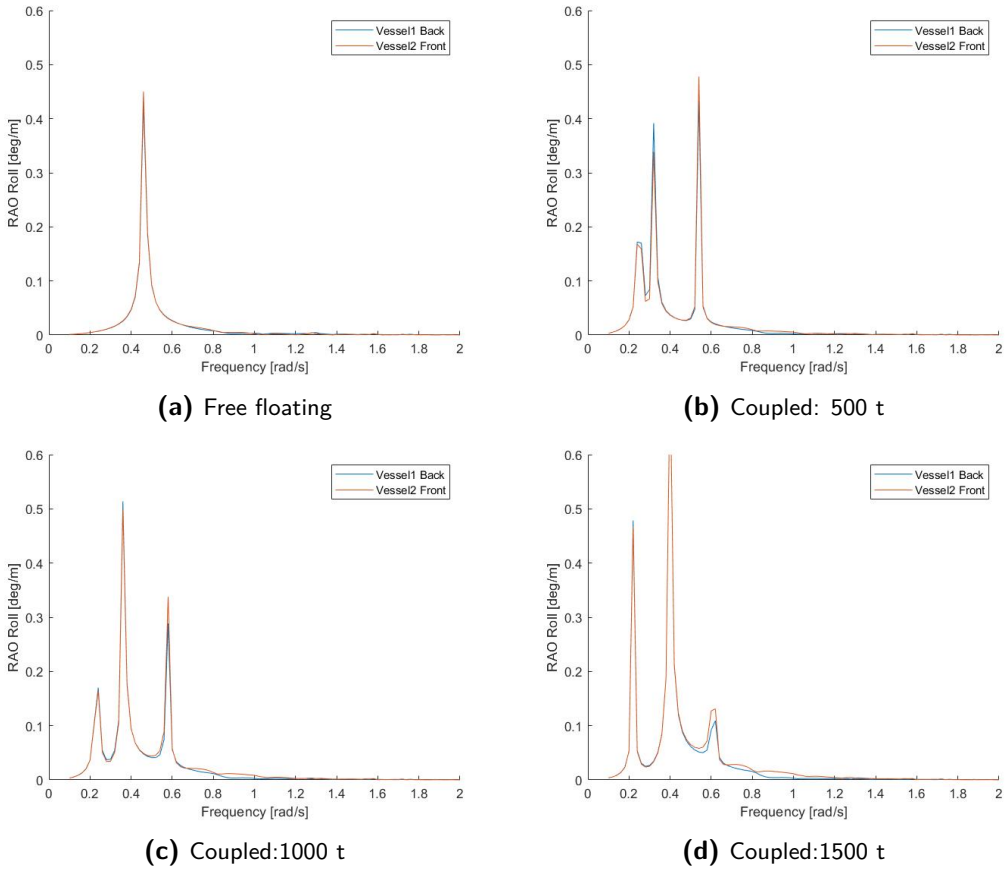

(a) Free floating

(b) Coupled: 500 t

(c) Coupled:1000 t

(d) Coupled:1500 t

Figure 4-9: Roll Responses for vessels in beam waves for different load conditions. The vessel to vessel distance is 40 m.

4-5-3 Vessel Roll Response

The lift has a large effect of the vessel roll motion. For the free floating vessels in beam waves, the roll motion is small except around the natural frequency at which a peak occur, shown in Figure 4-9a. When the motion is coupled, new peaks occur at different frequencies. The stiffness matrix of the QUAD Lift couples the roll motion to other degrees of freedom which leads to responses shown in Figure 4-9b, Figure 4-9c and Figure 4-9d. The mass of the load has an effect on the location of the CoG, which is directly linked to the vessel roll stiffness. Change of this term leads to a shift in the location of the peaks. The occurrence of new peaks in the roll response of the vessel is important for the analysis of the workability, which will be further elaborated in the next chapter.

4-5-4 Dynamic crane forces

The dynamic forces on each crane during the QUAD Lift are expressed as the total crane stiffness K times the relative displacement of each crane tip and the load attachment points. This vertical displacement can be calculated by the application of the transformation matrix on the RAO's on the vessels and load. The equation to calculate the dynamic crane force is

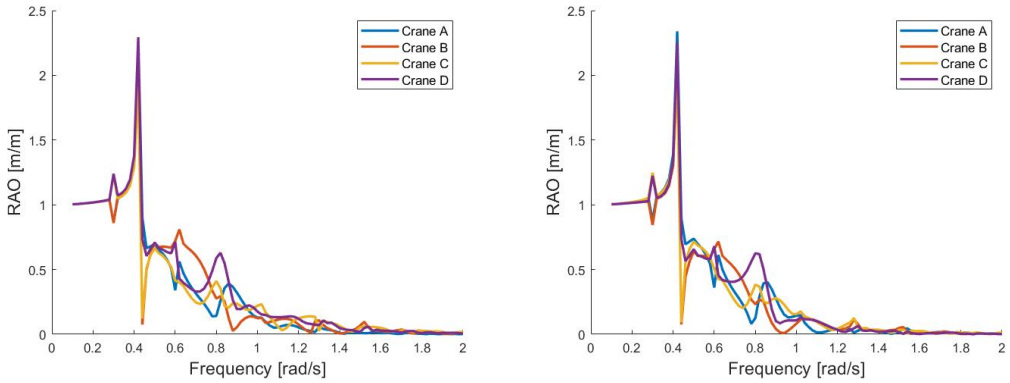

(a) Vertical response of crane tips **(b)** Vertical response of load attachment points

Figure 4-10: Vertical response of crane tips and load attachment points in QUAD Lift. The vessels are in head waves.

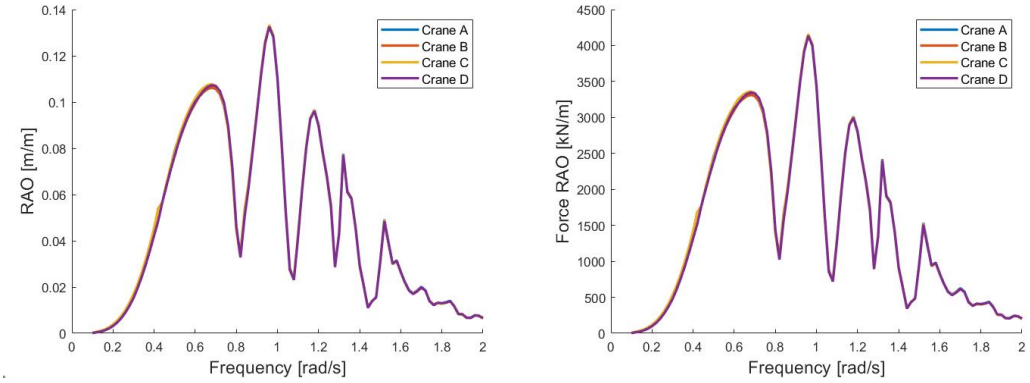

(a) Vertical elongation of the crane and crane cable **(b)** Vertical crane forces

Figure 4-11: Elongation and elongation forces of cranes and cables in QUAD Lift. The vessels are in head waves.

expressed as:

$$F_{dyn_{A,..,D}} = K \cdot (\Delta z_{A,..,D} - \Delta z_{L,A,..,D}) = K \cdot \Delta Z_{A,..,D} \tag{4-27}$$

The vertical response of each of the crane tips and attachment points $A, .., D$ are shown in Figure 4-10. From the figures it can be seen that there is a large influence of the roll response of the vessels. The vessel roll RAO is shown in Figure 4-6d. When the vessels roll, of course the crane tip will have a large vertical offset, since the crane tips are at a large vertical distance from the vessel origin.
The vertical responses of the cranes and corresponding attachment point are pretty similar. The difference in response is equal to the elongation of the cable shown in Figure 4-11. This elongation leads to large crane forces since the stiffness of the cranes is large. These vertical force RAO's of the cranes can be used to calculate the final dynamic force in the cranes by application of the sea-spectrum.

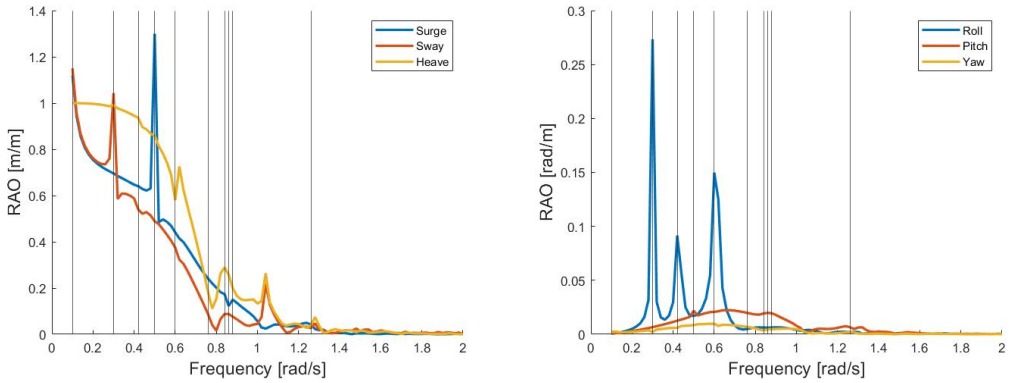

(a) Translational RAO's vessel **(b)** Rotational RAO's vessel

Figure 4-12: RAO's vessel during QUAD Lift including natural frequencies(vertical lines). The vessels are subjected to quarter waves.

4-6 Coupled Natural Frequencies

The natural frequencies of the system indicate at which frequencies resonance resonance peaks could occur. As written in section 3-6 the natural frequencies for the coupled QUAD Lift system can be calculated by:

$$\left(\mathbf{C} - \omega_n^2 \left(\mathbf{M} + \mathbf{A}\left(\omega_n\right)\right)\right) \vec{v} = 0 \tag{4-28}$$

This equation will give the natural frequencies ω_n and eigenvectors $\vec{v}$ of the coupled equation. The eigenvectors indicate the ratio of response between different degrees of freedom at the different natural frequencies in the system. However, the translations and rotations have different units. The rotations are given in radians which is quite a large unit compared to the translational unit which is given in meters. Therefore, the rotational values of the eigenvectors are expressed in degrees such that it gives a better comparison between the translational motions. The natural frequencies of the QUAD lift system are given in table 4-4. Based on the number of degrees of freedom 18 natural frequencies could be expected. However, all the natural frequencies are calculated with a corresponding added mass term which depends also on the frequency. Therefore, only the natural frequencies which have a matching added mass term are taking into account. The other natural frequencies of the system lay outside the region of the frequencies considered in this analysis. (0.1 till 2 rad/s)

Figure 4-12 gives an indication of the effect of the natural frequencies on the responses the vessel and load. The effect of the natural frequencies are visible in the different responses since the hydrodynamic as the hydrostatic matrices are coupled.

The normalized eigenvectors of the system are shown in Figure 4-13. The horizontal axis indicates the corresponding DoF. To create a better overview, the natural frequencies are divided in two sets of 5 and plotted in different figures. The subscripts 1,2 and L indicate the two vessels and load respectively. The 1^{st} natural frequency is strongly linked to the surge and yaw motions of the vessels.(DoF: 1,6,7 and 12) Both the DP-system and QUAD Lift coupling create this low frequent natural frequency. The 2^{nd} and 3^{rd} natural frequencies are linked to the roll motions of both the vessels and the load. The 3^{rd} natural frequency is also linked to the heave of the load. This could be explained by the direct connection between the roll and

Natural Frequency	Frequency [rad/s]
1	0.10
2	0.30
3	0.42
4	0.50
5	0.60
6	0.76
7	0.84
8	0.86
9	0.88
10	1.26

Table 4-4: Natural Frequencies QUAD Lift

the vertical displacement of the load. If the vessel rolls, the crane tip will have a large vertical displacement (since it is positioned at a large distance from the CoG), which creates a vertical displacement of the load. The 4^{th} and 5^{th} natural frequencies have large eigenvectors in the surge and sway motions of the load.(DoF: 13 and 14) Large peaks at these natural frequencies are clearly visible in the horizontal response plots in Figure 4-8. For the 4^{th} and 5^{th} natural frequencies, there is a small coupling between the the surge and sway motions of the vessels and the load. (DoF: 1,2,7,8,13 and 14) Since the horizontal load displacements are relative large, the effect of these natural frequencies are still visible in the horizontal response plots of the vessel in Figure 4-12b. The fifth natural frequency shows also large coupling between the sway of the load and roll of both the vessels.
The 7^{th} and 8^{th} natural frequencies have coupling between the heave and pitch motions of both the vessels and the load. (DoF: 3,5,9,11,15,17) The higher frequencies have a small effect on the motions and are not clearly visible in the response plots.

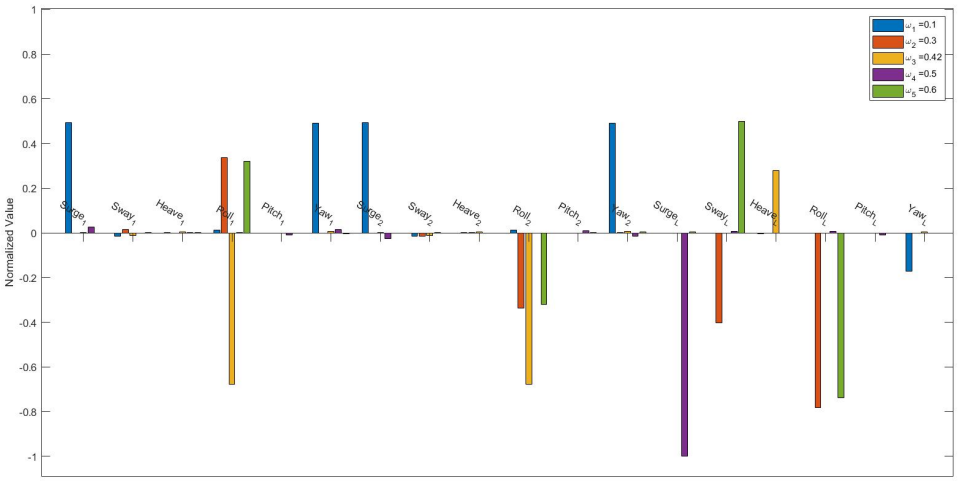

(a) Eigenvectors for each DoF of first set of 5 natural frequencies.

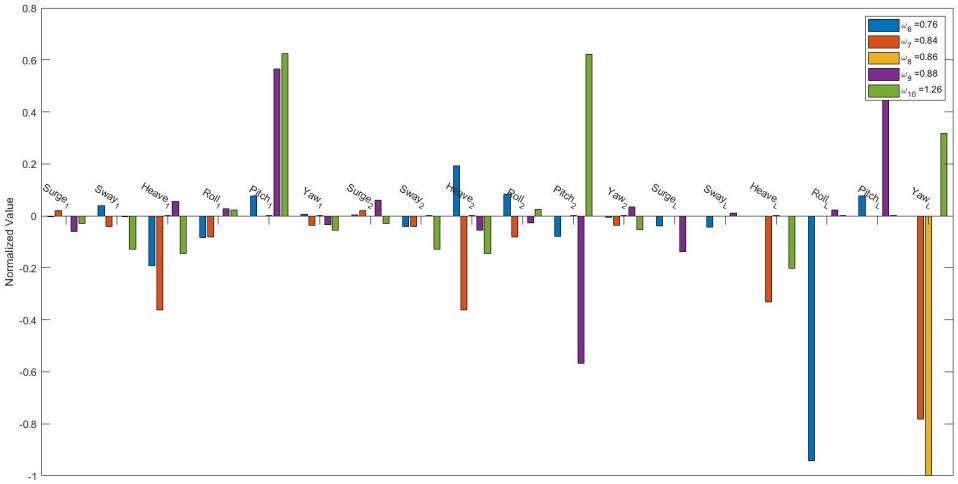

(b) Eigenvectors for each DoF of second set of 5 natural frequencies.

Figure 4-13: Eigenvectors for the 10 natural frequencies. The subscripts added to DoF on the x-axis indicate the DoF for the different bodies, 1: vessel 1, 2: vessel 2 and L: the load.

4-7 Tugger lines

As shown in Figure 4-8, the horizontal load responses are quite large for certain frequencies. Large displacements of the load is something which needs to be prevented during a lift for certain reasons: Large motions of the load could directly lead to unsafe situations and in collisions between the load and the vessel. The horizontal motions of the load are also coupled to the vessel motions, as shown by the eigenvalues in the previous section. Therefore, the load motions could create large vessel motions which makes it unsafe to perform an offshore lift.
A solution to prevent the horizontal load motions is the application of tugger lines. The tugger lines connect the load to the vessel. These lines could be attached to the load by padeyes. At the vessel the lines can be connected to tugger winches. These tugger winches care for the tension in the wires which prevents the lines from falling slack. In case of slack lines, slap loads (shock loads) could occur which could lead to really large forces and unsafe situations.

4-7-1 Tug method

The tugger lines are modelled as springs with a constant stiffness. It is assumed that there is no dissipation of energy via damping and that non-linearities in the lines are neglected. Just like the crane cables, the effect of mass of the lines is neglected as well. The axial stiffness of the lines depend on the type of material, the diameter of the lines and if the lines have a core. The axial stiffnesses of different ropes are formulated by Orcina based on the HER Group Marine Equipment & Wire Rope Handbook: [14]

$$\text{axial stiffness (AE)} = \begin{cases} 1.09e6 \cdot d^2 \text{ kN} & \text{for polyester ropes} \\ 1.06e6 \cdot d^2 \text{ kN} & \text{for polypropylene ropes} \\ 3.67e7 \cdot d^2 \text{ kN} & \text{for wire rope with fibre core} \\ 4.04e7 \cdot d^2 \text{ kN} & \text{for wire rope with wire core} \end{cases} \tag{4-29}$$

in which d is the nominal wire diameter. The wires with the core will give a considerable higher stiffness value than the fibre ropes. Since the diameter of the lines are bounded by the winches, different materials can be used to create another tugger line stiffness. The diameters of common used tugger lines can vary between 0.032 and 0.055 m. [13, 21] Therefore, the stiffness of the tugger line can vary in the range of 10 and 10000 kN/m, depending on the material properties and the line length of the tuggers. This large spread in stiffness values means that there is the freedom and possibility to look into the effects of different stiffness values.
The tugger lines are pre-tensioned by the use of winches. There are basically two types of controlling the winches. The first is a fixed tugger winch. The fixed tugger winch behaves as a passive system which pre-tension the line and will be put on a brake. A problem with fixed tugger winches is that the forces in the lines can become really large. If the load moves, it will directly lead to an elongation of the tugger line which requisites a large capacity of the line.
The second method to control the winch is by the constant tension method. The winch is set such that it delivers a constant tension in the line. This means that in case of motion

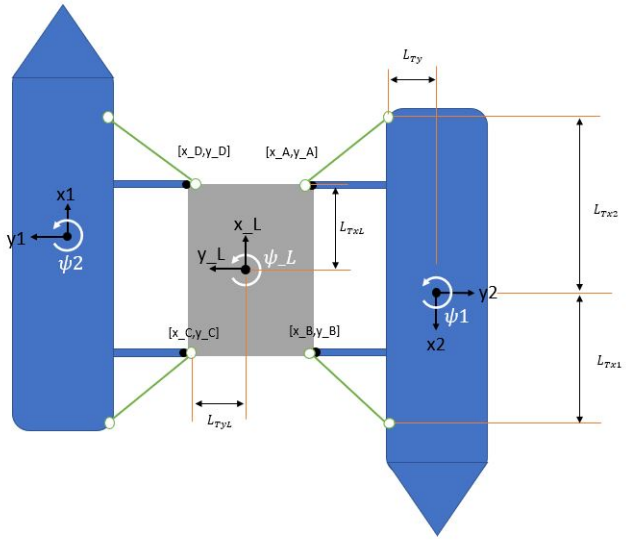

Figure 4-14: Top view of QUAD lift including green tugger lines.

of the load or vessel, the winch will be activated and will react such that the tension in the line is constant. A problem however is that the reaction of the winch is often delayed with respect to the motion of the load system. Therefore, the tension will fluctuate around the rated value.
In this analysis the working principal of a fixed winch is imitated since the line stiffness is a constant value, independent of the load motion.

4-7-2 Tugger line lay-out

The attachment points of the tugger lines on the vessel and load will have an influence on the effectiveness of the tuggers. The stiffness of the tugger line in a certain translational direction x, y, z depends on the length of the tugger line in this direction:

$$K_{tug_{x,y,z}} = K_{tug} \cdot \frac{L_{tug_{x,y,z}}}{L_{tug}} \tag{4-30}$$

in which K_{tug} is the stiffness of the tugger line, $L_{tug_{x,y,z}}$ is the length of the line in each translational direction, respectively. L_{tug} is the total tugger line length. This length can be calculated by:

$$L_{tug} = \sqrt{L_{tug_x}^2 + L_{tug_y}^2 + L_{tug_z}^2} \tag{4-31}$$

Since the tugger lines have only a stiffness in a certain direction if it bridges this direction, the tugger line lay-out shown in Figure 4-14 is chosen. The green diagonal tugger lines connect the vessel and the load such that it can prevent motion of the load in both horizontal directions. As shown in Figure 4-15, the tugger lines are attached to the deck of the vessel and the top of the load. Depending on the crane cable length, the tugger lines will also give a stiffness in the vertical direction.

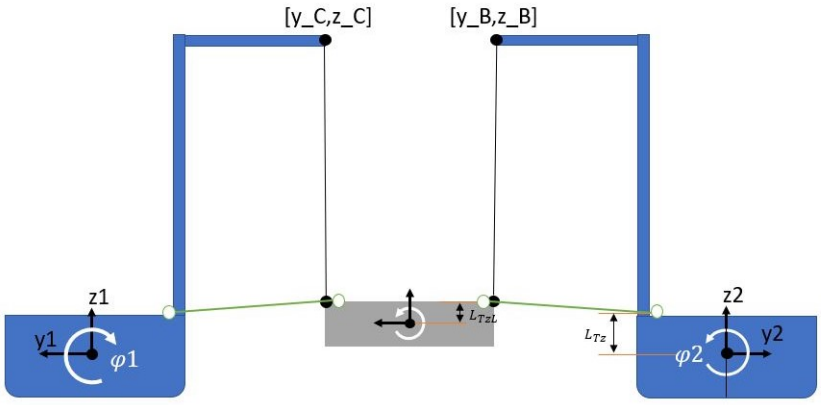

Figure 4-15: Front view of QUAD lift including green tugger lines.

4-7-3 Tugger line model

Just like the derivation of the QUAD Lifting model, use is made of the Lagrange method. Only stiffness terms are added to the system, so the Lagrange equation will result in a equivalent stiffness tugger matrix. The derivation starts by the definition of the motion of the attachment points $A, .., D$ of the tugger lines at the vessels written in the generalized values. The y and z position of each tugger winch at the vessel is at a distance L_{Ty} and L_{Tz} from the origin. The x position of the front and aft winch are located at L_{Tx1} and L_{Tx2}, respectively.

$$\begin{aligned}
\Delta x_{tug,A} &= x_2 + L_{Tz} \cdot \theta_2 + L_{Ty} \cdot \psi_2 \\
\Delta x_{tug,B} &= x_2 + L_{Tz} \cdot \theta_2 + L_{Ty} \cdot \psi_2 \\
\Delta x_{tug,C} &= x_1 + L_{Tz} \cdot \theta_1 + L_{Ty} \cdot \psi_1 \\
\Delta x_{tug,D} &= x_1 + L_{Tz} \cdot \theta_1 + L_{Ty} \cdot \psi_1
\end{aligned}$$

$$\begin{aligned}
\Delta y_{tug,A} &= y_2 - L_{Tz} \cdot \phi_2 - L_{Tx2} \cdot \psi_2 \\
\Delta y_{tug,B} &= y_2 - L_{Tz} \cdot \phi_2 + L_{Tx1} \cdot \psi_2 \\
\Delta y_{tug,C} &= y_1 - L_{Tz} \cdot \phi_1 - L_{Tx2} \cdot \psi_1 \\
\Delta y_{tug,D} &= y_1 - L_{Tz} \cdot \phi_1 + L_{Tx1} \cdot \psi_1
\end{aligned} \tag{4-32}$$

$$\begin{aligned}
\Delta z_{tug,A} &= z_2 - L_{Ty} \cdot \phi_2 + L_{Tx2} \cdot \theta_2 \\
\Delta z_{tug,B} &= z_2 - L_{Ty} \cdot \phi_2 - L_{Tx1} \cdot \theta_2 \\
\Delta z_{tug,C} &= z_1 - L_{Ty} \cdot \phi_1 + L_{Tx2} \cdot \theta_1 \\
\Delta z_{tug,D} &= z_1 - L_{Ty} \cdot \phi_1 - L_{Tx1} \cdot \theta_1
\end{aligned}$$

Also the attachment points of the load are described in the generalized coordinates. The padeyes of the load are located at about the same positions as the attachment points of the crane cable. Therefore, the positions are already given by eq. (4-19). The elongation of the

tugger lines $(A, .., D)$ in each translational direction can be written as:

$$\begin{aligned}
\Delta X_{tug,A,B} &= \Delta x_{tug,A,B} + \Delta x_{L,A,B} \\
\Delta Y_{tug,A,B} &= \Delta y_{tug,A,B} + \Delta y_{L,A,B} \\
\Delta X_{tug,C,D} &= \Delta x_{tug,C,D} - \Delta x_{L,C,D} \\
\Delta Y_{tug,C,D} &= \Delta y_{tug,C,D} - \Delta y_{L,D,C} \\
\Delta Z_{tug,A,..,D} &= \Delta z_{tug,A,..,D} - \Delta z_{L,A,..,D}
\end{aligned} \tag{4-33}$$

Since there is no addition of kinetic energy but only potential energy, the Lagrangian can be written as:

$$L = -V = 0.5K_{tug_x}X^2_{A,..,D} + 0.5K_{tug_y}Y^2_{A,..,D} + 0.5K_{tug_z}Z^2_{A,..,D} \tag{4-34}$$

The equations of motion are obtained by application of eq. (4-23). Again, Maple is used to determine the resulting tugger stiffness matix, $\mathbf{C_{tug}}$. The addition of the tugger lines to the QUAD lift system will result in the following new equation of motion:

$$\left(-\omega^2 \left(\mathbf{M} + \mathbf{A}(\omega) + \mathbf{M_L}\right) + i\omega\mathbf{B}(\omega) + \mathbf{C} + \mathbf{C_L} + \mathbf{C_{tug}}\right)\vec{X} = \vec{F}(\omega) \tag{4-35}$$

4-7-4 Tugger line stiffness analysis

The stiffness of the tugger lines can have a large effect on the behavior of the system. The stiffness values will influence the position of the natural frequencies. A increased stiffness value will normally shift the natural frequencies to a larger values. In terms of workability this is normally an unfavourable condition since the JONSWAP spectrum has a larger probability in the higher frequency region. On the other hand, increased stiffness terms can decrease the amplitude of the motion which could increase the workability. To perform a optimal and safe lift, it is necessary to look into the effect of different tugger lines stiffness. To give a clear overview of the effects of the tugger lines, different low stiffness terms are analysed first. Thereafter, the effects of larger stiffness terms of tugger lines are analysed.

Small stiffness values: Polypropylene wires

The relative low stiffness values of the tugger lines are: 30, 50, 100 and 200 kN/m. These stiffness values could be achieved by the application of polypropylene wires. The analysis is executed for the QUAD Lift configuration, given in Table 4-1 and Table 4-2. The QUAD Lift is analysed in quarter waves, since quarter waves responses tell something about the behaviour of the vessel in both horizontal directions. The tugger line parameters are given in Table 4-5.

Figure 4-16 shows the horizontal response(surge and sway) of the load for different tugger stiffnesses. The vertical black lines indicate the natural frequencies with the large eigenvector value for the horizontal motions of the load. In case of surge of the load, there is only one natural frequency for each tugger stiffness related to the large response of the horizontal motion of the load. With respect to the load sway motions, large responses occur at two natural frequencies. For both the surge and sway response of the load, a larger tugger stiffness shifts the natural frequency peaks to the higher frequencies. The natural frequencies related

Parameter	Symbol	Value
Pos. Winch A	$(L_{Tx2}, L_{Ty}, L_{Tz})$	(38,13.25,10) [m]
Pos. Winch B	$(L_{Tx1}, L_{Ty}, L_{Tz})$	(30,13.25,10) [m]
Dimensions tugger lines	$(L_{tug_x}, L_{tug_y}, L_{tug_z})$	(10,10,10) [m]
Length tugger lines	L_{tug}	17.32 [m]

Table 4-5: Tugger line parameters

Tugger Stiffness [kN/m]	Surge Load		Sway Load	
	ω_n [rad/s]	Crit. damping [kg/s]	ω_n [rad/s]	Crit. damping [kg/s]
0	0.5	1.38e7	0.3 & 0.6	1.11e7 & 1.27e7
30	0.58	1.46e7	0.32 & 0.66	1.28e7 & 1.05e7
50	0.62	1.51e7	0.34 & 0.7	1.09e7 & 1.02e7
100	0.72	1.64e7	0.36 & 0.78	1.01e7 & 1.14e7
200	0.9	1.73e7	0.38 & 0.94	9.8e6 & 1.37e7

Table 4-6: Natural frequencies and critical damping related to the horizontal load motions for different tugger stiffnesses.

to the surge and sway motions are given in Table 4-6. On average, a decrease of the peak values can be seen. Possible explanations for this trend are the increase of added mass or radiation damping at these frequencies. Also, the wave forces (diffraction and Froude Krylov) at the different natural frequencies influence the peak values.
The critical damping values of the horizontal load motion are calculated by:

$$C_c = 2\sqrt{\mathbf{K^i M^i}} \tag{4-36}$$

in which $\mathbf{K^i}$ and $\mathbf{M^i}$ are the diagonal generalized stiffness and mass matrices calculated by the frequency dependent eigenvector matrix $\mathbf{Q}$:

$$\begin{aligned} \mathbf{K^i} &= \mathbf{Q^T K Q} \text{ for which } \mathbf{K} = \mathbf{C} + \mathbf{C_L} + \mathbf{C_T} \\ \mathbf{K^i} &= \mathbf{Q^T M_s Q} \text{ for which } \mathbf{M_s} = \mathbf{M} + \mathbf{A}(\omega) + \mathbf{M_L} \end{aligned} \tag{4-37}$$

Since both $\mathbf{Q}$ and $\mathbf{A}(\omega)$ depend on the frequency of the system, there are different critical damping values for each natural frequency in the system. Increasing the tugger stiffness will normally increase the critical damping of the system since stiffness is added to the system. However, since the critical damping for the QUAD lift depends on the frequency dependent added mass, the critical damping can also decrease if stiffness is added to the system. This is shown in the critical damping for the load sway motion in Table 4-6

If we now look into the vessel roll response an interesting trend can be seen. Figure 4-17 shows the vessel roll response for different tugger line stiffness values. The natural frequency peak of the roll response without tugger lines(blue line) at 0.6 rad/s shifts to the higher frequencies when higher tugger stiffness are applied but the value of this peak will almost distinguish. The first peak of the vessel roll response shifts also the the right. In contrast to the third peak, the response increases for this peak. However, since this peak is still at relative low frequencies, the influence on the significant motions and workability could be limited.

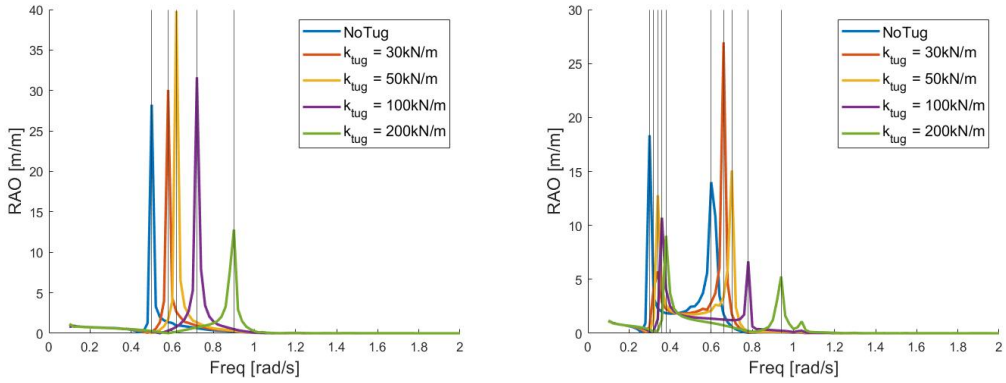

(a) Load surge RAO **(b)** Load sway RAO

Figure 4-16: Load RAO's for different low stiffness values of tugger lines. The vessels are in quarter waves.

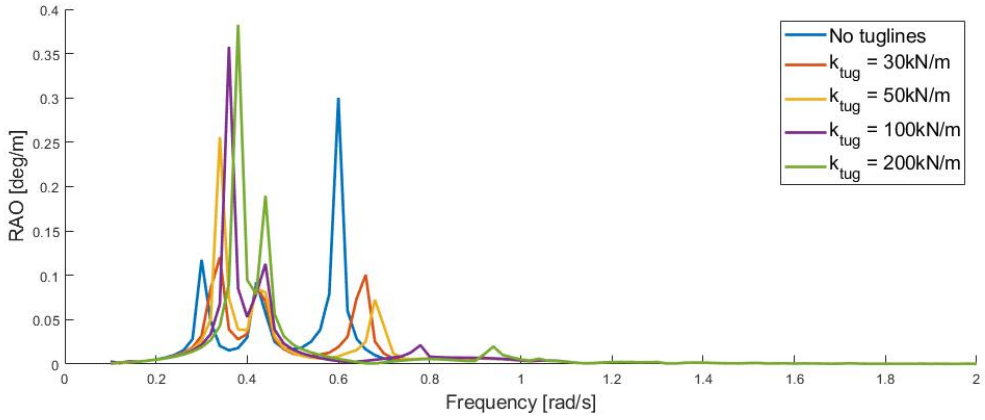

Figure 4-17: Vessel Roll RAO for different small stiffness values of tugger lines. The vessels are in quarter waves.

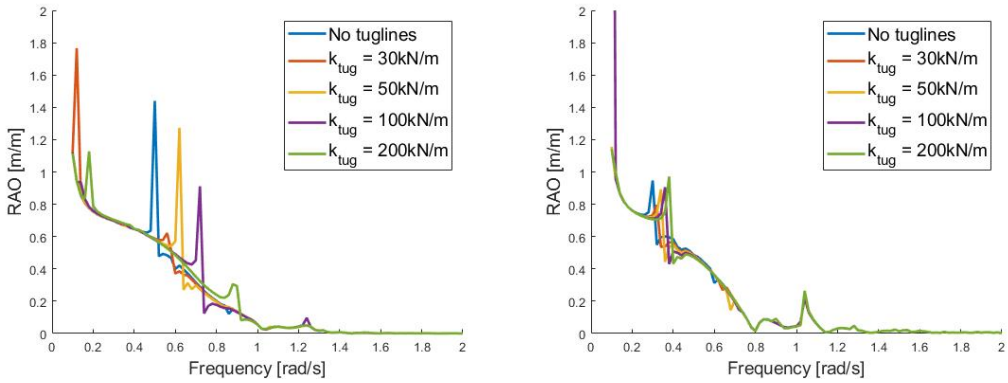

(a) Surge RAO **(b)** Sway RAO

Figure 4-18: Vessel RAO's for different small stiffness values of tugger lines. The vessels are in quarter waves.

The tugger lines have an effect on the horizontal motions of the vessel as well. Since the horizontal motions are directly coupled via the tugger lines, the shift of the natural frequency peaks should also be visbile in the vessel response. The horizontal vessel response plots are shown in Figure 4-18. The peak of the surge of the load(Figure 4-16a) is clearly coupled to the surge response of the vessel. A shift of this peak by the application of the tugger lines can be seen. Also for the first peak of the sway motion of the load this principal applies. The small shift of this peak can be seen in the sway motion of the load. However, the second peak of the load sway response(Figure 4-16b) is almost not visible in the vessel sway response. An explanation for the absence of this peak in the vessel sway response is that this peak is coupled to the roll response of the vessel. The vessel roll response results of course in a horizontal motion of the load but not directly in a horizontal motion of the vessel. A more elobarated analysis of this phenomenon will be given in the section 4-7-5. If stiffer tugger lines are applied two things could happen: the horizontal motions of the load will decrease or in case there is still a horizontal motion of the load there will be a coupling to the vessel.

Large stiffness values: Steel wires

Now the low stiffness values of the tugger lines are analysed, the principals of the effects are known. Since the loads during the QUAD lift could have large weights, the application of steel tugger lines with large stiffness values could be considered. For these large stiffness values, the connection between the load and the vessels will be more or less a rigid connection. Small relative motions between the vessels and load will give large resulting forces in the tugger lines. When an active control tugger winch is applied, continuous adaptation of the line lenght will happen to prevent to large tensions in the line. Since this study does not imply tugger control, the line length will be a constant. Only the direct effects of the fixed line length and stiffness on the motion are analysed.
The values of stiffness in this large stiffness analysis are respectively 1000, 2000 and 4000 kN/m. The resulting effects of this stiffness values on the horizontal motion of the load are shown in Figure 4-19. The figures show the effect of the stiff tugger lines: the natural frequency peaks are almost complete distinguished from the response plots. In case of load

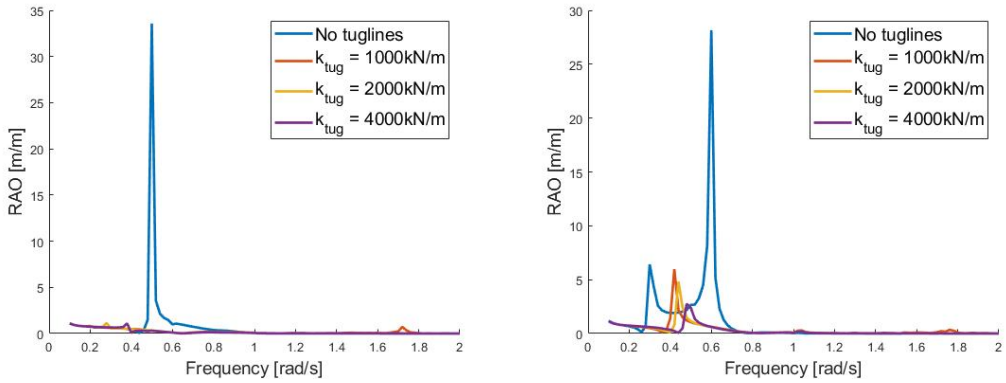

(a) Load surge RAO **(b)** Load sway RAO

Figure 4-19: Load RAO's for different large stiffness values of tugger lines. The vessels are in quarter waves.

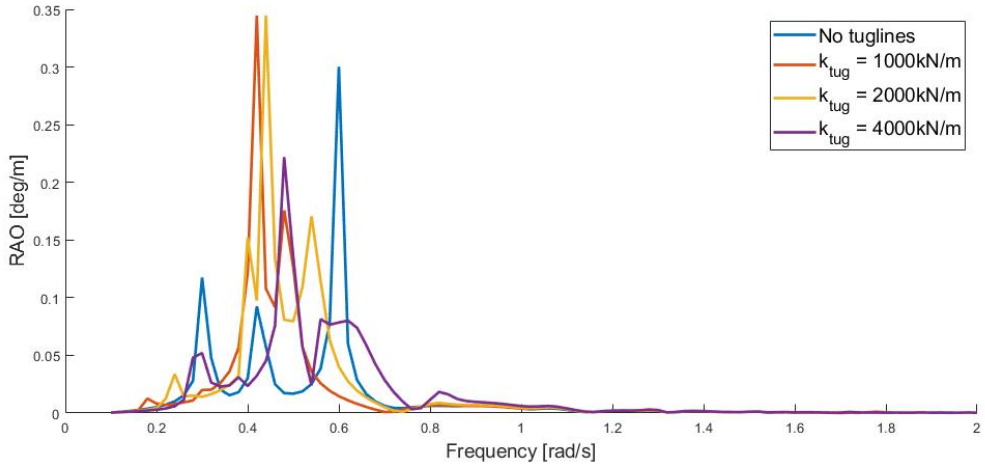

Figure 4-20: Vessel Roll RAO for different large stiffness values of tugger lines. The vessels are in quarter waves.

surge, the tugger lines dissapear the effect of the natural frequency of the surge motion. For load sway, the first peak of the response without tugger lines is still visible, although it is shifted to a larger frequency. The second peak is not visible in the response plot any more.

The roll response of the vessel shows a different behaviour than was shown in fig. 4-17 for the low stiffness. Figure 4-20 shows the roll response plots for the large stiffness values. Because of the large tugger line stiffness values, the lower natural frequencies peaks are shifted to the larger frequencies. For example, the roll response of the vessel with a tugger stiffness of 4000 kN/m (purple line in the figure) is relative large between 0.4 and 0.8 rad/s compared to the roll response of the vessel without tugger lines.

Another important observation in the analysis of the large stiffness values, is that the natural frequency of the horizontal motions of the vessel moves into the frequency analysis domain. Figure 3-19a already showed the influence of the DP-system on the response. The sway response increases when the frequency decreases. Since the DP system is modelled by hori-

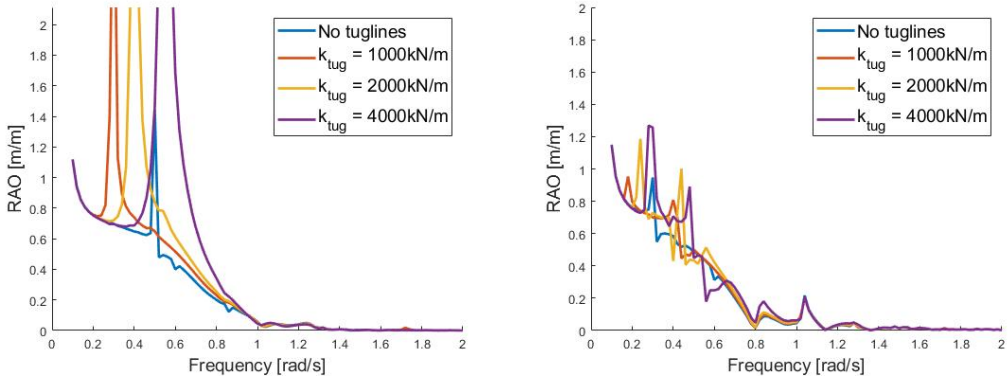

(a) Surge RAO **(b)** Sway RAO

Figure 4-21: Vessel RAO's for different large stiffness values of tugger lines. The vessels are in quarter waves.

zontal springs it adds stiffness terms to the equation of motion. These stiffness terms create a natural frequency for this motion which, since the DP system has a relative low stiffness, is at the low frequency region. However, if stiff tugger lines are applied, the natural frequencies of the horizontal motions of the vessels can shift into larger frequencies. In Figure 4-18 the natural frequencies of the vessel surge and sway motion are already visible and a shift of this natural frequency for larger stiffness values is shown. The effects of larger stiffness values on the horizontal motion of the vessels are shown in Figure 4-21. The tugger lines have a large effect on especially the surge motion of the vessel. The natural frequency of this motion shifts into the frequency bound of this analysis which creates really large peak values. The vessel sway response has a more limited character.
Since large horizontal motion of the vessel is something which should be prevented during the execution of the lift, the application of the stiff tugger lines is doubtable. Although it removes the large load motions, the vessel displacement responses are increased in both the surge and roll direction.

4-7-5 Natural Frequencies and Eigenvectors

Each different tugger line stiffness has its own set of natural frequencies and eigenvectors. Therefore, one small stiffness value and one large stiffness value is chosen for a elaborated analysis. These stiffness values are 200 kN/m and 1000 kN/m since, based on the response figures, these stiffness values produce the most preferable system responses. The natural frequencies of the different stiffness values are given in Table 4-7.

The first notable phenomenon is that some natural frequencies disappeared in the analysis with a larger tugger stiffness. Some of the natural frequencies are out of the spectrum bounds because of the increased stiffness. Also, the low natural frequencies for a tugger stiffness of 200 kN/m (0.12 and 0.16 rad/s) are shifted to larger values (0.18,0.2 and 0.3 rad/s, respectively).
Just for indication, the responses of the vessel and the natural frequencies are shown in Figure 4-22. To give a more clear view of all the responses, the roll RAO is given in [rad/m].

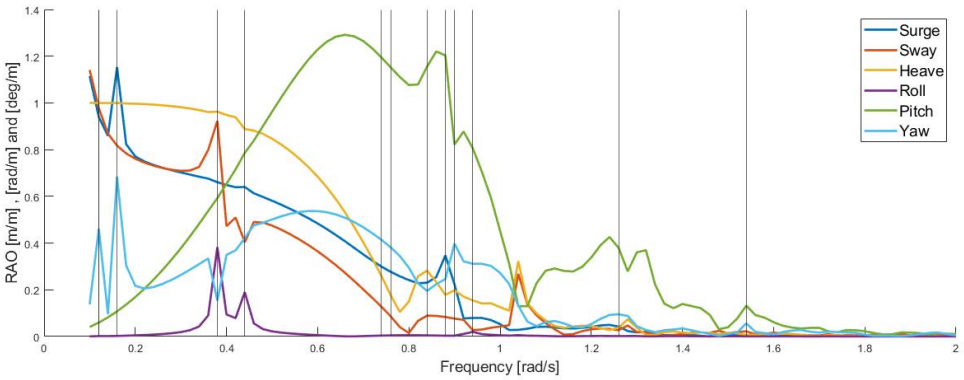

Figure 4-22: Vessel RAO's in a QUAD lift with tugger lines with a stiffness of 200 kN/m. The vertical black lines indicate the natural frequencies. The vessel is in quarter waves.

Natural Frequency	Freq. [rad/s] for $k_{tug} = 200$ [kN/m]	Freq. [rad/s] for $k_{tug} = 1000$ [kN/m]
1	0.12	0.18
2	0.16	0.2
3	0.38	0.3
4	0.44	0.42
5	0.74	0.48
6	0.76	0.76
7	0.84	0.84
8	0.88	0.88
9	0.90	1
10	0.94	1.74
11	1.26	1.76
12	1.54	-

Table 4-7: Natural Frequencies QUAD Lift with tugger lines with different stiffness values.

The other rotations are given in [deg/m]. The figure shows the coupling between the different vessel motions. Surge has coupled peaks matching with yaw (0.16 rad/s) and heave and pitch (0.88 rad/s). The sway motion has a clear coupling with the roll motion (0.38 and 0.44 rad/s).

In Figure 4-23 the eigenvectors for the different tugger line stiffnesses are shown. The first four natural frequencies for a stiffness of 200 kN/m ($\omega_1 : \omega_4$) have almost the same eigenvectors for the natural frequencies ($\omega_2 : \omega_5$) for a stiffness of 1000 kN/m. So only the natural frequencies have increased for the larger tugger stiffness. This confirms that the tugger line stiffness increases the natural frequencies and that the system shows the same behaviour at these larger frequencies.
The first natural frequency for a tugger stiffness of 1000 kN/m ($\omega 1 = 0.18 rad/s$) has large eigenvectors in the sway and roll motion of the vessels and the vertical motion of the load. This natural frequency is absent in the analysis with lower tugger stiffness. This was already discussed in the previous section 4-7-4. The large stiffness values shift the natural frequencies of the surge and sway motion of the vessel toward larger frequencies and into the frequency domain of this study. Therefore, a new natural frequency is visible in the analysis, since the lower limit starts at a frequency of 0.1 rad/s.

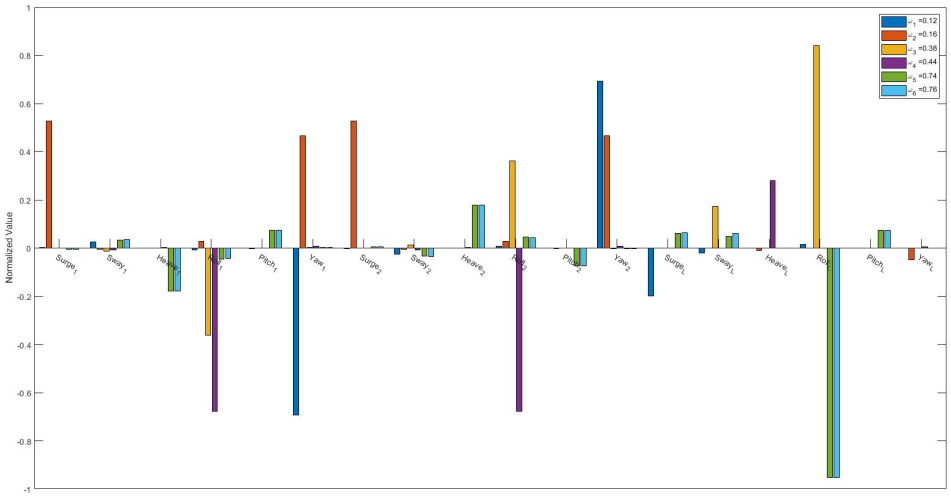

(a) Eigenvectors for each DoF of first set of 6 natural frequencies for a tugger stiffness of 200 kN/m.

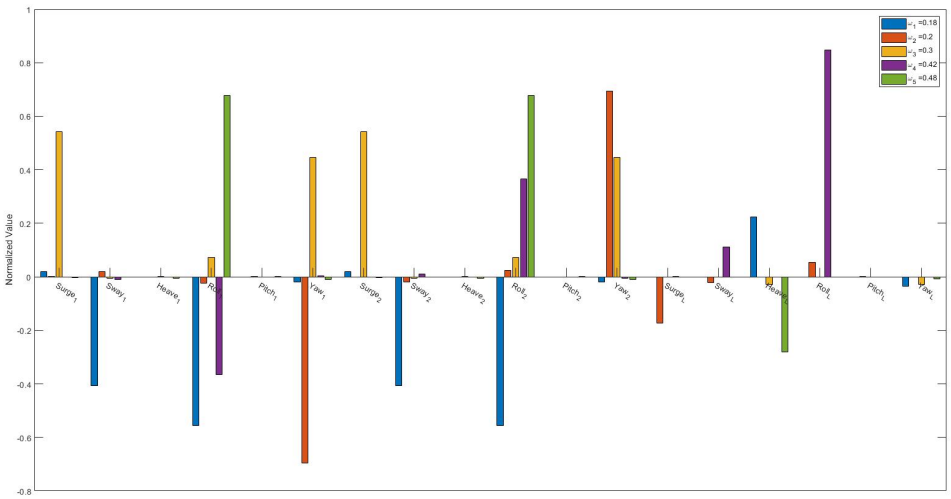

(b) Eigenvectors for each DoF of first set of 5 natural frequencies for a tugger stiffness of 1000 kN/m.

Figure 4-23: Eigenvectors for the first set of natural frequencies. The subscripts added to DoF on the x-axis indicate the DoF for the different bodies, 1: vessel 1, 2: vessel 2 and L: the load.

Chapter 5

Results: Parametric study and Workability

5-1 Introduction

Now the model is explained and analysed by the natural frequencies and eigenvectors, the results of the workability can be calculated. The workability is however, just a result for a certain parameter configuration. To create a good overview of the different stages of the Quad Lift, a parametric study will be executed in this chapter. Different examples of parameters are: cable length, tugger stiffness or load mass. For these parameters, the limiting SDA's are calculated for the different wave directions. These results will give an indication of the effects of these parameters on the system and the critical configurations in terms of workability.

5-2 Response Spectra

The RAO's of the system give the behaviour of the system for different set of wave frequencies and directions. The energy present at in different sea locations is given by a sea-spectrum. The response spectra is a energy spectrum of a certain body motion at a certain location. It is therefore formulated as the multiplication of a system response and the sea spectrum. For the determination of the workability a two-dimensional JONSWAP spectrum is used. This spectrum is not only a function of the wave frequencies but also a function of the wave directions. The formulation of this spectrum is explained in 2-2-1. The two-dimensional spectrum depends on the number of 100 frequencies and 8 different directions. Since the QUAD Lift analysis is symmetric, the behaviour of the vessels can be based on the behaviour of the second vessel. Therefore a 360 degree wave direction analysis can be done, based on 180 degree data.

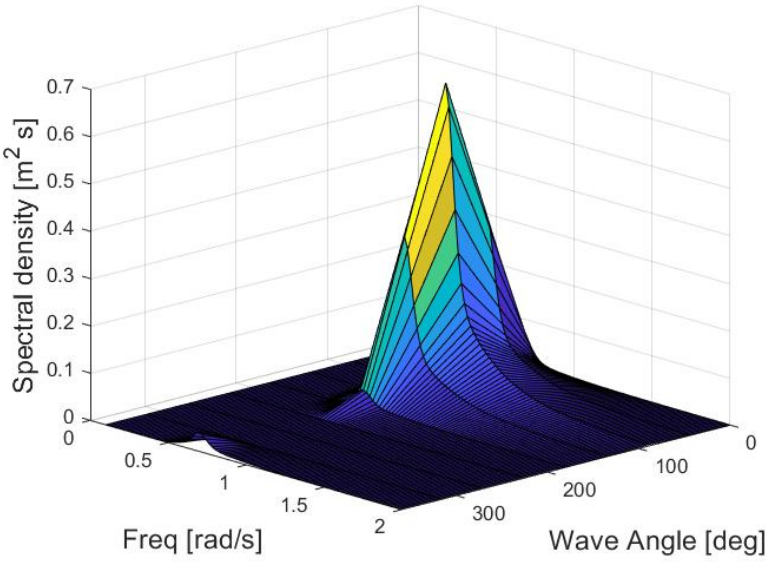

(a) Two-dimensional JONSWAP with a dominant direction of 90 degrees

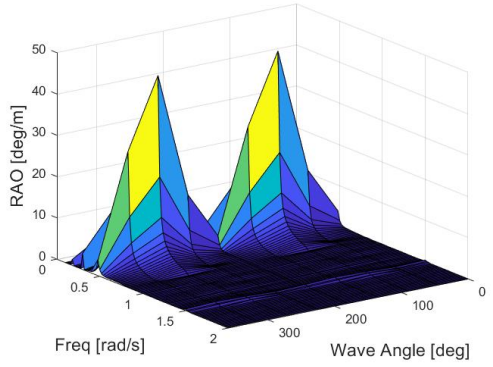

(b) Coupled Roll Response Fairplayer

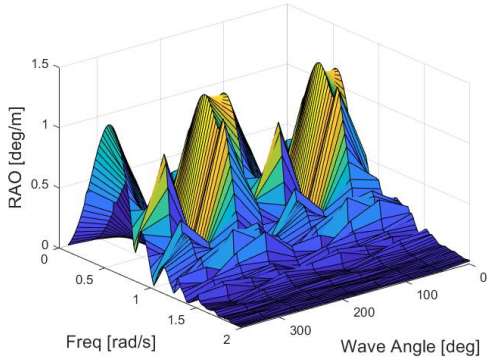

(c) Coupled Pitch Response Fairplayer

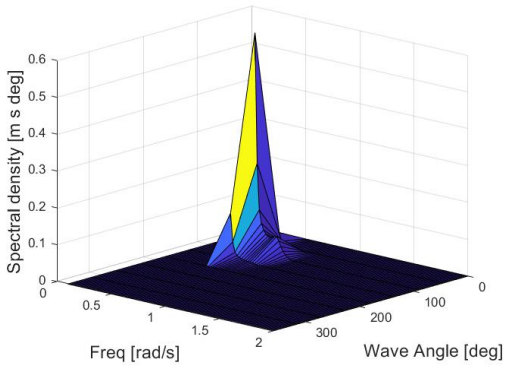

(d) Response spectra Roll Fairplayer

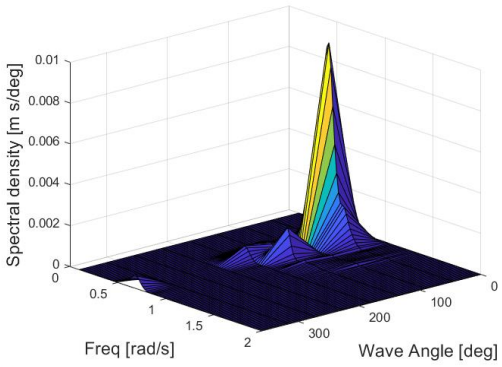

(e) Response spectra Pitch Fairplayer

Figure 5-1: Two dimensional response spectra for Fairplayer during QUAD Lift calculated by use of the JONSWAP spectrum with Hs = 2 m and Tp = 9 s and a dominant wave direction of 90 degrees

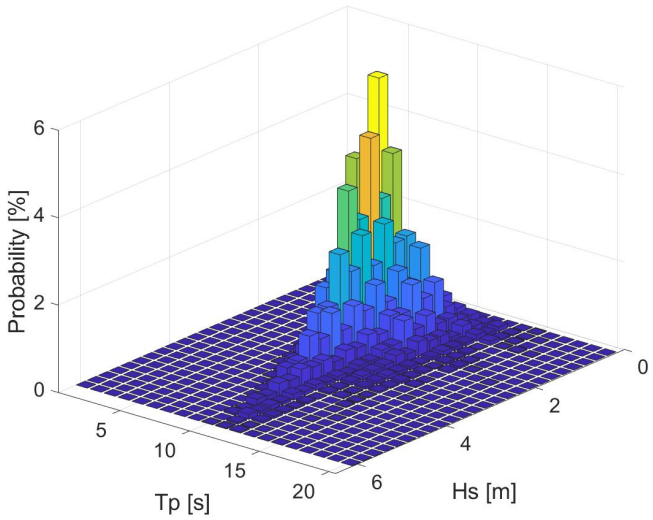

Figure 5-2: Probability of sea conditions at the Central North Sea as a function of specific significant wave height Hs and peak period Tp.

5-3 Parametric Study

When the response spectra of the different DoF are known, the SDA's of the motions of the vessel and load can be obtained. This section will shown the effect of different varying QUAD Lift parameters on the SDA of the motions and loads. The parametric study is performed for a sea condition with a significant wave height of 1.75 m and a peak period of 7 s. Similar conditions have a large probability of occurrence in the Central North Sea, based on the in-house scatter data from Jumbo Maritime as is shown in Figure 5-2. The complete scatter data table is shown in appendix C.

The SDA results are shown for different wave directions. This will give a indication of the influence of the direction of the waves. The parameters that change in this analysis are the load mass, the cable length and the tugger line stiffness. The calculations are executed for a load mass of 500, 1000 and 1500 ton. The crane cable length is set for 30 with steps of 5 m up to 45 m. Tugger line stiffness varies between 0 and 300 kN/m with steps of 100 kN/m. Linear interpolation is used to get analyse the effects of intermediate load masses and cable lengths. Since only 8 wave directions are considered, also linear interpolation is used to create a full 360 degrees result. The vessel to vessel distance is kept constant in this analysis and is equal to 40 m. Another gap distance requires a new diffraction calculation, since the hydrodynamic parameters will be different for another vessel configuration.
The vessel and load parameters for which the parametric study is performed are shown in Table 5-1. All four the cranes are in the same configuration, the same jib radius and the same vertical length between the crane tip and CoG. The different SDA results analysed in this section are the roll and pitch of the vessel, the side-lead and off-lead angles of the cranes and the force in the crane cables.
Since the parametric study is only executed for a single sea condition, the parametric results will only give a indication of the dependency of the SDA values on the different parameters

	Free Floating	QUAD Lift
Vessel mass $[kg]$	20048139	20048139
Draft $[m]$	7.5	7.5
VCOG $[m]$	9.6	9.6 - 11.04
GM $[m]$	3.09	3.09 - 1.65
Vessel Distances $[m]$	40	40
Crane tip z $[m]$	-	40
Jib Radius $[m]$	-	10
Cable length $[m]$	-	30 - 45
Load mass $[kg]$	-	500e3 - 1500e3
Load length $[m]$	-	48
Load width $[m]$	-	20
Load height $[m]$	-	10
Tugger line stiffness $[kN/m]$	-	0 - 4000e3

Table 5-1: Vessel and crane configurations for parametric and workability analysis. The cable length of the cranes and load masses change in the parametric analysis.

and the effect of the wave directions. The SDA results give however not a clear answer to the workability of the QUAD Lift. For some parametric configurations, the SDA values are far larger than the applicable limits, given in section 1-4. The next section, will give an answer to the workability of the QUAD lift.

5-3-1 Variation of Load mass

Vessel Roll and Pitch

In the first analysis, the load lifted during the QUAD lift is varied between 500 and 1500 tons. The cable length has a constant value of 40 m. The results show the vessel response without the addition of tugger lines. The SDA's of the vessel roll and pitch rotations are shown in Figure 5-3. The roll SDA is most dominant in the beam waves region, the pitch SDA has a dominant head direction. The vessel roll SDA increases for a larger load mass, the load mass does not have a big influence on the pitch SDA. For head waves, the roll SDA is very small with values of about 0.2 deg. In beam waves, the pitch SDA is small with values of about 0.4 deg.

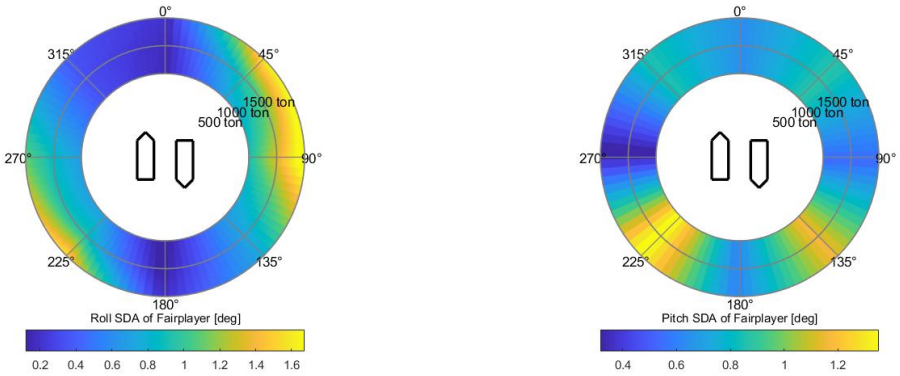

(a) Roll **(b)** Pitch

Figure 5-3: Polar plot of SDA of rotational motions of Fairplayer during QUAD Lift configuration for different loads. Tugger lines are not applied.

Crane side and off-lead angles and cable force

Figure 5-4 shows the side and off-lead angles of the crane. Both the side-lead angles and off-lead angles are too large. To decrease these angles, tugger lines need to be applied. The parametric change of the tugger line stiffness is shown given in section 5-3-2. Both these angles have the largest SDA's if the waves are coming from beam or quarter wave direction. Head waves causes smaller off-lead and side-lead angles.

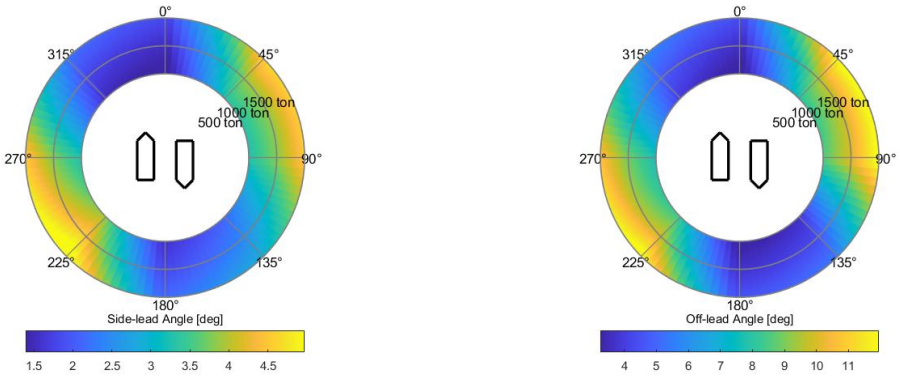

(a) Side-Lead angle **(b)** Off-lead angle

Figure 5-4: Polar plot of SDA of lead angles of Fairplayer during QUAD Lift configuration for different loads. Tugger lines are not applied.

The dynamic crane cable forces are shown in Figure 5-5. The crane cable forces are calculated by the elongation of the crane cables times the total stiffness of the cables. The forces are relative large in all wave directions. What can be seen is that the cable force does not depend largely on the applied load. The cable elongation is therefore, not directly caused by the mass of the load but the elongation is caused by the motion of the both vessels. Since these motion

create a different vertical response at the crane tips, the crane cables will be elongated, which creates the large cable forces.

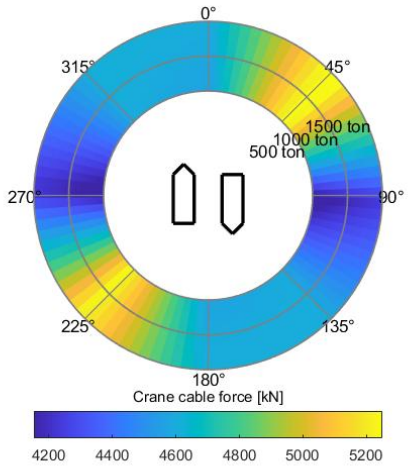

Figure 5-5: Polar plot of SDA of crane parameters during QUAD Lift for different loads. Tugger lines are not applied.

5-3-2 Variation of tugger stiffness values

The effect of tugger line stiffness is analysed to create a sufficient low SDA's for the lead angles. The lead angles as a function of the tugger line stiffness are shown in Figure 5-6. The mass of the load is 1000 ton and the cable length is 40 m. For larger tugger line stiffnesses (larger than 200 kN/m), the lead angles become small. This shows the effectiveness of the tugger lines. The tugger lines remove the large responses at higher frequencies of the load.

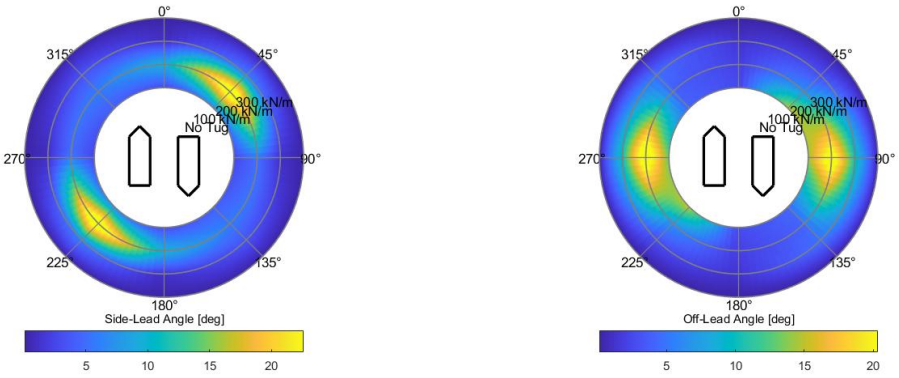

(a) Side-Lead angle **(b)** Off-lead angle

Figure 5-6: Polar plot of SDA of lead angles during QUAD Lift for different tugger lines stiffnesses.

5-3-3 Variation of cable length

During a lift, the cable length of the four cranes will change. The cable length has a large effect on the motion on the system. Not only the stiffness value of the cable line depends on this length, also the natural frequencies of the lead angles are related to the cable length. The cable length varies between 30 and 50 m. In Figure 5-7 the SDA values for the lead angles as a function of the cable length are shown. The load mass is again equal to 1000 ton. The tugger line stiffness is equal to 300 kN/m, since this showed a large decrease SDA value of the lead angles. The lead angles SDA increase if the cable length becomes shorter. The maximum lead angles SDA will happen if the QUAD lift is executed in quarter or beam waves.

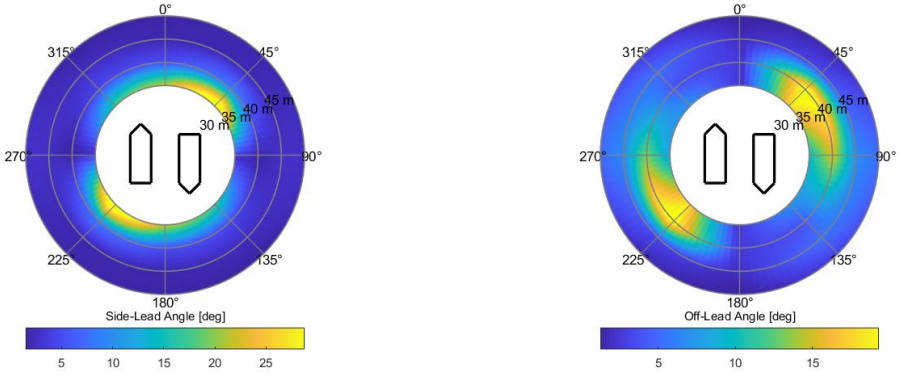

(a) Side-Lead angle **(b)** Off-lead angle

Figure 5-7: Polar plot of SDA of lead angles during QUAD Lift for different crane cable lengths.

Since the QUAD Lift system is a coupled system, the motions of the vessels will be, just as the lead angles, influenced by the crane cable length. In Figure 5-8 the vessel roll and pitch SDA's are shown. The roll of the vessels becomes larger if the cable length decreases. The pitch SDA has not a large dependency on the cable length.

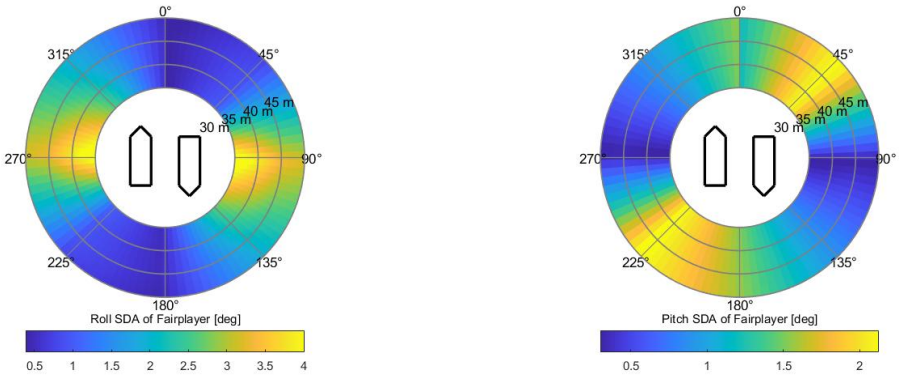

(a) Roll **(b)** Pitch

Figure 5-8: Polar plot of SDA of vessel rotations during QUAD Lift for different crane cable lengths.

5-4 Workability

The workability results indicate the percentage of the time at which a certain QUAD Lift configuration could be executed. If one of the QUAD lift motion SDA's in a certain sea-state exceeds one of the SDA limits, the QUAD lift is defined as not workable for this sea-state. The final percentage of the workability is based on the probability of occurrence of this sea-state in the Central North-Sea. Each workability calculation depends on a dominant wave direction. The workability of the QUAD lift is based on the following limiting SDA values of the vessel and load motions:

- Vessel Roll angle: 1.5 deg
- Vessel Pitch angle: 1.5 deg
- Vessel Roll + Pitch angle: 2.5 deg
- Crane Off-lead angle: 1 deg
- Crane Side-Lead angle: 2 deg

5-4-1 Free Floating Vessels

To compare the QUAD Lift workability, first the workability of the free-floating vessels is calculated. The vessel configuration is as given in Table 5-1. In this case only the motion of the vessels are considered, resulting in three different limiting SDA's: the vessel roll, the vessel pitch and the combined values of the roll and pitch. The workability of the Free-Floating vessels in both head and beam waves is shown in Figure 5-9. The left figure indicates the workability per sea-state, a certain peak period and a significant wave height. A green cell indicates that the SDA's are less than the limiting SDA's, so the situation is workable. A red cell indicates that one SDA is larger than the limiting SDA, so not workable. In head waves, the workability is equal to 84.24%. The bar graphs in Figure 5-10b and Figure 5-9d show the workability per SDA angle. For head waves, the workability is limited by the pitch response of the vessels. In beam waves, the workability decreases to 70.35%. Now, the roll response of the vessels is the limiting factor for the final workability.

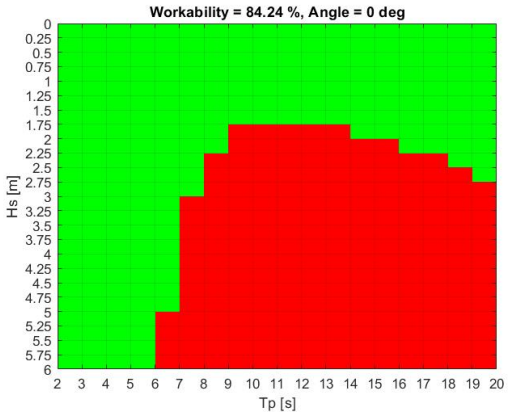

(a) Head Waves: Workability per sea state

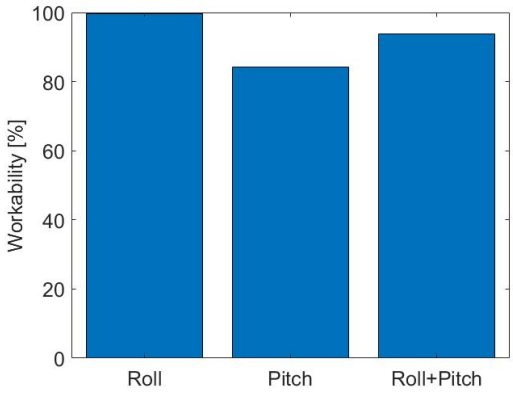

(b) Head Waves: Workability per SDA angle

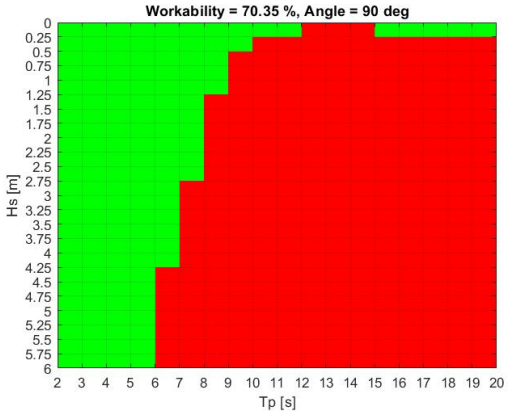

(c) Beam Waves: Workability per sea state

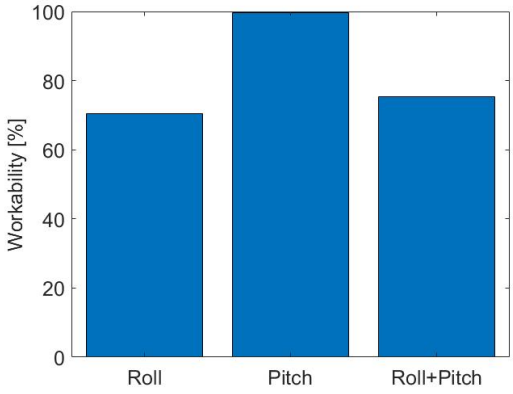

(d) Beam Waves: Workability per SDA angle

Figure 5-9: Workability results for free-floating vessels in beam waves. The green and red cells indicate a workable or not workable sea state, respectively.

5-4-2 QUAD Lift without tugger lines

To define the QUAD Lift as workable, also the off and side lead angles of the crane need to be below the limiting values. To give an indication of the importance of the tugger lines, the workability is calculated for a QUAD lift without tugger lines. The load mass is equal to 1000 ton, the cable length is 40 m.
Figure 5-10 shows the workability for the QUAD lift without the application of tugger lines. The workability is 21.38% and 9.08% in head and beam waves, respectively. This low workability is mainly caused by the off-lead angles as the bar plot show. The vessel rotations are not that large, therefore tugger lines need to be applied to decrease the large lead angles.

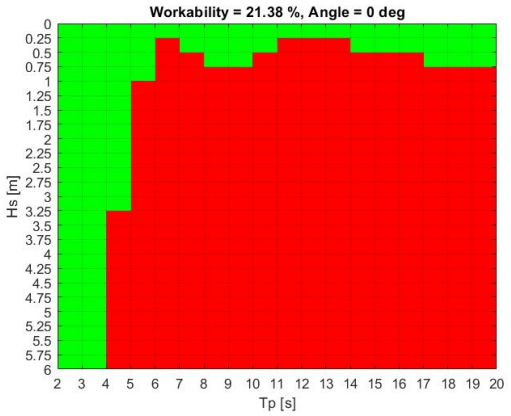

(a) Head Waves: Workability per sea state

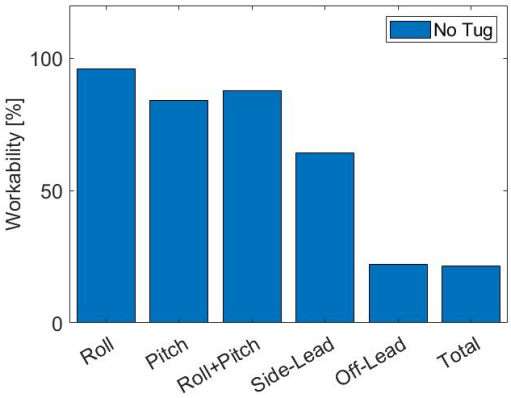

(b) Head Waves: Workability per SDA angle

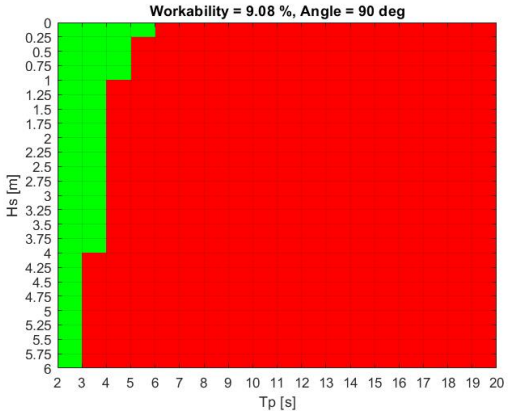

(c) Beam Waves: Workability per sea state

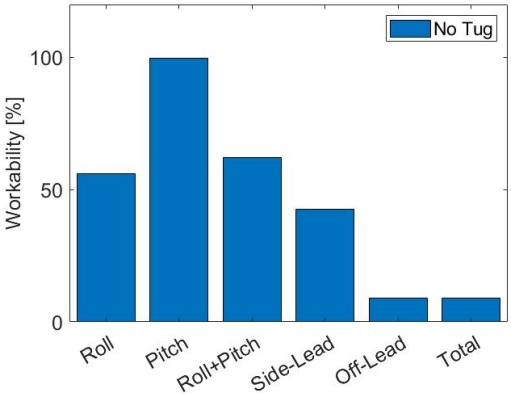

(d) Beam Waves: Workability per SDA angle

Figure 5-10: Workability results for QUAD Lift configuration without tugger lines in head and beam waves. The green and red cells indicate a workable or not workable sea state, respectively.

5-4-3 QUAD lift with tugger lines

In this section, the workability is analysed for different stiffness values of the tugger lines. In the previous chapter the effect of the tugger lines was explained. Tugger lines introduce stiffness values which result in the shift of the natural frequencies. Especially the horizontal motions of the load are effected which are related to the lead angles. The workability results are given for a load of 1000 ton and a cable length of 40 m.

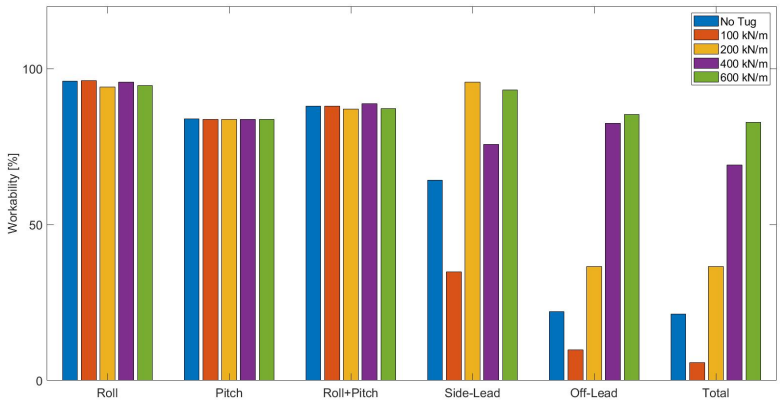

(a) Head Waves

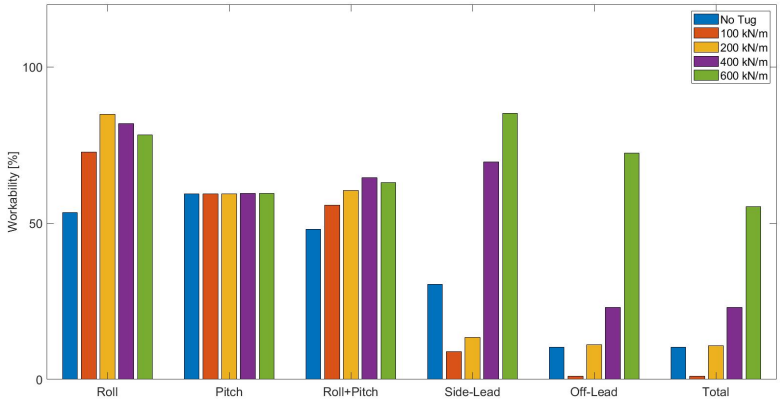

(b) Quarter Waves

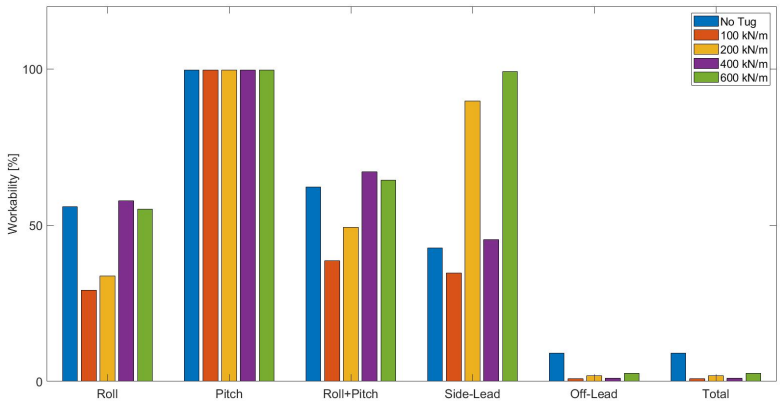

(c) Beam Waves

Figure 5-11: Workability results of QUAD Lift with different tugger stiffness values in head, quarter and beam waves.

Figure 5-11 show the workability for each SDA in head, beam and quarter waves for different

stiffness values. The application of stiffer tugger lines is quite effective for the workability in head and quarter waves. In head waves, a resulting workability of 83 % can be achieved by the application of tugger lines with a stiffness of 600 kN/m. This is much larger than the 21 % the workability when no tugger lines are applied.
Another remarkable result is that the application of tugger lines can decrease the workability. Tugger lines with a relative low stiffness of 100 kN/m create a total workability of less than 10%. The reason is that the tugger lines shift the peaks of the off-lead and side-lead angles into the the frequency spectrum with a large probability in the Central-North Sea. Then the resulting lead-angles will become unworkable in sea conditions with a frequent occurrence.
In quarter waves, the tugger lines have also a large positive effect. Tugger lines with a stiffness of 600 kN/m increase the total workability up to larger than 50%.

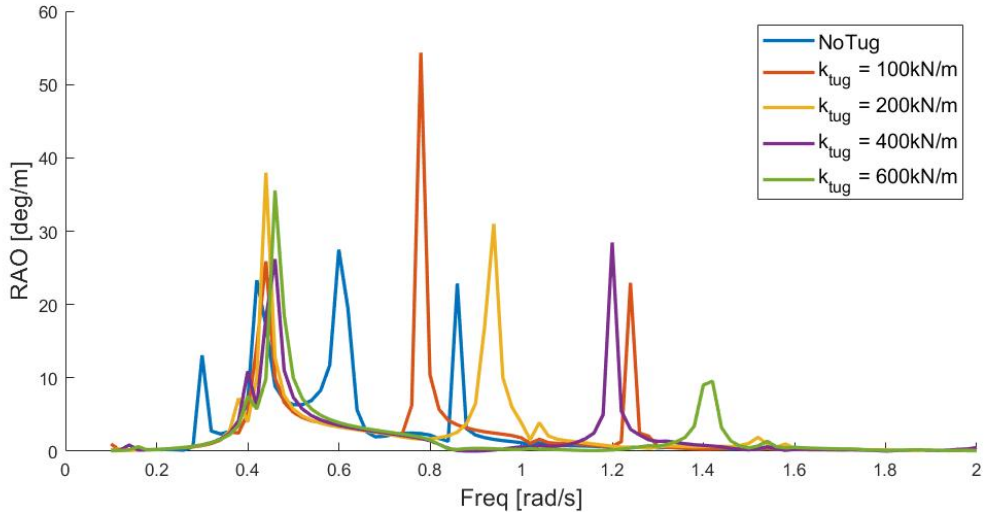

Figure 5-12: Off-lead angle response during QUAD Lift in beam waves for different tugger stiffness values.

In beam waves, the QUAD lift is practically not workable. The reason is that the off-lead angle stays large, even for large stiffness values. Figure 4-8b showed the large off-lead angles without the application of tugger stiffness. The application of tugger lines will lead to a shift of the frequency peaks but the peaks will still be present in both the lower and higher frequencies. The off-lead angle response in beam waves is shown in Figure 5-12. The left peak at a frequency of 0.4 rad/s does hardly not change positions for different stiffness values. Peaks at higher frequencies shift to larger frequencies for larger stiffness values. A problem for the workability however is that the off-lead angle is still non-zero between 0.2 and 0.8 rad/s. The calculation of the off-lead SDA angle by multiplication of the JONSWAP spectrum leads to large SDA values in frequent occuring seas and thus a low workability.
Really large stiffness values lead to the disappearance of the peaks at the larger frequencies. Figure 5-13 shows the workability with the application of tugger lines with a stiffness of 1000, 2000 and 4000 kN/m. These stiffness values can be achieved by the application of steel lines as was explained in the previous chapter. The workability in beam waves will eventually be 23.75% with a tugger stiffness of 1000 kN/m. Larger values of tugger stiffness do not only decrease the workability with respect to the off-lead angle but also the roll motion of the

vessels.

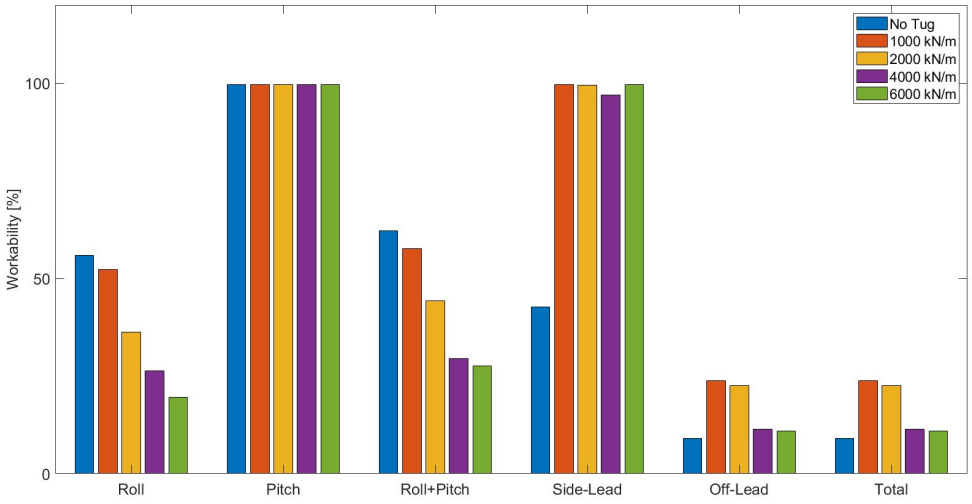

Figure 5-13: Off-lead angle response during QUAD Lift in beam waves for different tugger stiffness values.

Now it is known that in beam waves the workability is limited by the off-lead angle, the limiting off-lead SDA value can be adjusted to investigate the rate of the effect on the workability. When the limiting off-lead SDA is set to 2 degrees instead of 1 degree, the workability is increased to 44.2% when tugger lines are applied with a stiffness of 1000 kN/m. Figure 5-14 shows the workability of the QUAD lift in beam waves for the new limiting SDA off-lead angles.

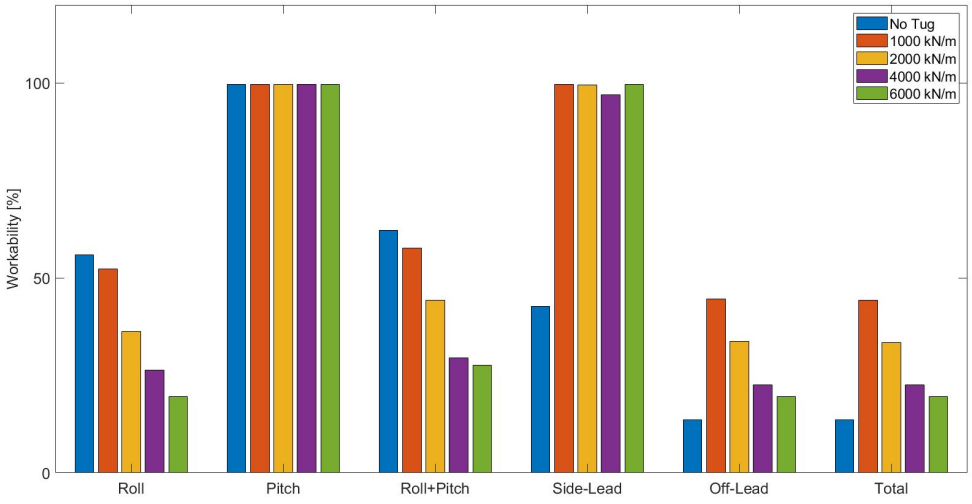

Figure 5-14: Off-lead angle response during QUAD Lift in beam waves for different tugger stiffness values. The limiting SDA off-lead angle is set to 2 degrees instead of 1 degree.

Chapter 6

Conclusions and Recommendations

6-1 Conclusions and Discussion

6-1-1 Vessel motions and interaction

A multi-vessel diffraction calculation for Jumbo's dual crane vessel Fairplayer Rotterdam is executed in both programs AQWA and OrcaWave. The vessel configuration is such that the cranes are perpendicular to each other. For a gap distance of 40 m, the data for the vessels in OrcaWave is validated to the output of diffraction program AQWA. The diffraction data of both programs is similar, only at gap resonance frequencies there are small differences. The linear equation of motion for the vessels has 12 degrees of freedom and are hydro-dynamically coupled, since the radiation forces of the vessels have an effect on each other. The DP systems of the vessels are modelled as a translational springs in both surge and sway direction and a rotational spring for the yaw direction. The natural period of the DP system for both the surge, sway and yaw direction is equal to 100 s. Viscous roll damping is added by application of the Ikeda method. The roll response of the diffraction calculation matches the response given by the model test of the Fairplayer executed by MARIN, with the exception of the natural frequency response value.
The transversal sloshing frequencies for different modes match the frequencies at which peaks occur in the frequency dependent hydrodynamic data. Potential theory, used in the diffraction calculations, overestimates the wave resonance effects. A damping lid on the wave surface in between the vessels successfully decreases the peak value effect, depending on the chosen damping factor. The operation effect of the damping lid was compared to literature since no model test were available. The damping lid had a negligible effect on the final workability of the QUAD lift. Therefore, the workability calculations are executed with the undamped diffraction data.
The natural frequencies of the vessels roll motion do not change for different vessel gap distances. The natural frequency for heave motion decreases if the gap distance increases, with a natural frequency of 0.86 rad/s for a gap distance of 20 m and a natural frequency of 0.80 rad/s for a gap distance of 40 m.

6-1-2 QUAD Lift

When four cranes of the vessels pick up the load, 6 DoF of the load motions are added, resulting in a 18 DoF system. A linear model of the QUAD lift is written in MATLAB. The load is modelled as a rectangular block with dimensions (48x20x5m). The jib radius of the cranes is 10 m. The stiffness of cables and cranes are modelled as linear springs in series, which stiffness is given by the manufacturer Huisman. Mass of the cables is neglected. When the vessels are attached to the load, the vertical position of the CoG of the vessels shifts vertically upward by attribution of one half of the static load mass to each vessel. The QUAD lift analysis is executed for a vessel gap width of 40 m.
For a load mass of 1000 ton and a cable length of 40 m, the roll response of the vessel is affected by three natural frequencies values 0.3, 0.4 and 0.62 rad/s. The load surge response has a large peak response at 0.50 rad/s. The load sway response has has a large peak response at 0.3 and 0.62 rad/s. The eigenvectors of the system show the large coupling between the roll of the vessel and the load sway motion for a frequency of 0.3 and 0.62 rad/s.
The dynamic cable elongation and therefore the dynamic crane forces are the same for each of the four cranes of both vessels. They only depend on the wave direction.
Tugger lines are added to prevent large horizontal motions of the load. Four tugger lines are added to the system in a cross configuration. The tugger lines are modelled as linear springs. The stiffness of the tugger lines can be changed by choice of the material or diameter of the cable.
For the horizontal load motions, increase of tugger stiffness results in a shift of the natural frequencies to higher frequency values. The natural frequency of the surge of the load shifts from 0.5 rad/s to a frequency of 0.9 rad/ for tuggers with a stiffness of 200 kN/m. For the load sway motion the natural frequency values 0.3 rad/s and 0.62 rad/s shift to values of 0.38 rad/s and 0.94 rad/s, respectively. Further increase of tugger line stiffness leads to the reduction of the responses for the natural frequencies. In quarter waves, the highest value of the load surge response peak for a stiffness of 1000 kN/m is equal to 2 m instead of of 33 m without tugger lines. For the load sway motion the maximum response reduces from 28 to 6 m.

6-1-3 Parametric study and Workability

A parametric study is executed for the QUAD Lift configuration. The effect of the load mass and the cable length on the system motions are analysed. The SDA values of the vessel motions and lead angles are calculated with the three dimensional response and JONSWAP spectra for the most probable sea condition in the Central North Sea. To identify the worst wave direction in terms of large motions, results are shown by use of polar plots.
An increase of the load mass leads to an increase in the roll and lead angles SDA of the Fairplayer. The SDA values are at its the largest in quarter and beam waves.
An increase of the cable length reduces the lead angle SDA's. The vessel roll and pitch motions of the vessel are not significantly influenced by the cable lengths. The SDA values are at its the largest in quarter and beam waves.

The workability is calculated by the SDA values and the wave scatter data for the Central North sea, representing the probability of each sea condition. For a safe installation

performance, the vessel motions SDA's are limited in the roll and pitch angles. During the QUAD lift, the crane angles need also be less than the SDA limit.
The workability of the free floating vessels in head waves, with a gap distance of 40 m, is 84 % and in beam waves 70 %. Limiting motions are the vessel pitch and roll, for head and beam waves respectively. In a QUAD lift with a load of 1000 ton and a cable length of 40 m, the workability in head and beam waves decreases to 21 and 9 %, respectively. The limiting factor for both wave directions is the crane off-lead angle.
With the addition of tugger lines, the workability can be increased. For a tugger stiffness of 600 kN/m, the workability in head waves is larger than 70 %. In quarter waves, the workability with these tugger lines increases from 10 to more than 50%. In beam waves however, this tugger stiffness does not increase the workability. The off-lead angle is still too large. Further increase of the tugger stiffness up to 1000 kN/m increases the workability of the QUAD lift in beam waves up to a maximum of 24 %. If the SDA limit for the off-lead angle is set from 1 to 2 degrees, the workability in beam waves increases to 44 %. Further increase of tugger stiffness has a negative effect on the workability in terms of off-lead angle and vessel roll response.

6-2 Recommendations

The thesis subject QUAD Lift started the research of a new possible method to improve the offshore capability of the Jumbo dual crane vessels. In this thesis, a workability study was performed. The workability indicates the extent of possibility to execute the QUAD lift with the J-Class vessels. Workability values of more than 80, 50 and 20 % in respectively head, quarter and beam waves show great perspective for the execution of the QUAD Lift. The workability calculations are only calculated for a fixed vessel gap distance of 40 m. In a further extended study, more vessel distances could be analysed. In this thesis, the application of a damped lid in between the vessels had negligible effects on the final workability values. Smaller or larger gap distances could have a different effect on the gap wave behaviour. Therefore, it would be interesting to perform a study on the hydrodynamic interaction between the J-Class vessels. Multi-vessel model testing could give the answer on the correct value of the damping factor.

The workability of the QUAD lift is only based on the following limiting motions: The roll and pitch angles of the vessels and the side and off-lead angles of the cranes. For a complete research on a safe execution of a QUAD lift also other limits should be required. For example, the horizontal motions of vessels and load during an installation, the dynamic crane or tugger line forces or the maximum heading rotation of the vessels during a lift. The different limits depend on the project conditions for which the QUAD lift is executed and need to be analysed for each different application.
The workability calculation of the QUAD lift is calculated for installation phase 4, shown in Figure 1-3. The load is hanging in the cranes and the hydrodynamic interaction is only caused by the vessels. The effects of external structures like barges or platforms are neglected. The effects of the moment of picking up or loosening the load should be further investigated.

The sea spectrum used in this thesis is the JONSWAP spectrum. This spectrum matches the spectral density for wind driven seas, like the North Sea. In seas with a lot of swell waves, this spectrum is not a good estimation. For the application of the QUAD lift in seas with

severe swell waves, another wave spectrum should be used.

The QUAD lift model equation of motion is just as the vessel equation of motions calculated in the frequency domain. This means only linear equations are used. Non-linear wave effects like drift forces and slamming are neglected in this study.
In the execution of the QUAD lift different types of control play a role. The DP-system of the vessels controls the horizontal position and the heading. Active winches of the tugger lines enable the adjustment of the line length to secure the maximum tension in the tuggers. Since these control systems will affect the motions of the system, it should be a topic of research in the further work.

Appendix A

Responses

This appendix contains the responses (RAO's) of the vessels and the load in quarter waves. All the translations of the system have the unit [m/m]. The rotations have the unit [deg/m]. The QUAD lift responses are given for a load mass of 1000 ton and a cable length of 40 m.

A-1 Free floating vessels

The labels FF1 and FF2 in the legend indicate each of the two vessels.

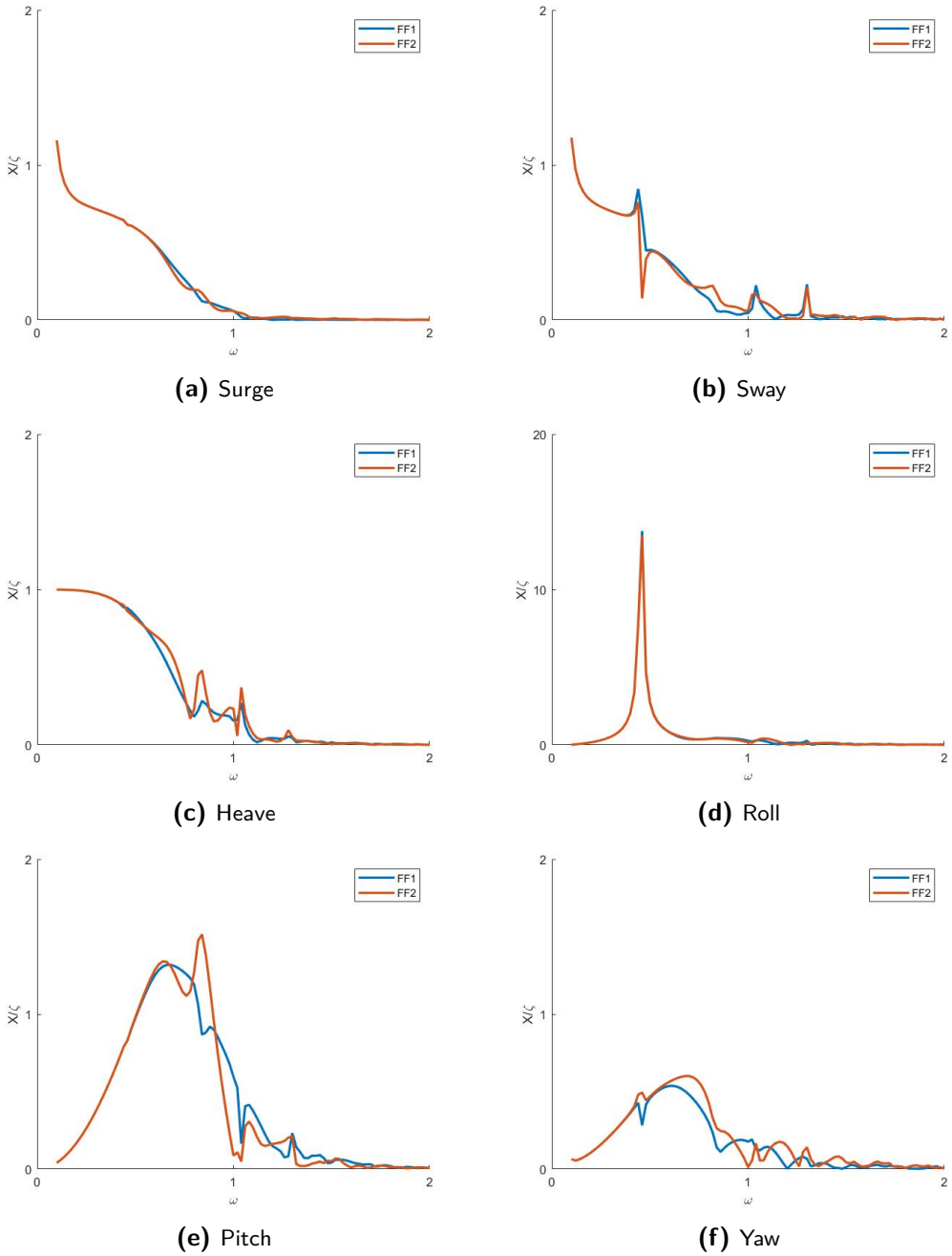

(a) Surge **(b)** Sway

(c) Heave **(d)** Roll

(e) Pitch **(f)** Yaw

Figure A-1: Comparison RAO's of free floating Fairplayers in quarter waves. The red line indicates the foremost vessel in the sense of that the wave first reaches this vessel.

A-2 QUAD Lift

The labels QUAD and Tug in the legend indicate the responses of the system without tugger lines and with a tugger stiffness of 600 kN/m.

A-2-1 Vessel Response

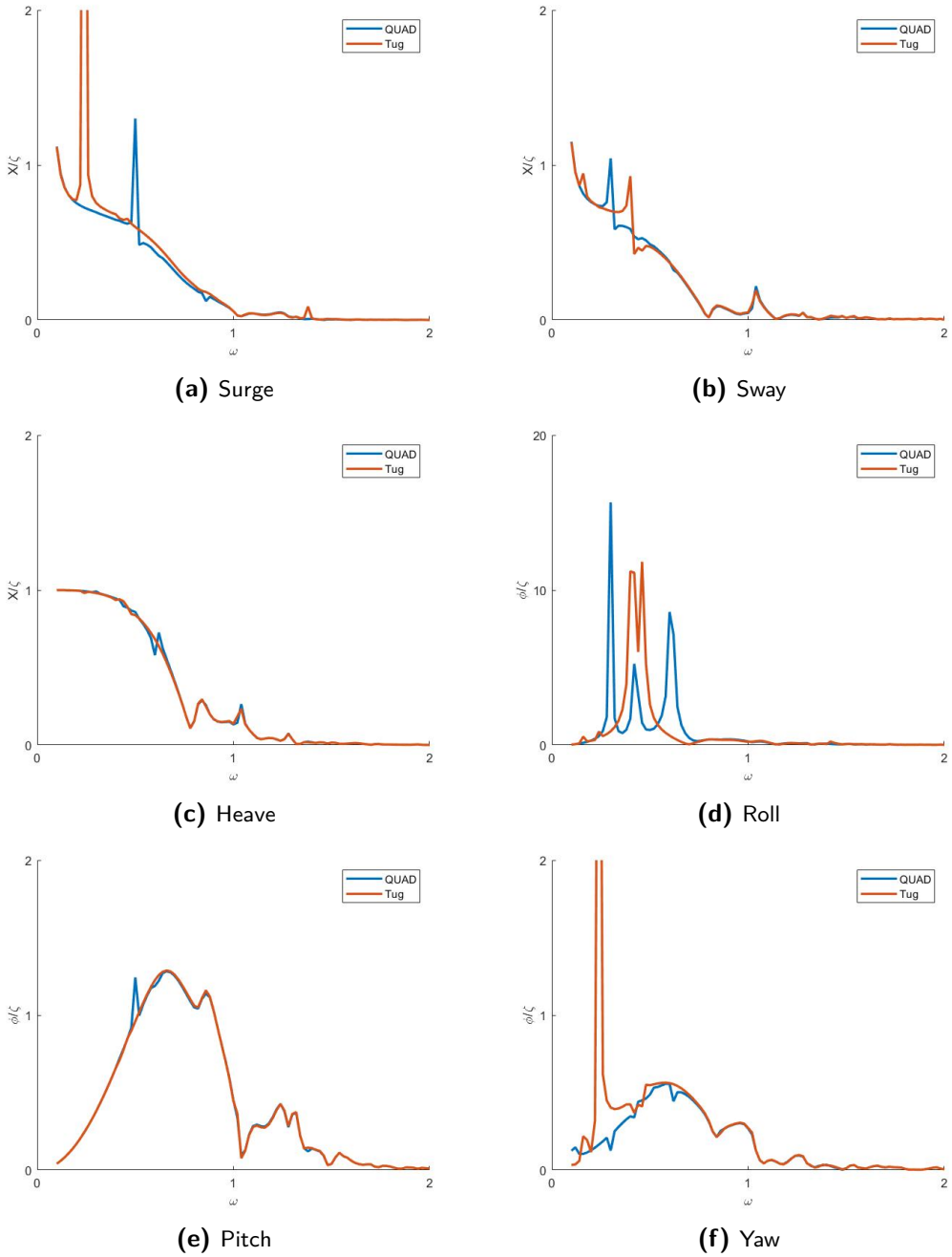

Figure A-2: RAO's of Fairplayer during QUAD lift in quarter waves.

A-2-2 Load Response

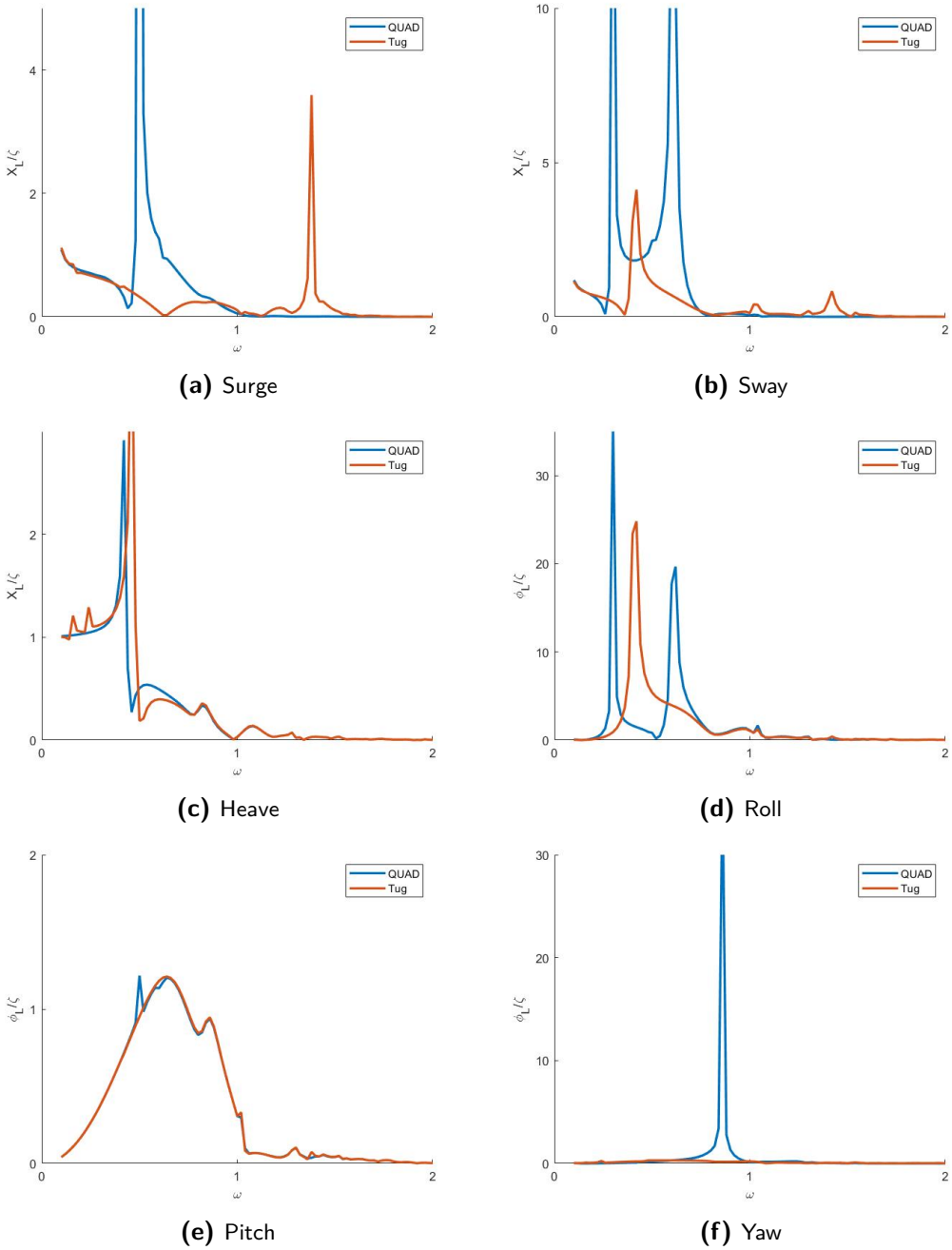

(a) Surge **(b)** Sway

(c) Heave **(d)** Roll

(e) Pitch **(f)** Yaw

Figure A-3: RAO's of load during QUAD lift in quarter waves.

Appendix B

QUAD Lift Matrices

This appendix shows the diagonal 18x18 QUAD lift and tugger line stiffness matrices generated by MAPLE.
Both the QUAD Lift and tugger line stiffness matrix have the same layout, which is shown on the next page.

The Maple output of the QUAD lift stiffness matrix C_L and tugger line stiffness matrix C_T are shown in Figure B-1 and Figure B-2, respectively.

$$\mathbf{C_L} = \mathbf{C_T} =$$

$$\begin{bmatrix}
C_{1,1} & 0 & 0 & 0 & C_{1,5} & C_{1,6} & 0 & 0 & 0 & 0 & 0 & 0 & C_{1,13} & 0 & 0 & 0 & C_{1,17} & C_{1,18} \\
0 & C_{2,2} & 0 & C_{2,4} & 0 & C_{2,6} & 0 & 0 & 0 & 0 & 0 & 0 & 0 & C_{2,14} & 0 & C_{2,16} & 0 & 0 \\
0 & 0 & C_{3,3} & C_{3,4} & C_{3,5} & 0 & 0 & 0 & 0 & 0 & 0 & 0 & 0 & 0 & C_{3,15} & C_{3,16} & 0 & 0 \\
0 & C_{4,2} & C_{4,3} & C_{4,4} & C_{4,5} & C_{4,6} & 0 & 0 & 0 & 0 & 0 & 0 & 0 & C_{4,14} & C_{4,15} & C_{4,16} & 0 & 0 \\
C_{5,1} & 0 & C_{5,3} & C_{5,4} & C_{5,5} & C_{5,6} & 0 & 0 & 0 & 0 & 0 & 0 & C_{5,13} & 0 & C_{5,15} & C_{5,16} & C_{5,17} & C_{5,18} \\
C_{6,1} & C_{6,2} & 0 & C_{6,4} & C_{6,5} & C_{6,6} & 0 & 0 & 0 & 0 & 0 & 0 & C_{6,13} & C_{6,14} & 0 & C_{6,16} & C_{6,17} & C_{6,18} \\
0 & 0 & 0 & 0 & 0 & 0 & C_{7,7} & 0 & 0 & 0 & C_{7,11} & C_{7,12} & C_{7,13} & 0 & 0 & 0 & C_{7,17} & C_{7,18} \\
0 & 0 & 0 & 0 & 0 & 0 & 0 & C_{8,8} & 0 & C_{8,10} & 0 & C_{8,12} & 0 & C_{8,14} & 0 & C_{8,16} & 0 & C_{8,18} \\
0 & 0 & 0 & 0 & 0 & 0 & 0 & 0 & C_{9,9} & C_{9,10} & C_{9,11} & 0 & 0 & 0 & C_{9,15} & C_{9,16} & 0 & 0 \\
0 & 0 & 0 & 0 & 0 & 0 & 0 & C_{10,8} & C_{10,9} & C_{10,10} & C_{10,11} & C_{10,12} & 0 & C_{10,14} & C_{10,15} & C_{10,16} & 0 & 0 \\
0 & 0 & 0 & 0 & 0 & 0 & C_{11,7} & 0 & C_{11,9} & C_{11,10} & C_{11,11} & C_{11,12} & C_{11,13} & 0 & C_{11,15} & C_{11,16} & C_{11,17} & C_{11,18} \\
0 & 0 & 0 & 0 & 0 & 0 & C_{12,7} & C_{12,8} & 0 & C_{12,10} & C_{12,11} & C_{12,12} & C_{12,13} & C_{12,14} & 0 & C_{12,16} & C_{12,17} & C_{12,18} \\
C_{13,1} & 0 & 0 & 0 & C_{13,5} & C_{13,6} & C_{13,7} & 0 & 0 & 0 & C_{13,11} & C_{13,12} & C_{13,13} & 0 & 0 & 0 & C_{13,17} & 0 \\
0 & C_{14,2} & 0 & C_{14,4} & 0 & C_{14,6} & 0 & C_{14,8} & 0 & C_{14,10} & 0 & C_{14,12} & 0 & C_{14,14} & 0 & C_{14,16} & 0 & 0 \\
0 & 0 & C_{15,3} & C_{15,4} & C_{15,5} & 0 & 0 & 0 & C_{15,9} & C_{15,10} & C_{15,11} & 0 & 0 & 0 & C_{15,15} & 0 & 0 & 0 \\
0 & C_{16,2} & C_{16,3} & C_{16,4} & C_{16,5} & C_{16,6} & 0 & C_{16,8} & C_{16,9} & C_{16,10} & C_{16,11} & C_{16,12} & 0 & C_{16,14} & 0 & C_{16,16} & 0 & 0 \\
C_{17,1} & 0 & 0 & 0 & C_{17,5} & C_{17,6} & C_{17,7} & 0 & 0 & 0 & C_{17,11} & C_{17,12} & C_{17,13} & 0 & 0 & 0 & C_{17,17} & 0 \\
C_{18,1} & 0 & 0 & 0 & C_{18,5} & C_{18,6} & C_{18,7} & 0 & 0 & 0 & C_{18,11} & C_{18,12} & 0 & 0 & 0 & 0 & 0 & C_{18,18}
\end{bmatrix}$$

$$
\begin{bmatrix}
\begin{bmatrix}
2.0\,kr, & 0, & 0, & 0, & 2.0\,kr{\cdot}LzCr, & 2.0\,kr{\cdot}LyCr, & 0, & 0, & 0, & 0, & 0, & 0, & -2.0\,kr, & 0, & 0, & 0, & -1.00\,kr{\cdot}Lz, & 1.00\,kr{\cdot}Ly
\end{bmatrix},\\
\begin{bmatrix}
0, & 2.0\,kr, & 0, & -2.0\,kr{\cdot}LzCr, & 0, & 0.5\,kr\,(-2.\,LxCr2 + 2.\,LxCr1), & 0, & 0, & 0, & 0, & 0, & 0, & -2.0\,kr, & 0, & 1.00\,kr{\cdot}Lz, & 0, & 0
\end{bmatrix},\\
\begin{bmatrix}
0, & 0, & 2.0\,kc, & -2.0\,kc{\cdot}LyCr, & 0.5\,kc\,(2.\,LxCr2 - 2.\,LxCr1), & 0, & 0, & 0, & 0, & 0, & 0, & 0, & 0, & -2.0\,kc, & -1.00\,kc{\cdot}Ly, & 0, & 0
\end{bmatrix},\\
\begin{bmatrix}
0, & -2.0\,kr{\cdot}LzCr, & -2.0\,kc{\cdot}LyCr, & 2.0\,kc{\cdot}LyCr^2 + 2.0\,kr{\cdot}LzCr^2, & 0.5\,kc\,(-2.\,LxCr2\,LyCr + 2.\,LxCr1\,LyCr), & 0.5\,kr\,(2.\,LxCr2\,LzCr - 2.\,LxCr1\,LzCr), & 0, & 0, & 0, & 0, & 0, & 0, & 2.0\,kr{\cdot}LzCr, & 2.0\,kc{\cdot}LyCr, & 1.00\,kc{\cdot}Ly\,LyCr - 1.00\,kr{\cdot}Lz\,LzCr, & 0, & 0
\end{bmatrix},\\
\begin{bmatrix}
2.0\,kr{\cdot}LzCr, & 0, & 0.5\,kc\,(2.\,LxCr2 - 2.\,LxCr1), & 0.5\,kc\,(-2.\,LxCr2\,LyCr + 2.\,LxCr1\,LyCr), & 0.5\,kc\left(2.\,LxCr2^2 + 2.\,LxCr1^2\right) + 2.0\,kr{\cdot}LzCr^2, & 2.0\,kr{\cdot}LyCr\,LzCr, & 0, & 0, & 0, & 0, & 0, & -2.0\,kr{\cdot}LzCr, & 0, & 0.5\,kc\,(-2.\,LxCr2 + 2.\,LxCr1), & & & &\\
0.5\,kc\,(-Ly\,LxCr2 + Ly\,LxCr1), & 0.5\,kc\,(-Lx\,LxCr2 - Lx\,LxCr1) - 1.00\,kr{\cdot}Lz\,LzCr, & 1.00\,kr{\cdot}Ly\,LzCr
\end{bmatrix},\\
\begin{bmatrix}
2.0\,kr{\cdot}LyCr, & 0.5\,kr\,(-2.\,LxCr2 + 2.\,LxCr1), & 0, & 0.5\,kr\,(2.\,LxCr2\,LzCr - 2.\,LxCr1\,LzCr), & 2.0\,kr{\cdot}LyCr\,LzCr, & 0.5\,kr\left(4.\,LyCr^2 + 2.\,LxCr2^2 + 2.\,LxCr1^2\right), & 0, & 0, & 0, & 0, & 0, & -2.0\,kr{\cdot}LyCr, & 0.5\,kr\,(2.\,LxCr2 - 2.\,LxCr1), & 0, & 0.5\,kr\,(&\\
-Lz\,LxCr2 + Lz\,LxCr1), & -1.00\,kr{\cdot}Lz\,LyCr, & 0.5\,kr\,(2.0\,Ly\,LyCr - Lx\,LxCr2 - Lx\,LxCr1)
\end{bmatrix},\\
\begin{bmatrix}
0, & 0, & 0, & 0, & 0, & 2.0\,kr, & 0, & 0, & 0, & 2.0\,kr{\cdot}LzCr, & 2.0\,kr{\cdot}LyCr, & -2.0\,kr, & 0, & 0, & 0, & -1.00\,kr{\cdot}Lz, & -1.00\,kr{\cdot}Ly
\end{bmatrix},\\
\begin{bmatrix}
0, & 0, & 0, & 0, & 0, & 0, & 2.0\,kr, & 0, & -2.0\,kr{\cdot}LzCr, & 0, & 0.5\,kr\,(-2.\,LxCr2 + 2.\,LxCr1), & 0, & -2.0\,kr, & 0, & 1.00\,kr{\cdot}Lz, & 0, & 0
\end{bmatrix},\\
\begin{bmatrix}
0, & 0, & 0, & 0, & 0, & 0, & 0, & 2.0\,kc, & -2.0\,kc{\cdot}LyCr, & 0.5\,kc\,(2.\,LxCr2 - 2.\,LxCr1), & 0, & 0, & 0, & -2.0\,kc, & 1.00\,kc{\cdot}Ly, & 0, & 0
\end{bmatrix},\\
\begin{bmatrix}
0, & 0, & 0, & 0, & 0, & 0, & 0, & -2.0\,kr{\cdot}LzCr, & -2.0\,kc{\cdot}LyCr, & 2.0\,kc{\cdot}LyCr^2 + 2.0\,kr{\cdot}LzCr^2, & 0.5\,kc\,(-2.\,LxCr2\,LyCr + 2.\,LxCr1\,LyCr), & 0.5\,kr\,(2.\,LxCr2\,LzCr - 2.\,LxCr1\,LzCr), & 0, & 2.0\,kr{\cdot}LzCr, & 2.0\,kc{\cdot}LyCr, & -1.00\,kc{\cdot}Ly\,LyCr &\\
-1.00\,kr{\cdot}Lz\,LzCr, & 0, & 0
\end{bmatrix},\\
\begin{bmatrix}
0, & 0, & 0, & 0, & 0, & 0, & 2.0\,kr{\cdot}LzCr, & 0, & 0.5\,kc\,(2.\,LxCr2 - 2.\,LxCr1), & 0.5\,kc\,(-2.\,LxCr2\,LyCr + 2.\,LxCr1\,LyCr), & 0.5\,kc\left(2.\,LxCr2^2 + 2.\,LxCr1^2\right) + 2.0\,kr{\cdot}LzCr^2, & 2.0\,kr{\cdot}LyCr\,LzCr, & -2.0\,kr{\cdot}LzCr, & 0, & 0.5\,kc\,(-2.\,LxCr2 + 2.\,LxCr1), &\\
0.5\,kc\,(Ly\,LxCr2 - Ly\,LxCr1), & 0.5\,kc\,(Lx\,LxCr2 + Lx\,LxCr1) - 1.00\,kr{\cdot}Lz\,LzCr, & -1.00\,kr{\cdot}Ly\,LzCr
\end{bmatrix},\\
\begin{bmatrix}
0, & 0, & 0, & 0, & 0, & 0, & 2.0\,kr{\cdot}LyCr, & 0.5\,kr\,(-2.\,LxCr2 + 2.\,LxCr1), & 0, & 0.5\,kr\,(2.\,LxCr2\,LzCr - 2.\,LxCr1\,LzCr), & 2.0\,kr{\cdot}LyCr\,LzCr, & 0.5\,kr\left(4.\,LyCr^2 + 2.\,LxCr2^2 + 2.\,LxCr1^2\right), & -2.0\,kr{\cdot}LyCr, & 0.5\,kr\,(2.\,LxCr2 - 2.\,LxCr1), & 0, & 0.5\,kr\,(&\\
-Lz\,LxCr2 + Lz\,LxCr1), & -1.00\,kr{\cdot}Lz\,LyCr, & 0.5\,kr\,(-2.0\,Ly\,LyCr + Lx\,LxCr2 + Lx\,LxCr1)
\end{bmatrix},\\
\begin{bmatrix}
-2.0\,kr, & 0, & 0, & 0, & -2.0\,kr{\cdot}LzCr, & -2.0\,kr{\cdot}LyCr, & -2.0\,kr, & 0, & 0, & 0, & -2.0\,kr{\cdot}LzCr, & -2.0\,kr{\cdot}LyCr, & 4.0\,kr, & 0, & 0, & 0, & 2.00\,kr{\cdot}Lz, & 0
\end{bmatrix},\\
\begin{bmatrix}
0, & -2.0\,kr, & 0, & 2.0\,kr{\cdot}LzCr, & 0, & 0.5\,kr\,(2.\,LxCr2 - 2.\,LxCr1), & 0, & -2.0\,kr, & 0, & 2.0\,kr{\cdot}LzCr, & 0, & 0.5\,kr\,(2.\,LxCr2 - 2.\,LxCr1), & 0, & 4.0\,kr, & 0, & -2.00\,kr{\cdot}Lz, & 0, & 0
\end{bmatrix},\\
\begin{bmatrix}
0, & 0, & -2.0\,kc, & 2.0\,kc{\cdot}LyCr, & 0.5\,kc\,(-2.\,LxCr2 + 2.\,LxCr1), & 0, & 0, & 0, & -2.0\,kc, & 2.0\,kc{\cdot}LyCr, & 0.5\,kc\,(-2.\,LxCr2 + 2.\,LxCr1), & 0, & 0, & 0, & 4.0\,kc, & 0, & 0, & 0
\end{bmatrix},\\
\begin{bmatrix}
0, & 1.00\,kr{\cdot}Lz, & -1.00\,kc{\cdot}Ly, & 1.00\,kc{\cdot}Ly\,LyCr - 1.00\,kr{\cdot}Lz\,LzCr, & 0.5\,kc\,(-Ly\,LxCr2 + Ly\,LxCr1), & 0.5\,kr\,(-Lz\,LxCr2 + Lz\,LxCr1), & 0, & 1.00\,kr{\cdot}Lz, & 1.00\,kc{\cdot}Ly, & -1.00\,kc{\cdot}Ly\,LyCr - 1.00\,kr{\cdot}Lz\,LzCr, & 0.5\,kc\,(Ly\,LxCr2 - Ly\,LxCr1), &\\
0.5\,kr\,(-Lz\,LxCr2 + Lz\,LxCr1), & 0, & -2.00\,kr{\cdot}Lz, & 0, & 1.000\,kc{\cdot}Ly^2 + 1.000\,kr{\cdot}Lz^2, & 0, & 0
\end{bmatrix},\\
\begin{bmatrix}
-1.00\,kr{\cdot}Lz, & 0, & 0, & 0, & 0.5\,kc\,(-Lx\,LxCr2 - Lx\,LxCr1) - 1.00\,kr{\cdot}Lz\,LzCr, & -1.00\,kr{\cdot}Lz\,LyCr, & -1.00\,kr{\cdot}Lz, & 0, & 0, & 0, & 0.5\,kc\,(Lx\,LxCr2 + Lx\,LxCr1) - 1.00\,kr{\cdot}Lz\,LzCr, & -1.00\,kr{\cdot}Lz\,LyCr, & 2.00\,kr{\cdot}Lz, & 0, & 0, & 0, & 1.000\,kc{\cdot}Lx^2 &\\
+ 1.000\,kr{\cdot}Lz^2, & 0
\end{bmatrix},\\
\begin{bmatrix}
1.00\,kr{\cdot}Ly, & 0, & 0, & 0, & 1.00\,kr{\cdot}Ly\,LzCr, & 0.5\,kr\,(2.0\,Ly\,LyCr - Lx\,LxCr2 - Lx\,LxCr1), & -1.00\,kr{\cdot}Ly, & 0, & 0, & 0, & -1.00\,kr{\cdot}Ly\,LzCr, & 0.5\,kr\,(-2.0\,Ly\,LyCr + Lx\,LxCr2 + Lx\,LxCr1), & 0, & 0, & 0, & 0, & 0.5\,kr\left(2.00\,Ly^2 + 2.00\,Lx^2\right)
\end{bmatrix}
\end{bmatrix}
$$

Figure B-1: QUAD Lift stiffness matrix generated by Maple

$$
\begin{bmatrix}
\begin{bmatrix} 2.0\,Ktug\_x, 0, 0, 0, 2.0\,Ktug\_x\,L\_Tz, 2.0\,Ktug\_x\,L\_Ty, 0, 0, 0, 0, 0, 0, -2.0\,Ktug\_x, 0, 0, 0, -2.0\,Ktug\_x\,L\_TzL, 2.0\,Ktug\_x\,L\_TyL \end{bmatrix},\\
\begin{bmatrix} 0, 2.0\,Ktug\_y, 0, -2.0\,Ktug\_y\,L\_Tz, 0, 0.5\,Ktug\_y\,(-2.\,L\_TxC + 2.\,L\_TxD), 0, 0, 0, 0, 0, 0, 0, -2.0\,Ktug\_y, 0, 2.0\,Ktug\_y\,L\_TzL, 0, 0 \end{bmatrix},\\
\begin{bmatrix} 0, 0, 2.0\,Ktug\_z, -2.0\,Ktug\_z\,L\_Ty, 0.5\,Ktug\_z\,(2.\,L\_TxC - 2.\,L\_TxD), 0, 0, 0, 0, 0, 0, 0, 0, 0, -2.0\,Ktug\_z, -2.0\,Ktug\_z\,L\_TyL, 0, 0 \end{bmatrix},\\
\begin{bmatrix} 0, -2.0\,Ktug\_y\,L\_Tz, -2.0\,Ktug\_z\,L\_Ty, 2.0\,Ktug\_y\,L\_Tz^2 + 2.0\,Ktug\_z\,L\_Ty^2, 0.5\,Ktug\_z\,(-2.\,L\_TxC\,L\_Ty + 2.\,L\_TxD\,L\_Ty), 0.5\,Ktug\_y\,(2.\,L\_TxC\,L\_Tz - 2.\,L\_TxD\,L\_Tz), 0, 0, 0, 0, 0, 0, 2.0\,Ktug\_y\,L\_Tz,\\
2.0\,Ktug\_z\,L\_Ty, -2.0\,Ktug\_y\,L\_TzL\,L\_Tz + 2.0\,Ktug\_z\,L\_TyL\,L\_Ty, 0, 0 \end{bmatrix},\\
\begin{bmatrix} 2.0\,Ktug\_x\,L\_Tz, 0, 0.5\,Ktug\_z\,(2.\,L\_TxC - 2.\,L\_TxD), 0.5\,Ktug\_z\,(-2.\,L\_TxC\,L\_Ty + 2.\,L\_TxD\,L\_Ty), 2.0\,Ktug\_x\,L\_Tz^2 + 0.5\,Ktug\_z\,(2.\,L\_TxC^2 + 2.\,L\_TxD^2), 2.0\,Ktug\_x\,L\_Ty\,L\_Tz, 0, 0, 0, 0, 0, 0, -2.0\,Ktug\_x\,L\_Tz,\\
0, 0.5\,Ktug\_z\,(-2.\,L\_TxC + 2.\,L\_TxD), 0.5\,Ktug\_z\,(-2.\,L\_TyL\,L\_TxC + 2.\,L\_TyL\,L\_TxD), -2.0\,Ktug\_x\,L\_TzL\,L\_Tz + 0.5\,Ktug\_z\,(-2.\,L\_TxL\,L\_TxC - 2.\,L\_TxL\,L\_TxD), 2.0\,Ktug\_x\,L\_TyL\,L\_Tz \end{bmatrix},\\
\begin{bmatrix} 2.0\,Ktug\_x\,L\_Ty, 0.5\,Ktug\_y\,(-2.\,L\_TxC + 2.\,L\_TxD), 0, 0.5\,Ktug\_y\,(2.\,L\_TxC\,L\_Tz - 2.\,L\_TxD\,L\_Tz), 2.0\,Ktug\_x\,L\_Ty\,L\_Tz, 2.0\,Ktug\_x\,L\_Ty^2 + 0.5\,Ktug\_y\,(2.\,L\_TxC^2 + 2.\,L\_TxD^2), 0, 0, 0, 0, 0, 0, -2.0\,Ktug\_x\,L\_Ty,\\
0.5\,Ktug\_y\,(2.\,L\_TxC - 2.\,L\_TxD), 0, 0.5\,Ktug\_y\,(-2.\,L\_TzL\,L\_TxC + 2.\,L\_TzL\,L\_TxD), -2.0\,Ktug\_x\,L\_TzL\,L\_Ty, 2.0\,Ktug\_x\,L\_TyL\,L\_Ty + 0.5\,Ktug\_y\,(-2.\,L\_TxL\,L\_TxC - 2.\,L\_TxL\,L\_TxD) \end{bmatrix},\\
\begin{bmatrix} 0, 0, 0, 0, 0, 0, 2.0\,Ktug\_x, 0, 0, 0, 2.0\,Ktug\_x\,L\_Tz, 2.0\,Ktug\_x\,L\_Ty, 2.0\,Ktug\_x, 0, 0, 0, 2.0\,Ktug\_x\,L\_TzL, 2.0\,Ktug\_x\,L\_TyL \end{bmatrix},\\
\begin{bmatrix} 0, 0, 0, 0, 0, 0, 0, 2.0\,Ktug\_y, 0, -2.0\,Ktug\_y\,L\_Tz, 0, 0.5\,Ktug\_y\,(-2.\,L\_TxA + 2.\,L\_TxB), 0, 2.0\,Ktug\_y, 0, -2.0\,Ktug\_y\,L\_TzL, 0, 0 \end{bmatrix},\\
\begin{bmatrix} 0, 0, 0, 0, 0, 0, 0, 0, 2.0\,Ktug\_z, -2.0\,Ktug\_z\,L\_Ty, 0.5\,Ktug\_z\,(2.\,L\_TxA - 2.\,L\_TxB), 0, 0, 0, -2.0\,Ktug\_z, 2.0\,Ktug\_z\,L\_TyL, 0, 0 \end{bmatrix},\\
\begin{bmatrix} 0, 0, 0, 0, 0, 0, 0, -2.0\,Ktug\_y\,L\_Tz, -2.0\,Ktug\_z\,L\_Ty, 2.0\,Ktug\_y\,L\_Tz^2 + 2.0\,Ktug\_z\,L\_Ty^2, 0.5\,Ktug\_z\,(-2.\,L\_TxA\,L\_Ty + 2.\,L\_TxB\,L\_Ty), 0.5\,Ktug\_y\,(2.\,L\_TxA\,L\_Tz - 2.\,L\_TxB\,L\_Tz), 0, -2.0\,Ktug\_y\,L\_Tz,\\
2.0\,Ktug\_z\,L\_Ty, 2.0\,Ktug\_y\,L\_TzL\,L\_Tz - 2.0\,Ktug\_z\,L\_TyL\,L\_Ty, 0, 0 \end{bmatrix},\\
\begin{bmatrix} 0, 0, 0, 0, 0, 0, 2.0\,Ktug\_x\,L\_Tz, 0, 0.5\,Ktug\_z\,(2.\,L\_TxA - 2.\,L\_TxB), 0.5\,Ktug\_z\,(-2.\,L\_TxA\,L\_Ty + 2.\,L\_TxB\,L\_Ty), 2.0\,Ktug\_x\,L\_Tz^2 + 0.5\,Ktug\_z\,(2.\,L\_TxA^2 + 2.\,L\_TxB^2), 2.0\,Ktug\_x\,L\_Ty\,L\_Tz, 2.0\,Ktug\_x\,L\_Tz, 0,\\
0.5\,Ktug\_z\,(-2.\,L\_TxA + 2.\,L\_TxB), 0.5\,Ktug\_z\,(2.\,L\_TyL\,L\_TxA - 2.\,L\_TyL\,L\_TxB), 2.0\,Ktug\_x\,L\_TzL\,L\_Tz + 0.5\,Ktug\_z\,(2.\,L\_TxL\,L\_TxA + 2.\,L\_TxL\,L\_TxB), 2.0\,Ktug\_x\,L\_TyL\,L\_Tz \end{bmatrix},\\
\begin{bmatrix} 0, 0, 0, 0, 0, 0, 2.0\,Ktug\_x\,L\_Ty, 0.5\,Ktug\_y\,(-2.\,L\_TxA + 2.\,L\_TxB), 0, 0.5\,Ktug\_y\,(2.\,L\_TxA\,L\_Tz - 2.\,L\_TxB\,L\_Tz), 2.0\,Ktug\_x\,L\_Ty\,L\_Tz, 2.0\,Ktug\_x\,L\_Ty^2 + 0.5\,Ktug\_y\,(2.\,L\_TxA^2 + 2.\,L\_TxB^2), 2.0\,Ktug\_x\,L\_Ty,\\
0.5\,Ktug\_y\,(-2.\,L\_TxA + 2.\,L\_TxB), 0, 0.5\,Ktug\_y\,(2.\,L\_TzL\,L\_TxA - 2.\,L\_TzL\,L\_TxB), 2.0\,Ktug\_x\,L\_TzL\,L\_Ty, 2.0\,Ktug\_x\,L\_TyL\,L\_Ty + 0.5\,Ktug\_y\,(-2.\,L\_TxL\,L\_TxA - 2.\,L\_TxL\,L\_TxB) \end{bmatrix},\\
\begin{bmatrix} -2.0\,Ktug\_x, 0, 0, 0, -2.0\,Ktug\_x\,L\_Tz, -2.0\,Ktug\_x\,L\_Ty, 2.0\,Ktug\_x, 0, 0, 0, 2.0\,Ktug\_x\,L\_Tz, 2.0\,Ktug\_x\,L\_Ty, 4.0\,Ktug\_x, 0, 0, 0, 4.0\,Ktug\_x\,L\_TzL, 0 \end{bmatrix},\\
\begin{bmatrix} 0, -2.0\,Ktug\_y, 0, 2.0\,Ktug\_y\,L\_Tz, 0, 0.5\,Ktug\_y\,(2.\,L\_TxC - 2.\,L\_TxD), 0, 2.0\,Ktug\_y, 0, -2.0\,Ktug\_y\,L\_Tz, 0, 0.5\,Ktug\_y\,(-2.\,L\_TxA + 2.\,L\_TxB), 0, 4.0\,Ktug\_y, 0, -4.0\,Ktug\_y\,L\_TzL, 0, 0 \end{bmatrix},\\
\begin{bmatrix} 0, 0, -2.0\,Ktug\_z, 2.0\,Ktug\_z\,L\_Ty, 0.5\,Ktug\_z\,(-2.\,L\_TxC + 2.\,L\_TxD), 0, 0, 0, -2.0\,Ktug\_z, 2.0\,Ktug\_z\,L\_Ty, 0.5\,Ktug\_z\,(-2.\,L\_TxA + 2.\,L\_TxB), 0, 0, 0, 4.0\,Ktug\_z, 0, 0, 0 \end{bmatrix},\\
\begin{bmatrix} 0, 2.0\,Ktug\_y\,L\_TzL, -2.0\,Ktug\_z\,L\_TyL, -2.0\,Ktug\_y\,L\_TzL\,L\_Tz + 2.0\,Ktug\_z\,L\_TyL\,L\_Ty, 0.5\,Ktug\_z\,(-2.\,L\_TyL\,L\_TxC + 2.\,L\_TyL\,L\_TxD), 0.5\,Ktug\_y\,(-2.\,L\_TzL\,L\_TxC + 2.\,L\_TzL\,L\_TxD), 0, -2.0\,Ktug\_y\,L\_TzL,\\
2.0\,Ktug\_z\,L\_TyL, 2.0\,Ktug\_y\,L\_TzL\,L\_Tz - 2.0\,Ktug\_z\,L\_TyL\,L\_Ty, 0.5\,Ktug\_z\,(2.\,L\_TyL\,L\_TxA - 2.\,L\_TyL\,L\_TxB), 0.5\,Ktug\_y\,(2.\,L\_TzL\,L\_TxA - 2.\,L\_TzL\,L\_TxB), 0, -4.0\,Ktug\_y\,L\_TzL, 0, 4.0\,Ktug\_y\,L\_TzL^2\\
+ 4.0\,Ktug\_z\,L\_TyL^2, 0, 0 \end{bmatrix},\\
\begin{bmatrix} -2.0\,Ktug\_x\,L\_TzL, 0, 0, 0, -2.0\,Ktug\_x\,L\_TzL\,L\_Tz + 0.5\,Ktug\_z\,(-2.\,L\_TxL\,L\_TxC - 2.\,L\_TxL\,L\_TxD), -2.0\,Ktug\_x\,L\_TzL\,L\_Ty, 2.0\,Ktug\_x\,L\_TzL, 0, 0, 0, 2.0\,Ktug\_x\,L\_TzL\,L\_Tz + 0.5\,Ktug\_z\,(2.\,L\_TxL\,L\_TxA\\
+ 2.\,L\_TxL\,L\_TxB), 2.0\,Ktug\_x\,L\_TzL\,L\_Ty, 4.0\,Ktug\_x\,L\_TzL, 0, 0, 0, 4.0\,Ktug\_x\,L\_TzL^2 + 4.0\,Ktug\_z\,L\_TxL^2, 0 \end{bmatrix},\\
\begin{bmatrix} 2.0\,Ktug\_x\,L\_TyL, 0, 0, 0, 2.0\,Ktug\_x\,L\_TyL\,L\_Tz, 2.0\,Ktug\_x\,L\_TyL\,L\_Ty + 0.5\,Ktug\_y\,(-2.\,L\_TxL\,L\_TxC - 2.\,L\_TxL\,L\_TxD), 2.0\,Ktug\_x\,L\_TyL, 0, 0, 0, 2.0\,Ktug\_x\,L\_TyL\,L\_Tz, 2.0\,Ktug\_x\,L\_TyL\,L\_Ty + 0.5\,Ktug\_y\,(\\
-2.\,L\_TxL\,L\_TxA - 2.\,L\_TxL\,L\_TxB), 0, 0, 0, 0, 0, 4.0\,Ktug\_x\,L\_TyL^2 + 4.0\,Ktug\_y\,L\_TxL^2 \end{bmatrix}\end{bmatrix}
$$

Figure B-2: Tugger line stiffness matrix generated by Maple

Appendix C

Scatter Diagram

The scatter data of the Central North Sea, generated by Jumbo Maritime.

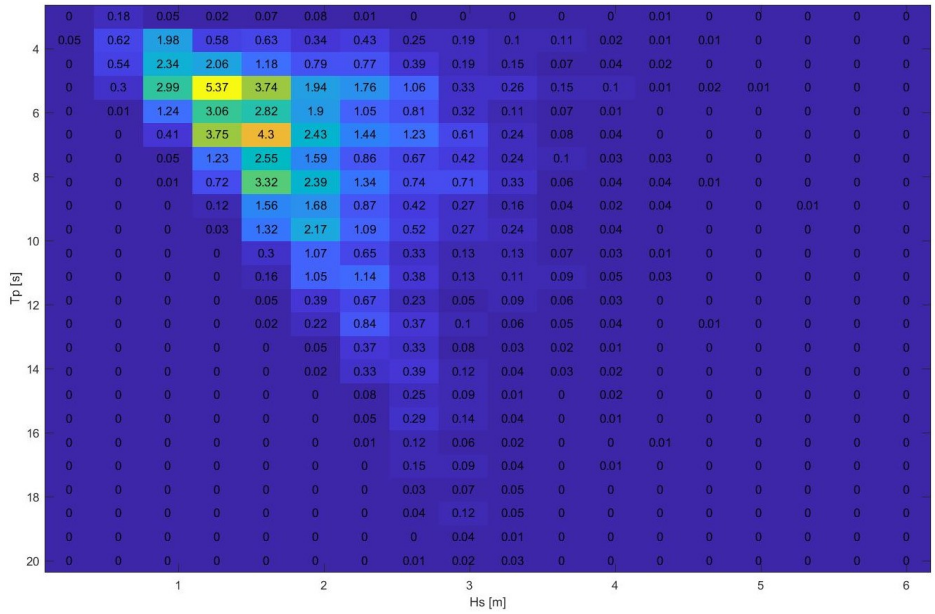

Figure C-1: Wave Scatter diagram of Central North sea, numbers in the diagram are given in percentages.

Appendix D

Literature Review

D-1 Introduction

The research on floating interaction bodies goes back to a long time since it is a relevant topic in the offshore working field. A lot of researchers use potential theory to investigate the motion of the fluid and body. Potential theory neglects viscous effects of the fluid. Mainly potential theory fits its purpose under these assumptions for the flow: the flow is incompressible, non-viscous, homogeneous, continuous and irrotational. Next to the flow assumptions it is assumed that the body motion is small compared to its size.
Based on potential theory there are different numerical methods to calculate the body motions. Widely known are the strip-theory, the panel method, also known as the boundary element method, and the finite element method [34].

D-2 Literature review hydrodynamic body interaction

D-2-1 Strip theory

The strip theory is applicable for slender bodies which have the length dimension substantially greater than the others. It is assumed that the force at one section of the body is not affected by the shape of the other parts of the body. I.e. each cross section of the body is considered to be part of a horizontal cylinder with constant cross section and infinite length, which is shown in Figure D-1. The three-dimensional coefficients for the body are found by an integration of the 2-D values over the ships length [18].

For multi-body systems, strip theory implies that there is only interaction between corresponding sections of structures. Regarding multi-body systems, Ohkusu (1970) used strip theory to analyse the interaction between multiple cylinders in heave, sway and roll motion [25]. In 1971, Ohkusu and Takaki extended this approach to create a theoretical calculation for the seakeeping qualities of twin hull ships in head and beam seas [26]. Kodan (1984) used Ohkusu's theory to describe the hydrodynamic interaction between two parallel slender structures in oblique waves and compared it to model experiments[20].

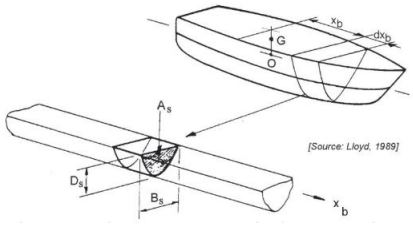

Figure D-1: Strip theory, the cross section is treated hydrodynamically as a infinite long cilinder.

D-2-2 Panel method

The panel method is a numerical method to calculate the potential flow around a body, based on the principle of Green's integral theorem. Compared to strip theory arbitrary body geometries can be used. The body surface is divided into multiple panels onto each the sources and doubled strengths as well as the fluid pressure can be calculated. By the use of Green's integral theorem, a three dimensional linear homogeneous differential equation can be transformed into a two dimensional integral equation. With the integral equation and its boundaries it is possible to determine the velocities on the body surface.

Faltinsen and Michelsen (1975) used this method to a floating object in regular waves [9]. Chakrabarti (2000) used the multiple-scattering method in combination with the panel method, to represent the interactions between different bodies [4]. In 2001, Fang and Chen analysed the hydrodynamic problems between two moving ships [5]. They solved the Green functions and derivatives by the use of the Telste and Noblesse's algorithm. In 2005, Ali and Khalil and Ali and Inoue, respectively, computed the hydrodynamic interaction coefficients for multiple freely floating cylinders and barges [2],[1].

D-2-3 Finite element method

The boundary integral method can create difficulties when the higher frequencies in the application of the Fourier Transform are needed. At higher frequencies, the phenomenon of irregular frequencies may occur. This problem can be tackled by the use of the finite element method which does not rely on boundary integral equations.

D-3 Potential Theory

D-3-1 Conservation Principles

Given a continuous and homogeneous flow, the increase of mass m per unit of time t of the fluid with density ρ through a fluid element with dimensions dx, dy, and dz is given by:

$$\frac{\partial m}{\partial t} = -\frac{\partial \rho}{\partial t} \cdot dx \cdot dy \cdot dz = \left\{ \frac{\partial(\rho u)}{\partial x} + \frac{\partial(\rho v)}{\partial y} + \frac{\partial(\rho w)}{\partial z} \right\} \tag{D-1}$$

In which u, v and w are the velocities in x, y and z direction, respectively. Equation (D-1) is known as the continuity equation which describes the conservation of mass. If we assume that

the fluid is incompressible, the density is considered to be constant, the continuity equation can be simplified to:

$$\frac{\partial u}{\partial x} + \frac{\partial v}{\partial y} + \frac{\partial w}{\partial z} = 0 \tag{D-2}$$

Next to the conservation of mass, there is conservation of momentum. According to Newtons second law, the force times acceleration for a non-viscous, incompressible fluid element as in eq. (D-1) in x-direction yields:

$$dm \cdot \frac{Du}{Dt} = \rho \cdot dxdydz \cdot \frac{Du}{Dt} = -\frac{\partial p}{\partial x} \cdot dxdydz \tag{D-3}$$

In which:

$$\frac{Du}{Dt} = \frac{\partial u}{\partial t} + \boldsymbol{u} \cdot \nabla u = \frac{\partial u}{\partial t} + \frac{\partial u}{\partial x}\frac{dx}{dt} + \frac{\partial u}{\partial y}\frac{dy}{dt} + \frac{\partial u}{\partial z}\frac{dz}{dt} = \frac{\partial u}{\partial t} + u\frac{\partial u}{\partial x} + v\frac{\partial u}{\partial y} + w\frac{\partial u}{\partial z} \tag{D-4}$$

Combining eq. (D-4) and eq. (D-3) gives the Euler equation in x-direction for a non-viscous and incompressible flow:

$$\frac{Du}{Dt} = \frac{\partial u}{\partial t} + u\frac{\partial u}{\partial x} + v\frac{\partial u}{\partial y} + w\frac{\partial u}{\partial z} = -\frac{1}{\rho}\frac{\partial p}{\partial x} \tag{D-5}$$

The same method can be used to obtain both the equations of Euler for the flow in the y and z direction.

D-3-2 Velocity Potential

Now a velocity potential function is introduced. A velocity potential is defined by the property that the derivative of the velocity potential to a certain direction is equal to the velocity in that direction. The velocity potentials in each Cartesian direction are shown in eq. (D-6).

$$u = \frac{\partial \Phi}{\partial x}, \quad v = \frac{\partial \Phi}{\partial y}, \quad w = \frac{\partial \Phi}{\partial z} \tag{D-6}$$

It is also possible to define the potential functions in other dimensions. For example in polar coordinates:

$$v_r = \frac{\partial \Phi}{\partial r}, \quad v_\theta = \frac{1}{r}\frac{\partial \Phi}{\partial \theta} \tag{D-7}$$

Combining eq. (D-2) and eq. (D-6) gives the Laplace equation for an incompressible fluid:

$$\frac{\partial^2 \Phi}{\partial x^2} + \frac{\partial^2 \Phi}{\partial y^2} + \frac{\partial^2 \Phi}{\partial z^2} = 0 \quad \text{or} \quad \nabla^2 \Phi = 0 \tag{D-8}$$

Next to the Laplace condition potential theory satisfies the rotation free condition:

$$\frac{\partial^2 \Phi}{\partial y \partial x} = \frac{\partial^2 \Phi}{\partial x \partial y} \quad \text{so} \quad \frac{\partial v}{\partial x} - \frac{\partial u}{\partial y} = 0 \tag{D-9}$$

The velocity terms in eq. (D-5) can be rewritten in terms of the velocity potential:

$$\begin{aligned} u\frac{\partial u}{\partial x} &= \frac{\partial \Phi}{\partial x}\cdot\frac{\partial^2 \Phi}{\partial x^2} = \frac{1}{2}\cdot\frac{\partial}{\partial x}\left(\frac{\partial \Phi}{\partial x}\right)^2 \\ v\frac{\partial u}{\partial y} &= \frac{\partial \Phi}{\partial y}\cdot\frac{\partial^2 \Phi}{\partial x \partial y} = \frac{1}{2}\cdot\frac{\partial}{\partial x}\left(\frac{\partial \Phi}{\partial y}\right)^2 \\ w\frac{\partial u}{\partial z} &= \frac{\partial \Phi}{\partial z}\cdot\frac{\partial^2 \Phi}{\partial x \partial z} = \frac{1}{2}\cdot\frac{\partial}{\partial x}\left(\frac{\partial \Phi}{\partial z}\right)^2 \end{aligned} \tag{D-10}$$

Substituting eq. (D-6) and eq. (D-10) in the Euler equation for flow in x-direction eq. (D-10) gives:

$$\frac{\partial}{\partial x}\left\{\frac{\partial \Phi}{\partial t} + \frac{1}{2}\left[\left(\frac{\partial \Phi}{\partial x}\right)^2 + \left(\frac{\partial \Phi}{\partial y}\right)^2 + \left(\frac{\partial \Phi}{\partial z}\right)^2\right] + \frac{p}{\rho}\right\} = 0 \tag{D-11}$$

The same can be done in the y and z direction, in this case only the partial derivative with respect to x at the beginning will change in y and z, respectively. So, the partial derivative with respect to x, y and z equals 0, which means the expressions are a function of time only. This provides the Bernoulli equation for an in-stationary flow:

$$\frac{\partial \Phi}{\partial t} + \frac{1}{2}V^2 + \frac{p}{\rho} + gz = f(t) \tag{D-12}$$

For a stationary flow, the Bernoulli equation can be written as:

$$p + \frac{1}{2}\rho V^2 + \rho g z = Constant \tag{D-13}$$

D-3-3 Potential Flow Elements

To solve the Laplace equation, eq. (D-8), one can use superposition. Multiple simple flow elements which are a solution of the Laplace equation can be superposed to recreate a more complex flow. Examples of these flow elements are an uniform flow, a source, a sink, a circulation and a doublet or dipole.

The simplest solution is an uniform flow in a certain direction:

$$\Phi = U \cdot x \quad \text{so} \quad u = \frac{\partial \Phi}{\partial x} = U \tag{D-14}$$

The second derivative of the potential in all directions is equal to zero. The first derivative with respect to x gives the fluid velocity which is equal to the uniform flow U. A negative uniform flow leads to a flow in the opposite direction. Both uniform flow elements are shown in Figure D-2.

Another flow element is a source point. This is a point from which to flow radiates in any outward direction. For a two-dimensional flow, its potential function is equal to:

$$\Phi = \frac{Q}{2\pi}\cdot \ln\sqrt{x^2+y^2}, \quad \text{or in polar coordinates} \quad \Phi = \frac{Q}{2\pi}\cdot \ln r \tag{D-15}$$

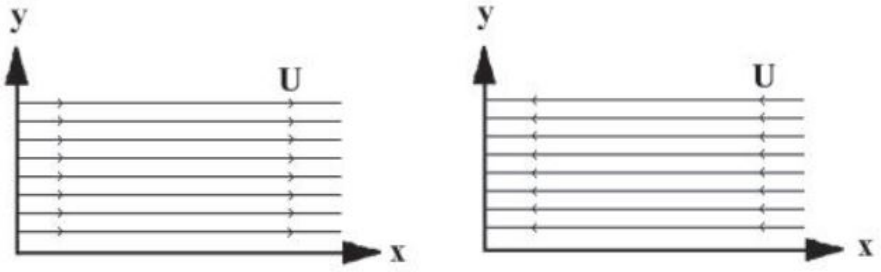

(a) Positive uniform flow element. **(b)** Negative uniform flow element.

Figure D-2: Uniform potential flow, [18].

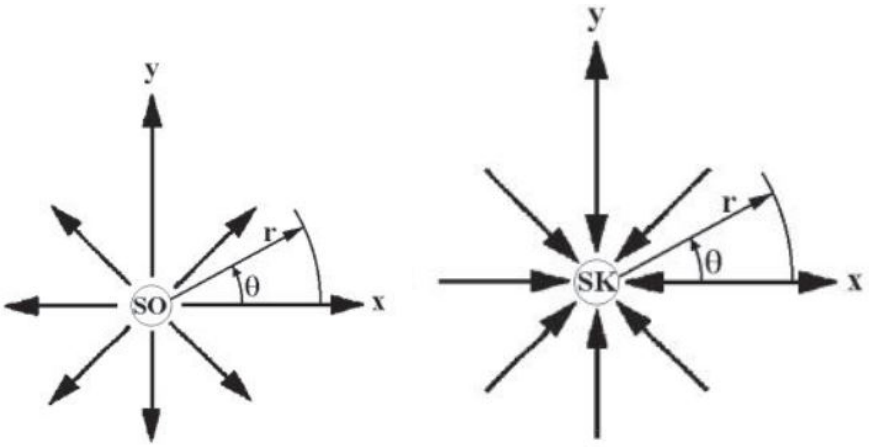

(a) Source flow element. **(b)** Sink flow element.

Figure D-3: Radial potential flow [18].

in which Q is the source strength, r defines the location of the potential lines circling around the origin and θ defines the location of the stream lines.

A sink is negative source so it has as inward radial flow. Its potential is the same as the source only with a negative sign. The source and sink point flow elements are shown in Figure D-3.

A circulation or a vortex is a tangential flow around a point. The potential function for this flow element is:

$$\Phi = \frac{\Gamma}{2\pi} \cdot \arctan \frac{y}{x}, \quad \text{or in polar coordinates} \quad \Phi = \frac{\Gamma}{2\pi} \cdot \theta \tag{D-16}$$

in which Γ is the circulation strength. The tangential velocity for a vortex is in a counter clockwise direction. If the potential has a negative sign the tangential velocity is in a clockwise direction. A circulation flow element is shown in Figure D-4.

If a source and a sink are only separated by a small distance s, which tends to go to zero, a doublet or a dipole will occur. A dipole is a superposition of source and a sink. The potential function for a dipole is:

$$\Phi = \mu \frac{x}{x^2 + y^2}, \quad \text{or in polar coordinates} \quad \Phi = \frac{\mu \cdot \cos\theta}{r} \tag{D-17}$$

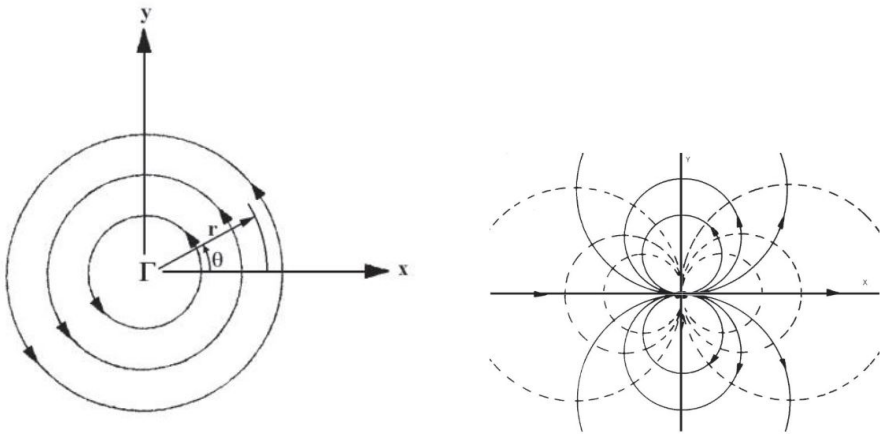

(a) Circulation flow element. **(b)** Doublet or Dipole flow.

Figure D-4: Potential flow elements and superposition [18].

in which μ is the doublet strength, which is equal to $\frac{Qs}{\pi}$. A example of a doublet flow is shown in Figure D-4.

D-4 Potential theory of a body in waves

With the basics and assumptions of potential theory known, the potential theory regarding a body in waves can be written. A freely floating body, with zero mean forward speed, oscillating in a fluid is considered. The linear wave velocity potential can be defined as:

$$\Phi(x,y,z,t) = \Phi_r(x,y,z,t) + \Phi_w(x,y,z,t) + \Phi_d(x,y,z,t) \tag{D-18}$$

in which Φ_r is the radiation potential, Φ_w the incident wave potential and Φ_d the diffraction potential. Each of these potentials has to fulfil several requirements and boundary conditions:

- Continuity condition
$$\frac{\partial^2\Phi}{\partial x^2} + \frac{\partial^2\Phi}{\partial y^2} + \frac{\partial^2\Phi}{\partial z^2} = 0 \tag{D-19}$$
- Seabed boundary condition
At the seabed, at a depth of $z = -d$, the velocity in the vertical direction has to be zero:
$$\frac{\partial\Phi}{\partial z} = 0 \quad \text{at} \quad z = -d \tag{D-20}$$
This is a no-leak condition. Water particles could not move into the soil.
- Free surface dynamic boundary condition
The pressure at the free surface ($z = \zeta$) of the fluid has to equal the atmospheric pressure. Based on the Bernoulli equation for in-stationary, irrotational flow the boundary condition is expressed as:
$$\frac{\partial\Phi}{\partial t} + g\zeta = 0 \quad \text{for} \quad z = \zeta \tag{D-21}$$

- Free surface kinematic boundary condition
  At the free surface of the flow ($z = \zeta$) the vertical velocity of a water particle has to be the same as the vertical velocity of the the free surface itself. For linear waves it yields:

$$\frac{dz}{dt} = \frac{\partial \Phi}{\partial z} = \frac{\partial \zeta}{\partial t} \quad \text{for} \quad z = \zeta \tag{D-22}$$

  This is also a no-leak condition. Particles could not pass through the free surface. Combining the dynamic and kinematic boundary condition for the free surface, eq. (D-21) and eq. (D-22) delivers the Cauchy-Poisson condition:

$$\frac{\partial^2 \Phi}{\partial t^2} + g\frac{\partial \Phi}{\partial z} = 0 \quad \text{for} \quad z = 0 \tag{D-23}$$

- Kinematic boundary condition at the oscillating body surface
  The velocity of a water particle at the body surface has to be equal to the velocity of the body hull at this point, v_n. So the velocity potential in normal direction, n is:

$$\frac{\partial \Phi}{\partial n} = v_n(x, y, z, t) \tag{D-24}$$

  This is also a no-leak condition. Water particles cannot move through the wetted surface of the body. Because the solution of the potential can be linearised, the outward normal velocity at the surface of the body can be written in terms of the summation of the oscillatory velocities v_j and generalized direction cosines on the surface of the body:

$$v_n(x, y, z, t) = \sum_{j=1}^{6} v_j \cdot f_j(x, y, z) \tag{D-25}$$

  The generalized direction cosines for each mode are given by:

$$\begin{aligned} f_1 &= \cos(n, x) \\ f_2 &= \cos(n, y) \\ f_3 &= \cos(n, z) \\ f_4 &= yf_3 - zf_2 \\ f_5 &= zf_1 - xf_3 \\ f_6 &= xf_2 - yf_1 \end{aligned} \tag{D-26}$$

- Radiation condition
  At large distant from the body, the potentials caused by the diffraction or motion of the body disappear:

$$\lim_{x \to \infty} \Phi = 0 \tag{D-27}$$

The boundary conditions apply to all possible wave conditions. Superposition can then be used to study all sorts of irregular wave conditions, even those with directional spreading.

D-4-1 Forces and moments

The forces and moments can be calculated by an integration of the pressure over the wetted body surface, S:

$$\vec{F} = -\iint_S (p \cdot \vec{n}_j) \cdot dS \tag{D-28}$$

The vector $\vec{n}_j$ creates the distinction between the forces and the moments:

$$\vec{n}_j = \begin{cases} \vec{n} & \text{for j} = 1, 2, 3 \\ \vec{n} \times \vec{r} & \text{for j} = 4, 5, 6 \end{cases} \tag{D-29}$$

in which $\vec{n}$ the outward normal vector and $\vec{r}$ is the position vector of the surface dS with respect to the origin of the reference frame of the body.

Substituting eq. (D-18) in the Bernoulli equation, eq. (D-12), with the assumption of zero mean forward speed gives an equation for the fluid pressure:

$$p = -\rho \frac{\partial \Phi}{\partial t} - \rho g z = -\rho \left(\frac{\partial \Phi_r}{\partial t} + \frac{\partial \Phi_w}{\partial t} + \frac{\partial \Phi_d}{\partial t} \right) - \rho g z \tag{D-30}$$

When the equation for the pressure is substituted in the force and moment equations, eq. (D-28), four different categories of forces and moments can be defined:

- Force and moments by radiated waves from oscillating body

$$\vec{F}_r = \rho \iint_S \left(\frac{\partial \Phi_r}{\partial t} \right) \vec{n}_j \cdot dS \tag{D-31}$$

- Force and moments by approaching waves on fixed floating body

$$\vec{F}_w = \rho \iint_S \left(\frac{\partial \Phi_w}{\partial t} \right) \vec{n}_j \cdot dS \tag{D-32}$$

- Force and moments by diffraction of waves due to fixed floating body

$$\vec{F}_d = \rho \iint_S \left(\frac{\partial \Phi_d}{\partial t} \right) \vec{n}_j \cdot dS \tag{D-33}$$

- Force and moments by hydrostatic buoyancy

$$\vec{F}_s = \rho \iint_S (g z) \vec{n}_j \cdot dS \tag{D-34}$$

Radiation Forces

The radiation forces and moments are the loads caused by the fluid due to the body oscillation in still water. The radiation potential Φ_r can be written as a summation over all the body modes of a separated space and time dependent term:

$$\Phi_r(x, y, z, t) = \sum_{j=1}^{6} \Phi_j(x, y, z, t) = \sum_{j=1}^{6} \phi_j(x, y, z) \cdot v_j(t) \tag{D-35}$$

in which ϕ_j is the space dependent potential in in each mode j and $v_j(t)$ is the time dependent oscillatory motion of the body in mode j.

So the normal velocity on the body surface can be written as:

$$\frac{\partial \Phi_r}{\partial n} = \sum_{j=1}^{6} \left(\frac{\partial \phi_j}{\partial n} \cdot v_j \right) = \sum_{j=1}^{6} (f_j \cdot v_j) \tag{D-36}$$

in which:

$$f_j = \frac{\partial \phi_j}{\partial n} \tag{D-37}$$

The function f_j are the generalized cosines for each mode j given in **??**. Substituting eq. (D-35) in the force and moments equation for radiated waves, eq. (D-31), gives the force equation for each DoF, $k = 1, .., 6$:

$$F_{r_k} = \rho \iint_S \left(\frac{\partial}{\partial t} \sum_{j=1}^{6} \phi_j v_j \right) n_k \cdot dS = \rho \iint_S \left(\frac{\partial}{\partial t} \sum_{j=1}^{6} \phi_j v_j \right) f_k \cdot dS = \rho \iint_S \left(\frac{\partial}{\partial t} \sum_{j=1}^{6} \phi_j v_j \right) \frac{\partial \phi_k}{\partial n} \cdot dS \tag{D-38}$$

Since both potentials, ϕ_j and ϕ_k are not time dependent one can write:

$$F_{r_k} = \sum_{j=1}^{6} F_{r_{kj}} \tag{D-39}$$

in which:

$$F_{r_{kj}} = \frac{\mathrm{d}v_j}{\mathrm{d}t} \rho \iint_S \phi_j \frac{\partial \phi_k}{\partial n} \cdot dS \tag{D-40}$$

The oscillatory motion for the body can be defined. Suppose it has an amplitude s_A in direction j, its time dependent motion is:

$$s_j = s_{A_j} e^{-i\omega t} \tag{D-41}$$

Then oscillatory velocity and acceleration are:

$$\begin{aligned} \dot{s}_j &= v_j = -i\omega s_{A_j} e^{-i\omega t} \\ \ddot{s}_j &= \frac{\mathrm{d}v_j}{\mathrm{d}t} = -\omega^2 s_{A_j} e^{-i\omega t} \end{aligned} \tag{D-42}$$

The hydrodynamic radiation forces can be split in a load in-phase with the acceleration and a load in-phase with the velocity. The load in-phase with the acceleration is the added mass of the body, A_{kj} and the load in-phase with the velocity is the radiation damping of the body, B_{kj}.

$$\begin{aligned} F_{r_{kj}} &= -A_{kj}\ddot{s}_j - B_{kj}\dot{s}_j \\ &= (\omega^2 s_{A_j} A_{kj} + i\omega s_{A_j} B_{kj}) e^{-i\omega t} \\ &= \left(-\omega^2 s_{A_j} \rho \iint_S \phi_j \frac{\partial \phi_k}{\partial n} \cdot dS \right) e^{-i\omega t} \end{aligned} \tag{D-43}$$

So the added mass and damping coefficients are given by:

$$A_{kj} = -\mathfrak{Re} \left\{ \rho \iint_S \phi_j \frac{\partial \phi_k}{\partial n} \cdot dS \right\} \quad B_{kj} = -\mathfrak{Im} \left\{ \rho\omega \iint_S \phi_j \frac{\partial \phi_k}{\partial n} \cdot dS \right\} \tag{D-44}$$

Wave and Diffraction Forces

The wave and diffraction forces are the loads caused by the incoming and diffracted waves on and due to the fixed body. Just as for the radiation potentials, the wave and diffraction potential can be written in terms of a isolated space and time dependent term:

$$\begin{aligned}\Phi_w(x,y,z,t) &= \phi_w(x,y,z)\cdot e^{-i\omega t}\\ \Phi_d(x,y,z,t) &= \phi_d(x,y,z)\cdot e^{-i\omega t}\end{aligned} \tag{D-45}$$

The kinematic boundary condition at the body surface implies:

$$\frac{\partial \Phi}{\partial n} = \frac{\partial \phi_w}{\partial n} + \frac{\partial \phi_d}{\partial n} = 0 \tag{D-46}$$

By application of the this condition and the generalized direction cosines from **??** in the forces and moments equations eq. (D-32) and eq. (D-33), the force and moments in each DoF k are:

$$F_{w_k} = -i\rho e^{-i\omega t}\iint_S (\phi_w + \phi_d) f_k \cdot dS = -i\rho e^{-i\omega t}\iint_S (\phi_w + \phi_d)\frac{\partial \phi_k}{\partial n}\cdot dS \tag{D-47}$$

The British mathematician George Green has elaborated three identities in vector calculus relating bulk to the boundary region on which the differential operators act. For a body in deep water, his second identity implies:

$$\iint_S \phi_j \frac{\partial \phi_k}{\partial n}\cdot dS = \iint_S \phi_k \frac{\partial \phi_j}{\partial n}\cdot dS \tag{D-48}$$

Using both eq. (D-47) and Green's second identity, eq. (D-48), one can eliminate the diffraction potential which results in the so-called Haskind relations. As a result the wave force is only a function of the wave potential ϕ_w and the radiation potential ϕ_k:

$$F_{w_k} = -i\rho\omega e^{-i\omega t}\iint_S (\phi_w \frac{\partial \phi_k}{\partial n} - \phi_k \frac{\partial \phi_w}{\partial n})\cdot dS \tag{D-49}$$

The wave potential for deep water can be written as:

$$\Phi_w = \frac{\zeta_a g}{\omega}\cdot e^{kz}\cdot \sin(\omega t - kx\cos\mu - kysin\mu) = \frac{i\zeta_a g}{\omega}\cdot e^{kz}\cdot e^{-ik(x\cos\mu + ysin\mu)}\cdot e^{-i\omega t} = \phi_w \cdot e^{-i\omega t} \tag{D-50}$$

With the potential given, the velocity of the water particles on the surface of the body in the outward normal direction is:

$$\begin{aligned}\frac{\partial \phi_w}{\partial n} &= \frac{i\zeta_a g}{\omega}\cdot k\left\{\frac{\partial z}{\partial n} - i(\frac{\partial x}{\partial n}\cos\mu + \frac{\partial y}{\partial n}\sin\mu)\right\}\cdot e^{kz}\cdot e^{-ik(x\cos\mu + ysin\mu)}\\ &= \phi_w \cdot k\left\{\frac{\partial z}{\partial n} - i(\frac{\partial x}{\partial n}\cos\mu + \frac{\partial y}{\partial n}\sin\mu)\right\}\\ &= \phi_w \cdot k\left\{f_3 - i(f_1\cos\mu + f_2\sin\mu)\right\}\end{aligned} \tag{D-51}$$

Substituting both eq. (D-51) and eq. (D-37) into the wave force equation eq. (D-49) gives the final expression for the wave loads:

$$F_{w_k} = -i\rho\omega e^{-i\omega t} \iint_S \phi_w f_k \cdot dS + i\rho\omega e^{-i\omega t} k_w \iint_S \phi_k \phi_w \Big\{ f_3 - i(f_1 \cos\mu + f_2 \sin\mu) \Big\} \cdot dS \quad \text{(D-52)}$$

in which k_w is the wave number to prevent mistakes.
The first term in the expression for the wave loads is known as the Froude-Krylov force and moments, the loads caused by the incident wave. The second term is known as the diffraction force and moments, the loads caused by the wave disturbance, due to the presence of the body.

Hydrostatic bouyancy

The final force and moment terms acting on a body are the hydrostatic loads. These are the loads caused by the bouyancy forces of the water. The load component in each DoF $k = 1, .., 6$ is given by:

$$F_{s_k} = \rho g \iint_S z f_k \cdot dS \quad \text{(D-53)}$$

D-4-2 Solving the potentials

Now, a general description of potential theory is given. The loads on a stationary oscillating body in wave are expressed in the terms of the potentials. The potential of the incident wave is known and given. The radiation and diffraction potential however, are more complex to define. To define these potentials and to solve the potential problem, different methods have been developed in the past.
Regarding 2D strip theory, in 1949 Ursell developed a analytical solution for the potentials for a circular section [30]. Tasai used the theory of Ursell and a conformal mapping method to solve the potentials for a more ship-like cross section [29]. In 1967, Frank used a method of pulsating sources to solve the potentials for ship-like cross sections. Since strip theory will not be used in this thesis, no more details regarding these solutions are given. A detailed elaboration of this methods can be found in [18].
For the 3D panel method a lot of diffraction software programs make use of the so called Green's function to solve the potential problem.

Green's Function Method

The potential at the surface of a mean wetted body, S_0 due to the motion modes of the body $j = 1, .., 6$ and the diffraction potential $j = 7$ can be represented by a continuous distribution of single sources on the surface body:

$$\phi_j = \frac{1}{4\pi} \iint_{S_0} \sigma_j(\hat{x}, \hat{y}, \hat{z}) \cdot G(x, y, z, \hat{x}, \hat{y}, \hat{z}) \cdot dS_0 \quad \text{for} \quad j = 1, .., 7 \quad \text{(D-54)}$$

in which σ_j is the complex pulsating source strength in a point located at $(\hat{x}, \hat{y}, \hat{z})$ on the mean wetted surface S_0 due to the motion of the body in the j mode. G is the Green's function of

the pulsating source in a point located at $(\hat{x}, \hat{y}, \hat{z})$ on the potential ϕ_j located at point (x, y, z). The Green's function as well as the potential function satisfy all the boundary conditions. Possible Green's function to solve the potential are given by [**?**] and [16]. Depending on the specific problem it preferable to use one over the other. Also, a lot of diffraction software use a combination of both formulation of Green's functions to speed up the calculations based on the work of [24].
The source strength can be calculated using the kinematic boundary condition on the body.

$$\frac{\partial \phi_j}{\partial n} = n_j = -\frac{1}{2}\sigma_j(x,y,z)\frac{1}{4\pi}\iint_{S_0}\sigma_j(\hat{x},\hat{y},\hat{z})\cdot\frac{\partial G(x,y,z,\hat{x},\hat{y},\hat{z})}{\partial n}\cdot dS_0 \quad \text{for} \quad j = 1,..,6 \tag{D-55}$$

in which n_j is equal to the generalized cosines as in eq. (D-37).
The solution of the diffraction potential, ϕ_7 is given by:

$$\frac{\partial \phi_7}{\partial n} = -\frac{\partial \phi_w}{\partial n} \tag{D-56}$$

When the source strength can be known using eq. (D-55), it can be substituted in eq. (D-54) to find the radiation potentials. With the radiation potentials both the added mass and the damping coefficients of the body can be calculated.

Bibliography

[1] M T Ali and Y Inoue. On hydrodynamic interaction between two rectangular barges floating side-by-side in regular waves. *Proceedings of the International Conference on Mechanical Engineering 2005*, 2005(December):6 (Paper ICME05–FL–03), 2005.

[2] Mir Tareque Ali and Gazi Md Khalil. On hydrodynamic interaction between several freely floating vertical cylinders in waves. *Proceedings of the International Conference on Offshore Mechanics and Arctic Engineering - OMAE*, 1 A(Omae 2005):391–398, 2005.

[3] ANSYS. Aqwa Theory Manual. 15317(November):174, 2013.

[4] Subrata Chakrabarti. Hydrodynamic interaction forces on multi-moduled structures. *Ocean Engineering*, 27(10):1037–1063, 2000.

[5] Gung Rong Chen and Ming Chung Fang. Hydrodynamic interactions between two ships advancing in waves. *Ocean Engineering*, 28(8):1053–1078, 2001.

[6] X. B. Chen, F. Rezende, S. Malenica, and J. R. Fournier. Advanced hydrodynamic analysis of LNG terminals. *10th International Symposium on Practical Design of Ships and other Floating Structures, PRADS 2007*, 1(January):224–233, 2007.

[7] Chen XB. Hydrodynamic analysis for offshore LNG terminals. *In: Proc 2nd int workshop on applied offshore hydrodynamics.*, 2005.

[8] DNV. Offshore Standard DNV-RP-H103 -Modelling And Analysis Of Marine Operations. *Det Norske Veritas*, (April):150, 2011.

[9] O. M. Faltinsen and F. C. Michelsen. Motions of Large Structures in Waves At Zero Froude Number., 1975.

[10] Jean Robert Fournier, Mamoun Naciri, and Xiao Bo Chen. Hydrodynamics of two side-by-side vessels experiments and numerical simulations. *Proceedings of the International Offshore and Polar Engineering Conference*, 4:158–165, 2006.

[11] Peter Harenberg. *Developing the optimal design solution for Jumbo to increase the offshore stability of a heavy crane lift vessel Peter Harenberg*. PhD thesis, Delft University of Technology, 2016.

[12] Heerema Marine Contractors. Revolutionary way of lifting offshore successfully tested. Technical Report 0, 2018.

[13] A J Van Der Heiden. Vessel and cargo motions. page 160, 2019.

[14] HER Group. *Marine Equipment and Wire Rope Handbook*. 1990.

[15] ITTC. ITTC Recommended Procedures: Numerical Estimation of Roll Damping. pages 1–33, 2011.

[16] Fritz John. On the motion of floating bodies. I. *Communications on Pure and Applied Mathematics*, 2(1):13–57, 1949.

[17] Fritz John. On the motion of floating bodies II. Simple harmonic motions. *Communications on Pure and Applied Mathematics*, 3(1):45–101, 1950.

[18] J M J Journée, W W Massie, and R H M Huijsmans. OFFSHORE HYDROMECHANICS Third Edition (2015) Based on Original Lecture Notes (2000). 2015.

[19] Yuki Kawahara, Kazuya Maekawa, and Yoshiho Ikeda. A simple prediction formula of roll damping of conventional cargo ships on the basis of Ikeda's method and its limitation. *Fluid Mechanics and its Applications*, 97(1):465–486, 2011.

[20] N Kodan. The motions of adjacent floating structures in oblique waves. *Journal of Energy Resources Technology, Transactions of the ASME*, 106(2):199–205, 1984.

[21] H Lageveen. Modelling and Steering of Tuggerwinch. 2014.

[22] Edward M. Lewandowski. Multi-vessel seakeeping computations with linear potential theory. *Ocean Engineering*, 35(11-12):1121–1131, 2008.

[23] B. Molin. On the piston and sloshing modes in moonpools. *Journal of Fluid Mechanics*, 430:27–50, 2001.

[24] J.N Newman. Algorithms for the free-surface Green function. *Department of Ocean Engineering, Massachusetts Institute of Technology*, 53(2-4):271–288, 1985.

[25] Ohkusu. On the motion of multihull ships in waves (I). XVIII(60), 1970.

[26] Makoto Ohkusu and Mikio Takaki. On the Motion of Twin Hull Ship in Waves. 1390.

[27] Willemijn H. Pauw, René H.M. Huijsmans, and Arjan Voogt. Advances in the hydrodynamics of side-by-side moored vessels. *Proceedings of the International Conference on Offshore Mechanics and Arctic Engineering - OMAE*, 4(April):597–603, 2007.

[28] Blanca Peña and Aaron McDougall. An investigation into the limitations of the panel method and the gap effect for a fixed and a floating structure subject to waves. *Proceedings of the International Conference on Offshore Mechanics and Arctic Engineering - OMAE*, 7:1–13, 2016.

[29] Fukuzo Tasai. On the Damping Force and added Mass of Ships Heaving and Pitching. *Journal of Zosen Kiokai*, 1959(105):47–56, 1959.

[30] F. Ursell. On the heaving motion of a circular cylinder on the surface of a fluid. *Quarterly Journal of Mechanics and Applied Mathematics*, 2(2):218–231, 1949.

[31] US Army. Directional Wave Spectra using cosine-squared and cosine 2S spreading Functions. *Technical Note*, 1, 2015.

[32] Jasper van Heijst. *Improvement of the workability of monohull heavy lift vessels during lifting operations by reducing roll motion.* PhD thesis, Delft University of Technology, 2015.

[33] Regina I Irene Williams. propagation analyses A Comparison of Monochromatic , One-Dimensional Spectral , and Two- Dimensional Spectral Wave ... May 2004. 2004.

[34] C Xie. Characterization of Coupled Body Response in Random Sea. *Ocean Engineering*, Msc Disser(December):125, 2005.

Glossary

List of Acronyms

CSVs	Construction Support Vessels
DP	Dynamic Positioning
CoG	Center of Gravity
DoF	Degree of Freedom
RAO	Response Amplitude Operator
SDA	Significant Double Amplitude
FSRU	Floating Storage and Regasification Unit
LNG	Liquified Natural Gas
JONSWAP	Joint North Sea Wave Project
CoB	Center of Buoyancy
MARIN	Maritime Research Institute Netherlands
ART	Anti Roll Tank
MPM	Most Probable Maximum
HLCV's	Heavy Lift Crane Vessels